Investigations on the Non-Photochemical Laser Induced Nucleation (NPLIN) mechanisms : case studies of Potassium Sulfate and EthyleneDiamine Sulfate

Melody Briard

Normandie Université

THÈSE

Pour obtenir le diplôme de doctorat

Spécialité CHIMIE

Préparée au sein de l'Université de Rouen Normandie

Investigations on the Non-Photochemical Laser Induced Nucleation (NPLIN) mechanisms : case studies of Potassium Sulfate and EthyleneDiamine Sulfate

Présentée et soutenue par
MELODY BRIARD

Thèse soutenue le 08/12/2022 devant le jury composé de		
M. ANDREW ALEXANDER	MAITRE DE CONFERENCES HDR, Université d'Edinbourg (UK)	Rapporteur du jury
MME ANNE SPASOJEVIC	PROFESSEUR DES UNIVERSITES, Université Paris-Saclay	Rapporteur du jury
M. CLEMENT BRANDEL	MAITRE DE CONFERENCES, Université de Rouen Normandie	Membre du jury
MME NADINE CANDONI	PROFESSEUR DES UNIVERSITES, Aix-Marseille Université	Membre du jury
M. SAMUEL PETIT	PROFESSEUR DES UNIVERSITES, Université de Rouen Normandie	Président du jury
MME VALÉRIE DUPRAY	MAITRE DE CONFERENCES HDR, Université de Rouen Normandie	Directeur de thèse

Thèse dirigée par VALÉRIE DUPRAY (SCIENCES ET METHODES SEPARATIVES)

UNIVERSITÉ DE ROUEN NORMANDIE

ED 591 PSIME

SMS Sciences et Méthodes Séparatives

"The way I see it, every life is a pile of good things and bad things. The good things don't always soften the bad things but vice versa, the bad things don't necessarily spoil the good things or make them unimportant"

The 11th doctor, Doctor Who

Acknowledgments

First, I would like to express all my gratitude to Dr. Valérie Dupray, for supervising my work with such kindness, for spending time with me changing the laser set-up and sharing her knowledge in optics and laser. I would like also to thanks Dr. Clément Brandel, who co-supervised this work. Thank you for your kindness, all your advices and ideas about this thesis. Thank you for having read and re-read my writings and for the feedback that always helps me to do better. Thank you both for the trust you have placed in me since the beginning, I could not have a better supervising team.

Then, many thanks to Prof. Gérard Coquerel who gave me the opportunity to learn about crystallization and solid-state during summer jobs and my M2 internship. Thank you for sharing your knowledge, I would not be here today without your help.

Now, I would like to thank all the jury members, Dr. Andrew Alexander and Prof. Anne Spasojevic as reviewers, Prof. Nadine Candoni and Prof. Samuel Petit as examiners for accepting to review my thesis. I hope that the defense of my PhD work will lead to interesting discussions.

I have to thanks people who contributed to this work : Dr. Sandrine Morin-Grognet for accepting to perform AFM analyses on my samples; Dr. Arnaud Barbier for his help with ICP analyses; Dr. Fabrice Barbe for supplying the stainless steel particles.

A special thanks to the CSI members Prof. Angela Vella and Dr. Yohann Cartigny for taking some of your time to follow my thesis work and evaluate it. Thanks for the discussion we had during CSI meeting.

J'écris à présent en français pour remercier tous les membres du laboratoire SMS, en particulier Nicolas Couvrat, Morgane Sanselme, Gabin Gbabode, Simon Clevers, Pascal Cardinaël et Marie Vaccaro pour leur gentillesse et leur aide. Merci à mes camarades doctorants, ceux qui sont devenus docteurs FX, Manon, Lina, Aliou, Chloé, Marine et ceux qui le seront bientôt Laureline et Aurélien, puis Clément, Hugo, Chrystal, Félix et Nino. Merci pour la bonne ambiance au quotidien et bon courage pour la suite.

Je remercie également les étudiants que j'ai encadré en stage et qui ont contribués à collecter des données pour ce sujet Nino, Charles et Clément.

Merci à mes amis, la team Molkkredi, pour la bonne humeur, les moments détentes autour de parties de mölkky, les discussions et les rires mais également pour leur soutien et l'entraide dans les moments plus sérieux de travail et de rédaction. Merci à vous tous Kevin, Markus, Vincent, Chloé, Claire, Tiffen et tout particulièrement merci à Guillaume (Guigui) pour ton amitié et ton soutien depuis notre première année de licence chimie.

Je remercie ma famille, mon frère Alain, et mes sœurs Sabrina et Amandine (Dine-sama) pour m'avoir encouragé dans mes études. Un grand merci à mes parents pour leur soutien sous toutes ses formes tout au long de mes études et dans tous mes projets. Merci à Dimitri pour son amour et son soutien ses cinq dernières années.

Merci à tous
Mélody

TABLE OF CONTENTS

GENERAL INTRODUCTION

Crystallization is a complex physico-chemical process, which involves two steps, nucleation and growth, the former being a key element in this work. Crystallization permits to control chemical purity, polymorphism and chirality. Because of kinetic reasons, spontaneous nucleation of the compound of interest can sometimes be difficult. Thus, various techniques have been developed to trigger nucleation in solution, such as seeding, mechanical energy, ultrasounds etc.

This thesis work focused on a rather recent technique called NPLIN (for Non-photochemical laser induced Nucleation). In NPLIN, a laser delivering very short nanosecond pulses at high energy is used to irradiate and induce nucleation of supersaturated solutions. The process is called non-photochemical as the laser does not induce any chemical reaction or degradation of the solvent or the solute.

NPLIN allows a significant decrease of the induction time, a control of the number and size of crystals. Moreover, the choice of the adequate laser polarization (linear to circular) has been reported as a way to control polymorphism and chirality.

This technique has thus a great potential to help control the nucleation, however the interaction between the laser light and the supersaturated solution is not yet fully understood. Indeed, the efficiency of the NPLIN seems to be compound and solvent dependent and, for some compounds, no NPLIN process is even observed (i.e., the nucleation is not induced). So, many questions about the NPLIN mechanism require a detailed study to be answered.

Since its discovery by Garetz *et al.* in 1996, the NPLIN process has been studied and applied to numerous compounds from small organic molecules to inorganic salts and proteins. Through these experiments, the different teams of researchers have developed their own theory about the mechanism and the influence of the laser on the supersaturated solution. Four mechanisms have been proposed : (i) Optical Kerr Effect (OKE) , (ii) Dielectric Polarisation (DP) (iii) Cavitation and (iv) nanoparticle heating.

The aim of this thesis is to provide new information to understand the mechanism by studying new compounds and applying an original

approach of NPLIN experiments. For this purpose, we focussed our work on two compounds : potassium sulfate and ethylenediamine sulfate. Each compound is the subject of a proper chapter.

The manuscript is organized as follows:

Chapter 1 is devoted to the definition of generalities concerning the solid state, crystallization and the interaction laser light-matter. These generalities are necessary for the good understanding of this work.

Chapter 2 is a literature review of the NPLIN process from its discovery in 1996 to the time of this writing, with a description of each proposed mechanism.

Chapter 3 is dedicated to the material and methods, protocol and laser set-up used during this work.

Chapter 4 focuses on the application of NPLIN to potassium sulfate for which we investigate the influence of different parameters on NPLIN kinetics. In particular the content and nature of dissolved gas in the solution was examined in order to discuss the potential formation of gaseous bubbles during NPLIN.

Chapter 5 focuses on the study of ethylenediamine sulfate, and particularly the influence of (solid) impurities in solution through filtration and doping of supersaturated solutions. Removed impurities are analysed for identification. In addition, different polarization geometries are used to explore the possible stereoselectivity of NPLIN as ethylenediamine sulfate exhibits supramolecular chirality.

Chapter 6 consists in a general discussion and final conclusions of this work. The different mechanisms are reviewed considering all the results we collected. With a particular attention to the nanoparticle heating mechanism, an additional study is presented to show how gold nanoparticles can trigger NPLIN in a system with long induction time at high supersaturation. Finally, a conclusion on the most likely mechanism and perspectives for the future work are proposed.

Chapter 1. GENERALITIES

1.1 INTRODUCTION

This chapter presents the basic notions that are required for a good understanding of the manuscript. It is dedicated to the fundamentals of crystallization with a specific focus on the mechanisms of nucleation. Besides, a comprehensive description of the laser technology will be given.

1.2 SOLID STATE

1.2.1 Crystallography

Crystallography is the science that describe the spatial arrangement of atoms, molecules or ions in crystal structures. In a crystal, there is a periodical repeating unit of a minimum volume composed of a minimum of molecules called the unit cell. The translations of the unit cell in the three dimensions forms the crystal lattice (Figure 1-1). The lattice geometry has been described by Bravais in 1849. From a mathematical point of view lattices are a set of three independent translation vector defined by (i) the norm of the vector called a, b and c representing the size of the lattice and (ii) the direction of the vector given by the angle between two vectors : α, β and γ. Bravais described the seven crystal systems depending on the relation between the cell parameters The combination of the 7 crystal systems with the four different and non-equivalent modes (i.e., position of the lattice points) gives 14 possible lattices (Figure 1-2) in which each lattices point have the same environment.

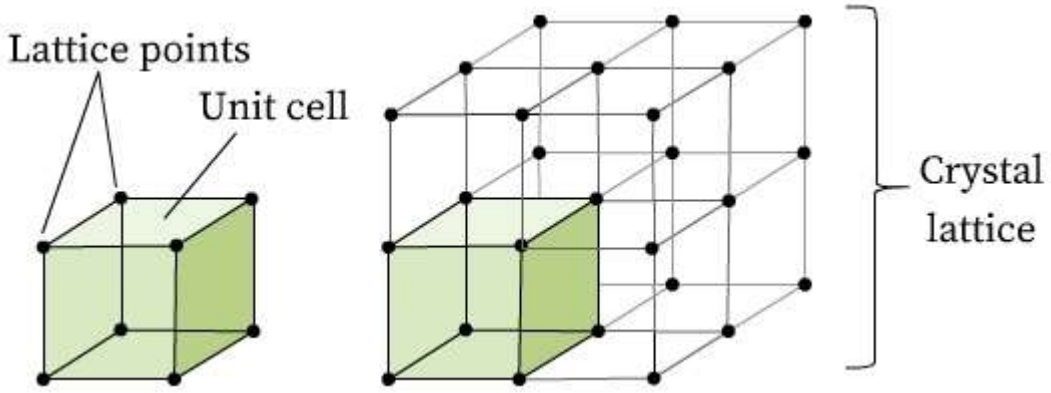

Figure 1-1-Representation of a unit cell (left) and its crystal lattice (right).

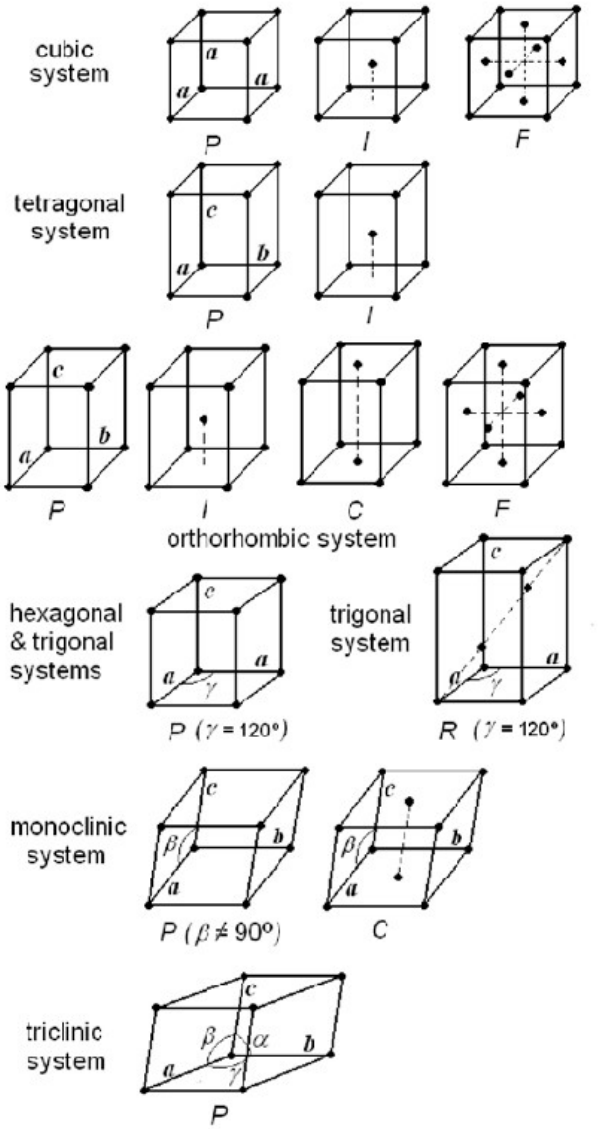

Figure 1-2-The 14 Bravais lattices

To completely describe a crystal structure the 14 Bravais lattices are not sufficient. The molecules inside the crystal lattice are usually linked by symmetry. There are two types of symmetry to be distinguished: (i) The macroscopic symmetries expressed by rotations, reflections and rotary-reflections which define the crystal shape and (ii) the microscopic symmetries, applied to the molecules, are associations of translations and either rotations or reflections giving respectively screw axes or glide planes.

The combination of the macroscopic symmetries and the Bravais lattices gives 32 points groups. The addition of microscopic symmetry leads to 230 possible spatial arrangement for a crystal, called space groups (SG).

1.2.2 **Classification of space groups**

According to the nature of the symmetry operations contained in its space group, the crystal exhibits different properties.

1.2.2.1 Centrosymmetry And Non-centrosymmetry

Centrosymmetry is related to the presence of an inversion center (or center of symmetry), noted i, in the set of symmetry operations contained in the SG of the structure. A SG containing i is a centrosymmetric SG. i is a symmetry operation by which the initial coordinate (x,y,z) of a point becomes (-x,-y,-z). When applied to a chiral object, application of i changes the handedness of the object (Figure 1-3). Thus, considering chiral molecules, centrosymmetric SG are incompatible with pure chiral molecules (only one enantiomer) since i would generate the counter enantiomer. Centrosymmetric SG are however common for racemic crystals. (See §1.2.4 for the chirality concepts)

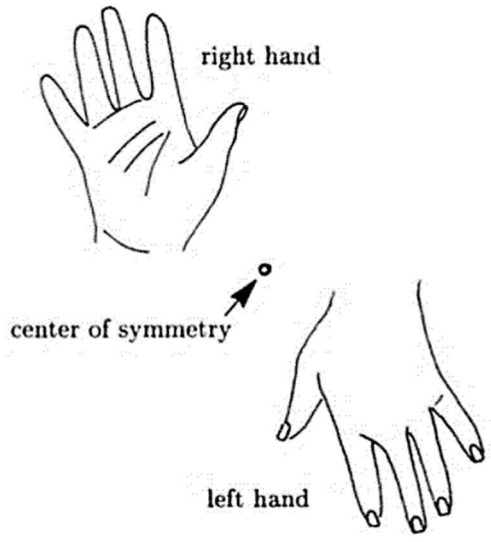

Figure 1-3-Example of an inversion center on hand adapted from[1]

Conversely, the absence of i qualifies the SG as non-centrosymmetric. Non centrosymmetric crystals can be recognised by the second harmonic generation (SHG) phenomenon[2]. Indeed, when exposed to a laser light, non-centrosymmetric crystals will respond by doubling the initial frequency which result in half the initial wavelength. Typically, when exposed to a 1064 nm laser light, a non-centrosymmetric crystal will re-emit a green radiation at 532 nm. There are however exceptions to this phenomenon when Kleinman symmetry is applicable: in point groups 422, 622 and 432 no SHG signal is generated even though they are non-centrosymmetric.[3]

1.2.2.2 Chiral space group

Chiral SG are compatible with crystals structures containing only one enantiomer. Thus, chiral SG are inevitably non-centrosymmetric, but the opposite is not true since a non-centrosymmetric SG can contain achiral molecules.

There are 22 chiral SG corresponding to 11 enantiomorphic pairs SG. Pairs of enantiomorphic space groups are mirror image related (for example $P6_1$ to $P6_5$ or $P4_1$ and $P4_3$) and said to be enantiomorphous: If one enantiomer crystallizes via $P4_1$, then the counter enantiomers crystallizes in $P4_3$. Chiral molecules can crystallise either in a chiral or in an achiral SG provided it contains only operations of the first kind (i.e., proper rotation, translation, screw axis). They are called the Sohncke space groups[4]. A comprehensive classification of the different type of SG is given in Figure 1-4.

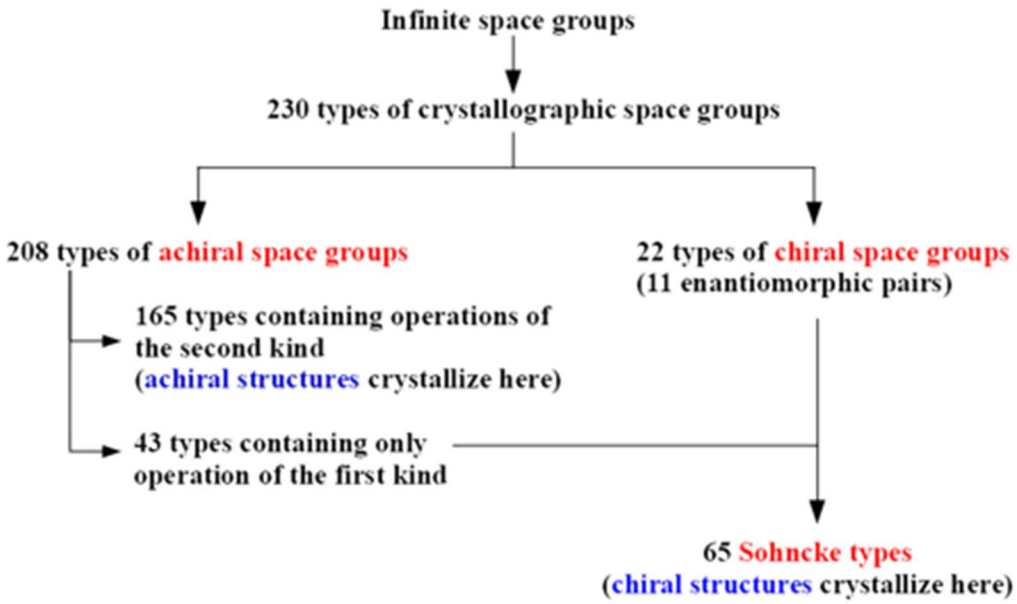

Figure 1-4-Classification of space groups in terms of chirality (adapted from [5])

1.2.3 **Polymorphism and Solvates**

Polymorphism is the ability of a compound to crystallize into different crystalline phase.[6] As represented in Figure 1-5, the two polymorphs differ from the arrangement of the building blocks in the 2D space. Polymorphism can also be due to different molecular conformations (torsion, rotation of chemical bond or group) which generate packing differences.

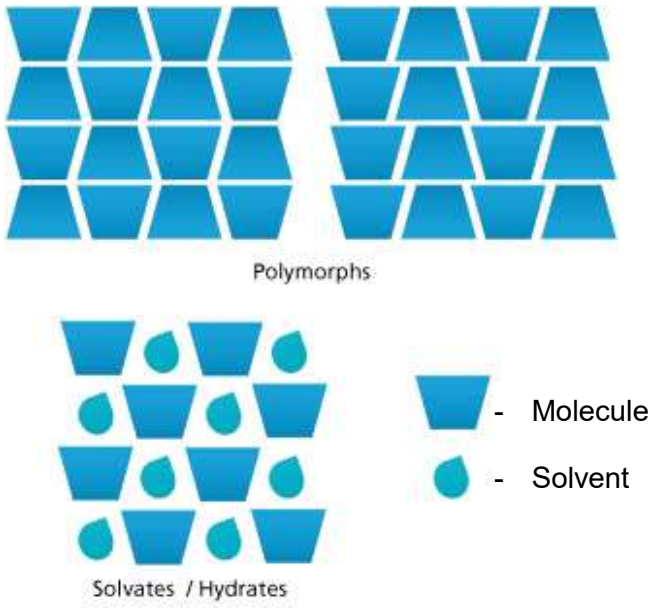

Figure 1-5-Representation of two polymorphs with packing differences, and illustration of solvate /hydrate form (adapted from reference[7]) .

The difference in packing between polymorphs gives specific physico-chemical properties to each polymorph such as solubilities, morphology, bioavailability or melting point. Those different polymorphs are thermodynamically different, and their stability varies with temperature and pressure.

The relation of stability between two polymorphic forms can be monotropic or enantiotropic. In a monotropic relation, one polymorph can only exist in a metastable state while the other is thermodynamically stable at all temperature (Figure 1-6,b) whereas in an enantiotropic relation, each polymorph has its stability range and determined temperature of transition (Figure 1-6,a). In 1979, Burger and Ramberger[8] published rules to easily distinguish monotropic from enantiotropic systems. One rule is the heat of fusion rule which say: “if the higher melting form (T_f) has the lower heat of fusion (ΔH_f) the two forms are usually enantiotropic, otherwise they are monotropic”. When translated into an equation the rule gives for an enantiotropic system the following (Equation 1-1)

$$T_f, B > T_f, A \Rightarrow \Delta H_f, B < \Delta H_f, A \qquad \textit{Equation 1-1}$$

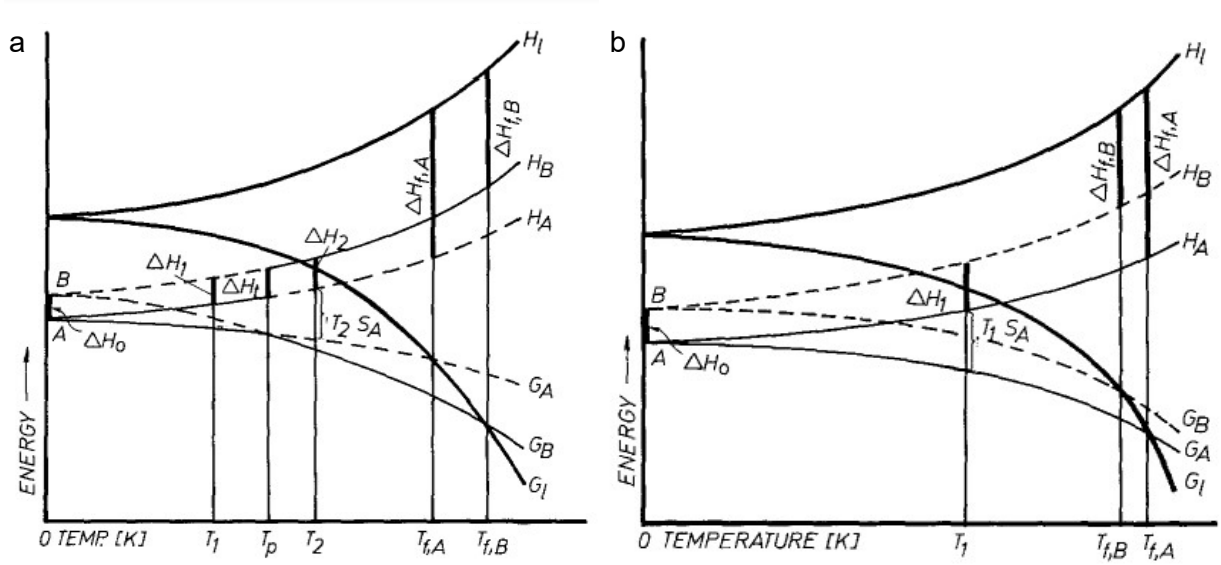

Figure 1-6-Energy in function of temperature for two polymorphs A and B in the case of enantiotropic relation (a) or monotropic relation (b).

When solvent molecules such as water are trapped in the crystalline structure of a compound, the crystal is called a solvate or a hydrate in case of water molecules (Figure 1-5). Solvates are sometimes referred to as pseudo-polymorphs, as they cannot be classified as polymorphic forms since the chemical composition of the crystal differs from the non-solvated form. Once again, the properties of the solvate will differ from the initial crystal.

1.2.4 **Chirality and Supramolecular chirality**

1.2.4.1 History

The discovery of Chirality goes back to 1801, well before the use of the word “chirality”, when René-Just Haüy discovered two forms of quartz crystal that mirrored each other[9]. Then, in 1815, Jean-Baptiste Biot observed the deviation of the plane of polarized light by several compounds such as quartz or sugar. Moreover, he observed that only crystalline quartz was able to deviate the light while only solutions of sugar could do so. As a result, he concluded that the phenomenon had a different origin: in quartz, it is the crystal structure itself that is responsible for this phenomenon, whereas in sugar, it is due to the individual constituents[10]. In 1820, Herschel linked the theory of Haüy and Biot and said that the crystalline form of quartz and the optical activity are related[11].

In 1848, Pasteur[12] found that a solution of “racemic” tartaric acid (called racemic acid) had no effect on the plane of polarized light since it is composed of crystals that are mirror images. After manual separation of the two kind of crystals, he found that both left and right crystal rotate the plane of polarized light but in opposite direction. An equal mixture of the two cancelled the effect.

Finally, it is in 1884 that Lord Kelvin[13] introduced the word “chiral” with the following definition : “*I call any geometrical figure, or group of points, 'chiral', and say that it has chirality if its image in a plane mirror, ideally realized, cannot be brought to coincide with itself.”* and the term enantiomorph was introduced in 1894 by Pierre Curie[14].

To summarize, chirality refers to a molecule or a system which is not superimposable to its mirror image. Chiral systems have the same properties but are recognized through their optical activity (i.e., ability to rotate the plane of polarized light), morphologies or behaviour in chiral environment. There are three kind of chirality[4]: (i) molecular chirality, (ii) chirality from the structural arrangement, and (iii) chirality of the space groups (described in § 1.2.2.2).

1.2.4.2 Molecular Chirality

Molecular chirality is due to different conformations or configurations of the molecules. The first kind (and most known) is the point chirality, where the presence of at least one stereogenic center, such as an asymmetric carbon or heteroatoms (Phosphorus, Nitrogen, Sulfur) induces chirality (Figure 1-7a). The molecules are called enantiomers. In the case of n stereogenic center, a number of 2^n molecules are related[15,16], the ones which are not superimposable and not mirror image are diastereomers (Figure 1-7b).

Three kind of blocked configurations (i.e., restricted rotation around a bond) lead to chirality : axial chirality (Figure 1-7,c), planar chirality (Figure 1-7,d) or helical chirality (Figure 1-7,e). They are called atropisomers[17,18], and can easily racemize (i.e., convert to the other isomer) under heat or in solution.

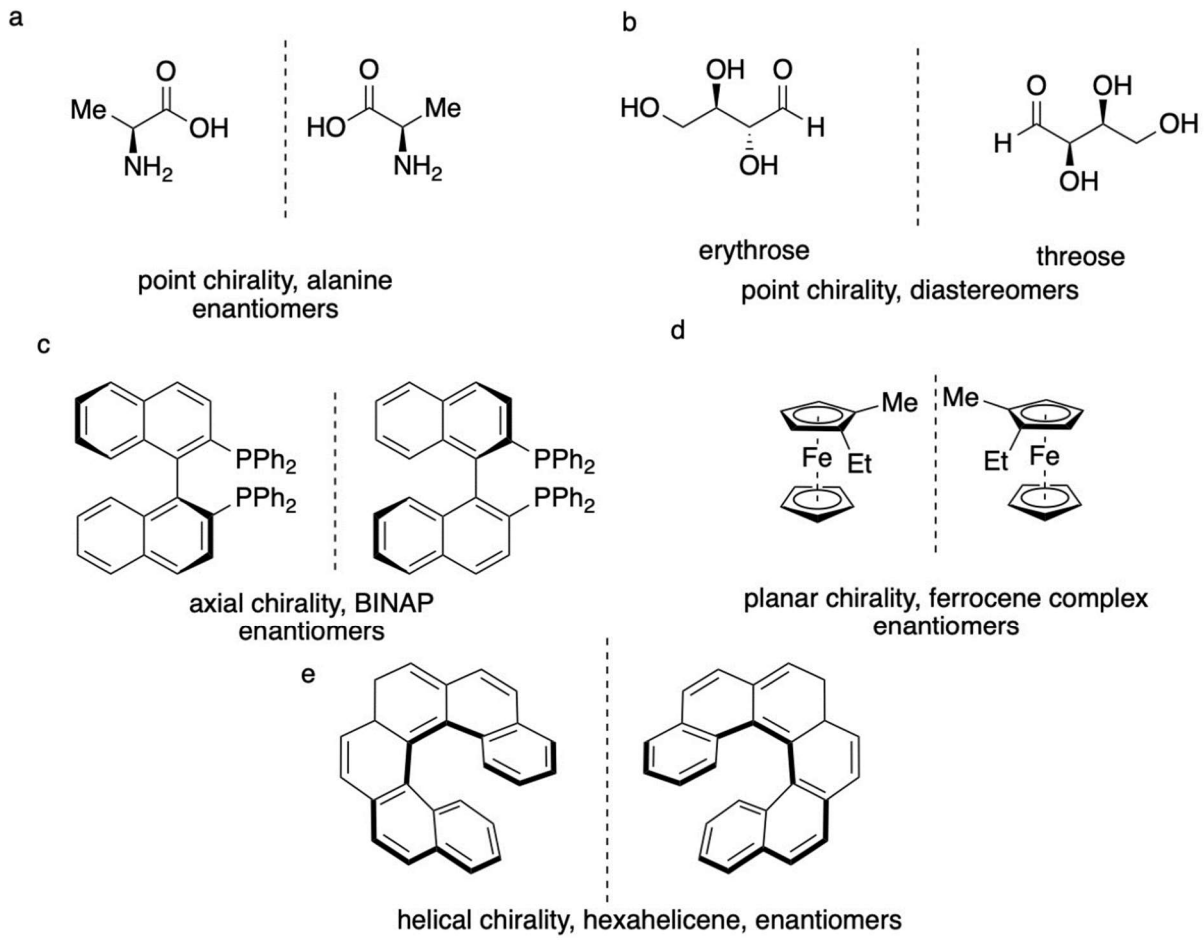

Figure 1-7-Different kind of molecular chirality. a) point chirality b) point chirality with 2 stereogenic center c) axial chirality (BINAP:2,2'-bis(diphenylphosphanyl)-1,1'-binaphthalene) d) planar chirality e) helical chirality

1.2.4.3 Chirality from structural arrangement

In 1898, Kipping and Pope described two kind of enantiomorphism one related to the molecules and the other to their arrangement[19]. The latter is the one of interest in this paragraph. It will be referred as Supramolecular chirality[20] or Chiral crystallization[21]. Achiral molecules (without optical activity in liquid or amorphous state) crystallize in enantiomorphous solid (Chiral SG) and may exhibit optical activity.

The chirality arises from the helical arrangement of the molecules in the crystal structure due to the presence of a screw axis. Several organic and inorganic achiral compounds have shown the ability to crystallize in chiral SG[22]. Three examples of supramolecular chirality will be described (i) Quartz, (ii) Sodium Chlorate, (iii) Ethylenediamine Sulfate.

1.2.4.3.1 The case of quartz

Quartz is a well-known example of supramolecular chirality since the observations of Haüy (§1.2.4.1). Quartz are made of silicates groups which are achiral. However, once the silicate groups are arranged in the crystal structure around the screw axis, according to the direction of rotation, clockwise or anticlockwise, the crystal acquires chiral properties. As seen in Figure 1-8, α-Quartz possesses two enantiomorphs which crystallizes in either in the $P3_221$ or $P3_121$ SG. The crystal handedness can be recognised by examining the crystal habit or the ability to deviate polarized light. The same phenomenon occurs with β-Quartz (polymorph at high temperature), which crystallize in SG $P6_421$ or $P6_221$[23].

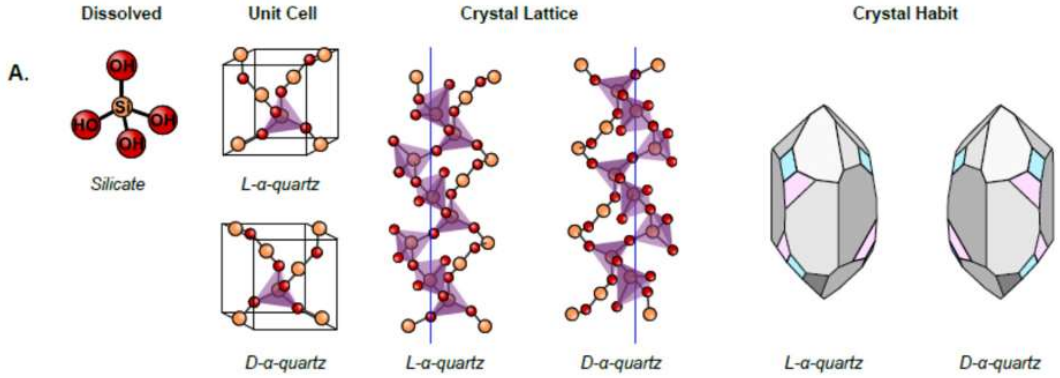

Figure 1-8-Quartz supramolecular chirality adapted from [24]

1.2.4.3.2 The case of sodium chlorate

Another example is Sodium chlorate ($NaClO_3$) or bromate ($NaBrO_3$). Sodium chlorate is composed of an association of achiral anion ClO_3^- and cation Na^+ and crystallizes in two enantiomorphic forms that both belong to the same SG $P2_13$ [25,26]. Figure 1-9 shows how the 2_1 screw axis confers chiral properties. Crystals are easily differentiated by polarized light microscopy since they interact differently with the plane of polarized light and exhibit different colours as seen in Figure 1-10.

Sodium Chlorate has been used as a model compound to investigate the mechanisms of deracemization: starting from an aqueous suspension of racemic crystals, a specific type of ripening, called Viedma ripening, occurs and the suspensions converts to a pure enantiomorph[27,28]. Another process of deracemization of $NaClO_3$ that have shown good results is Temperature Cycling Induced Deracemization (TCID)[29].

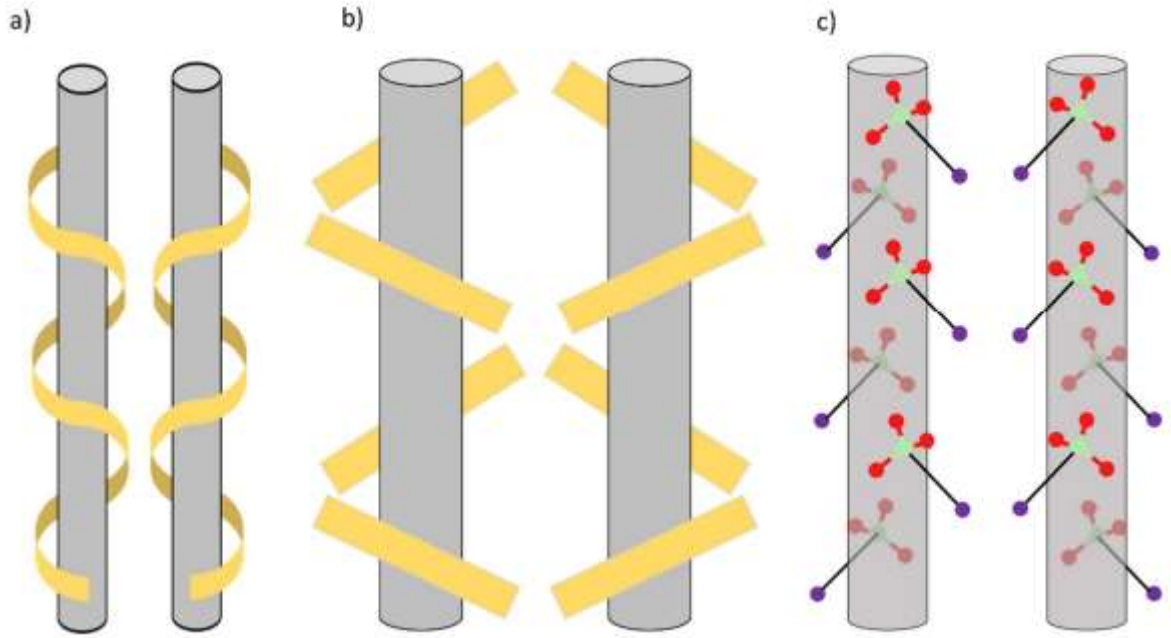

Figure 1-9-Representation of the 2_1 screw axis in a) helix b) bars and c) sodium chlorate structure

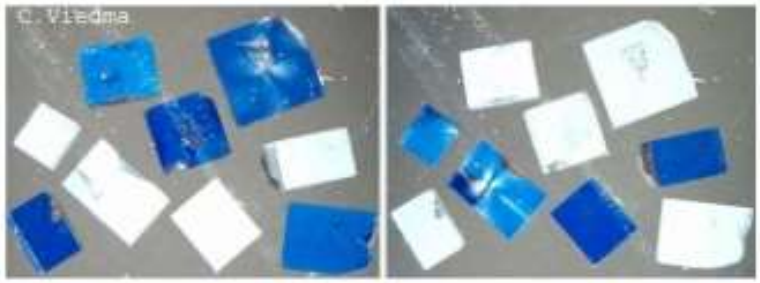

Figure 1-10-$NaClO_3$ crystal under polarized light microscopy, (adapted from Viedma [27]). On the left d-$NaClO_3$ are white and l-$NaClO_3$ appear blue when polariser is rotated clockwise. On the right, the colours are inversed when polarizer is rotated anti-clockwise.

1.2.4.3.3 Ethylene diamine sulfate

Ethylenediamine sulfate (EDS) is a salt made of an ethylenediammonium cation and a sulfate anion whose crystal structure forms a helical arrangement (Figure 1-11). EDS crystallizes in the chiral SG $P4_12_12$ (or $P4_32_12$ for the enantiomorph)[30,31]. As for $NaClO_3$ crystals, EDS enantiomorphs are recognised using a polarized microscope. when polarizer is rotated anti-clockwise with respect to the analyser, l-crystals appear blue and d-crystal appear light-brown and vice-versa if the polarizer is rotated clockwise.(Figure 1-12)

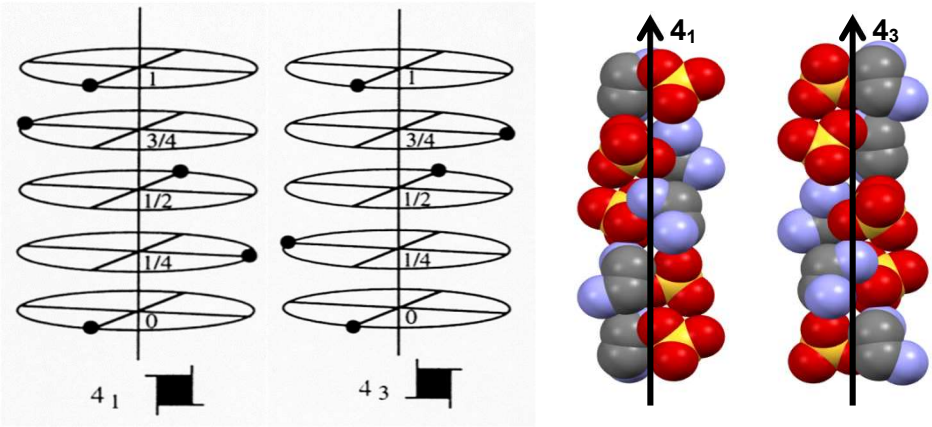

Figure 1-11-Representation of the helical axes 4_1 and 4_3, schematically (on the left) and as seen in the EDS structure (on the right). H atoms have been omitted for clarity.

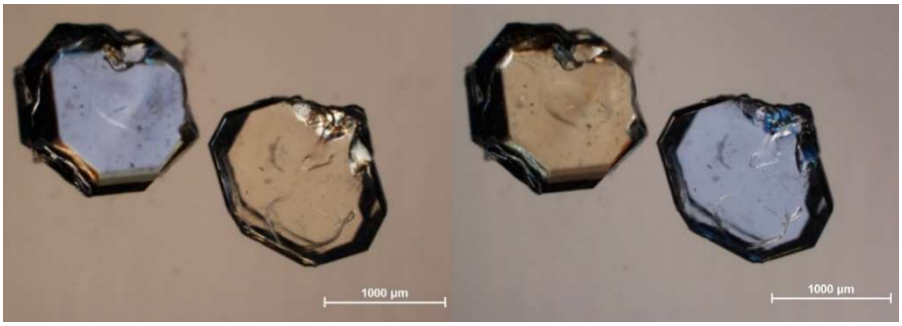

Figure 1-12-EDS crystals observed with a polarized light microscope. The picture shows the colour change of d-crystal (on the left) and l-crystal (on the right) when polarizer is rotated anti-clockwise with respect to the analyser.

1.3 CRYSTALLIZATION

Crystallization is a peculiar case of solidification: the change of state from a less ordered system to an ordered solid system. The solid obtained is a crystal and must be differentiated from an amorphous solid: A crystal has an ordered structure made of periodically arranged atoms, ions or molecules. Crystallization can occur from a gas phase, a melt, an amorphous solid or a solution. This work is only concerned with crystallization from solutions.

Different methods exist to achieve crystallization in solutions, such as cooling, evaporation, anti-solvent addition, etc. Yet, whatever the crystallization process, the phenomenon is always conceptually divided into four steps: (i) the establishment of the driving force, (ii) nucleation followed by (iii) the growth of the crystals and finally (iv) Ostwald ripening. The steps (i) and (ii) are of central interest for this study and will be described in detail hereafter.

1.3.1 **Solubility and supersaturation**

In order to understand the process of crystallization from solution, we need to define the solution itself, the solubility and the supersaturated state.

A solution is a homogeneous mixture composed at a minimum of one solvent and one solute. The solute is the compound of interest which is dissolved in the solvent. The concentration of the compound is limited by its solubility in the solvent.

The solubility is defined as the maximum quantity of compound that can be dissolved in a given quantity of solvent. The solubility value of the compound depends on the solvent, temperature and pressure. This quantity can be expressed either in mole or mass. The solubility can be expressed using different unit. In this work, we chose to express solubility values in weight percentage (%wt) which is equal to the mass of the compound dissolved over the total mass of the solution.

It is customary to represent the evolution of S as a function of Temperature, which is referred to as the “solubility curve” (Figure 1-13a). All along the solubility curve the solution is said saturated: no more solute can be added nor removed without departing from that saturation situation. Below the solubility curve, the domain is called undersaturated.

Each compound/solvent pair has a specific S=f(T) behaviour. In most cases, S is an increasing function of T (normal solubility) but in some cases the solubility will decrease with temperature. This behaviour is called indirect or retrograde solubility (Figure 1-13b).

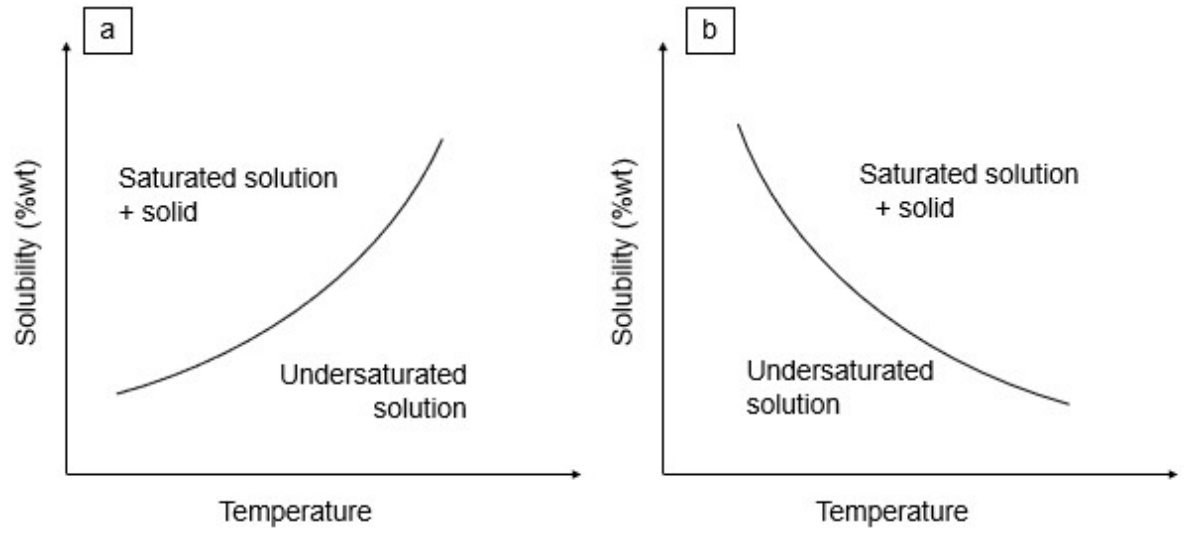

Figure 1-13-Schematic representation of solubility curves with (a) normal and (b) retrograde solubility.

The supersaturation is the fact that the solution has a higher concentration than permitted by the solubility.

There are three expressions to quantify supersaturation (Equation 1-2, 1-3 and 1-4). In this work the degree of supersaturation β has been used: it is the ratio between the concentration of the solution (C) over the solubility of the compound in the solvent (S) at a given temperature (Equation 1-2). The other expressions of supersaturation are the absolute supersaturation (ΔC) and the relative supersaturation (σ).

$$\beta = C/S \qquad \textit{Equation 1-2}$$

$$\Delta C = C - S \qquad \textit{Equation 1-3}$$

$$\sigma = \frac{C-S}{S} = \beta - 1 \qquad \textit{Equation 1-4}$$

A supersaturated solution is in a metastable state that can be achieved either by cooling an undersaturated solution or by increasing its concentration by evaporation above the solubility curve in Figure 1-14. Two situations have to be distinguished which are conceptually separated by the metastable zone limit (dashed line) in Figure 1-14. When the solution is brought above the limit (referred to as the labile zone), supersaturation is high enough to make nucleation happens spontaneously. The solution return to the thermodynamic equilibrium by crystallization: solid crystals are in equilibrium with a saturated solution. At lower supersaturation below the metastable limit, the solution remains in a metastable state where nucleation is delayed. This is the induction time. The larger the metastable zone, the longer the induction times.

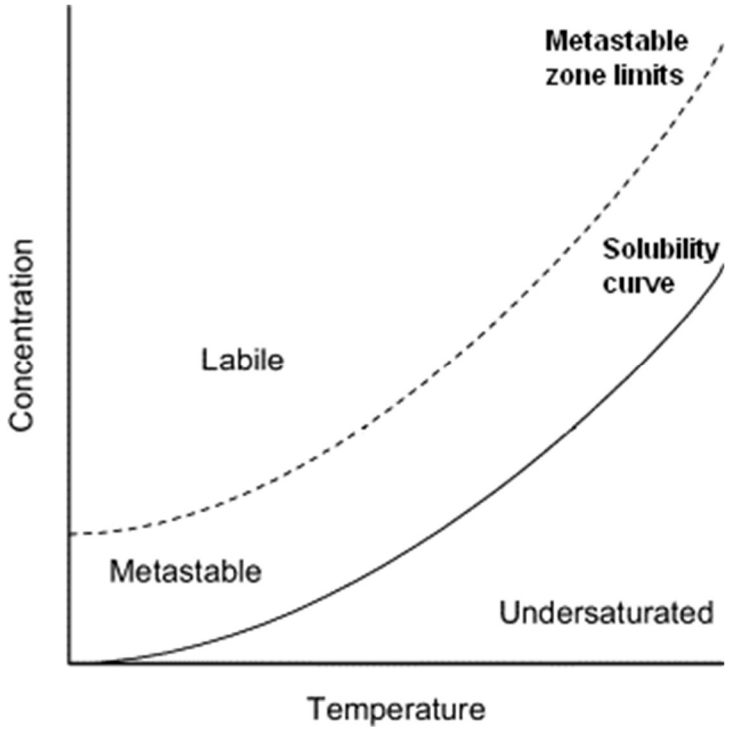

Figure 1-14-Illustration showing the three zone of saturation. Undersaturated, saturated and supersaturated

1.3.2 **The metastable zone limits**

The metastable zone limits were introduced by Wilhelm Ostwald[32] and named after him the Ostwald limits. The domain between the solubility curve and the Ostwald limits is called the metastable zone width (MSZW). This limit is different for each compound and can be impacted by the cooling rate, stirring rate, volume of solution[33], supersaturation or impurities[34].

The MSZW is expressed as the difference between two temperatures: cloud point and clear point. If ones apply the heating-cooling cycles presented in Figure 1-15 to a suspension, a clear solution will be obtained upon heating up to the clear point which corresponds to the solubility point. Upon slow cooling down from the clear point, the solution first become supersaturated and the temperature at which the first crystals are observed corresponds to the cloud point (which correspond to the Ostwald limit). Detection of the cloud point is not so easy and different techniques have been proposed[35–37]. In Figure 1-15, turbidimetry is used to detect the nucleation. However, the value is an approximation since the detection of the first nuclei is not possible due to its size, only grown crystals to a certain size can be detected.

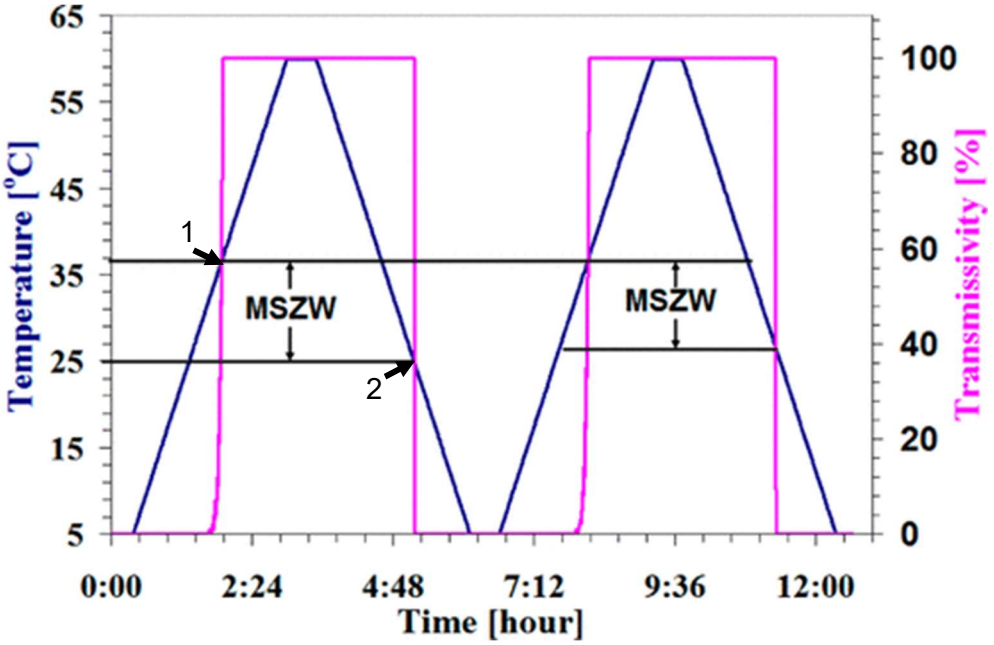

Figure 1-15-Example of MSZW measurements (from reference [38]). (1: clear point 2: cloud point)

1.3.3 **Nucleation**

Nucleation is a physico-chemical phenomenon by which a new phase emerges from another. In the framework of this thesis, nucleation refers to the production of crystal embryos from supersaturated solutions. The nucleation of gas from solution will be referred as cavitation.

Indeed, once supersaturation is established in the medium, the appearance of such tiny associations is likely to happen. Two kinds of nucleation will be considered: primary and secondary nucleation (Figure 1-16). Furthermore, the two theories explaining the nucleation mechanism will be discussed: classical nucleation theory (CNT) and two-step nucleation (TSN).

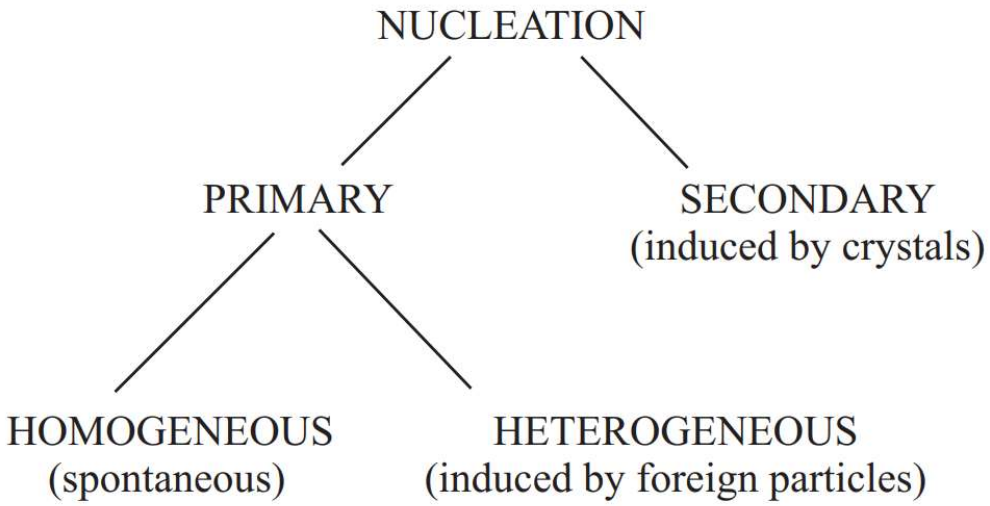

Figure 1-16-The different types of nucleation according to the classical nucleation theory (From Mullin[39])

1.3.3.1 Classical Nucleation Theory (CNT)

The Classical Nucleation Theory is the most used model to study nucleation. It was initiated by the work of Volmer and Weber in 1926[40] who used the work of Gibbs on thermodynamics to describe the nucleation as a one-step mechanism.

In this theory, the compound in solution gather to form clusters or aggregates exhibiting the same structure as the final crystal. Figure 1-17 shows the evolution of the solute to form a crystal structure and the corresponding evolution of Gibbs free energy in function of reaction coordinate (size of the cluster).

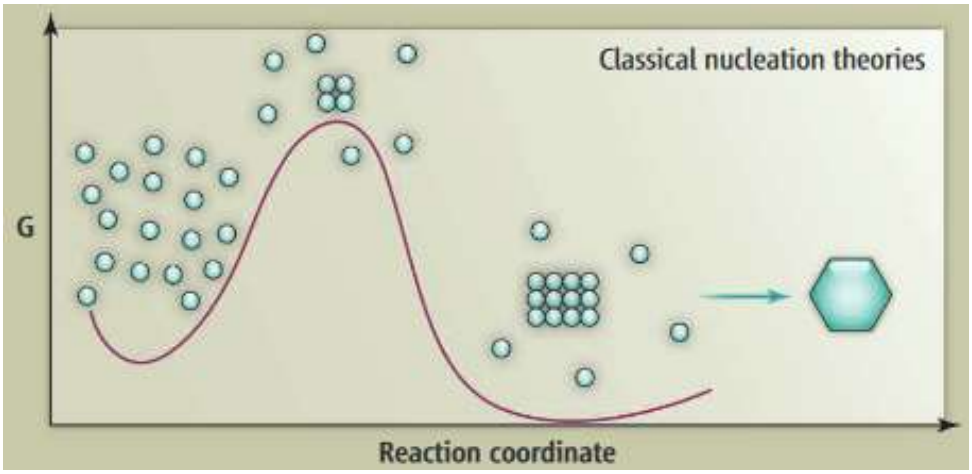

Figure 1-17-Schematic representation of the nucleation mechanisms according to the classical nucleation theory (from Myerson[41])

Then, two kinds of primary nucleation can be described according to the conditions of nucleation using CNT.

1.3.3.1.1 Homogeneous nucleation

Homogeneous primary nucleation describes the spontaneous nucleation of the compound in the bulk solution.

To form an aggregate (in the CNT, the nucleus is assimilated to a sphere of radius r), the system requires the creation of an interface between the daughter phase (i.e., the solid phase) and the mother phase (i.e., the liquid solution). Such interface destabilizes the system by an amount of $+4\pi r^2\gamma$, but it is counterbalanced by the creation of a bulk solid phase that stabilizes the system by a decrease of $-\frac{4}{3}\pi r^3$ [39]. The nuclei energy is represented by ΔG in Equation 1-5.

$$\Delta G = -\frac{4}{3}\pi r^3 \Delta Gv + 4\pi r^2\gamma \qquad \textit{Equation 1-5}$$

With ΔGv: the free energy change of the transformation per unit volume and γ: interfacial energy

The evolution of the free enthalpy of nucleation ΔG in function of the radius r is presented in Figure 1-18 alongside the energy of bulk formation and the interfacial energy. The Figure 1-18 shows that nucleation requires that the aggregates must be superior to a critical radius (r*) and overcome a barrier of energy ΔG*. This show the existence of a critical nuclei in the CNT. The system always tries to minimise its energy. When the nucleus size is close to r* it can either dissolve (smaller than r*) or grow to macroscopic crystal (larger than r*). It is worth noting that ΔG* is inversely proportional to β, that is to say that the higher β, the lower the barrier to overcome for nucleation, and thus lower the induction time.

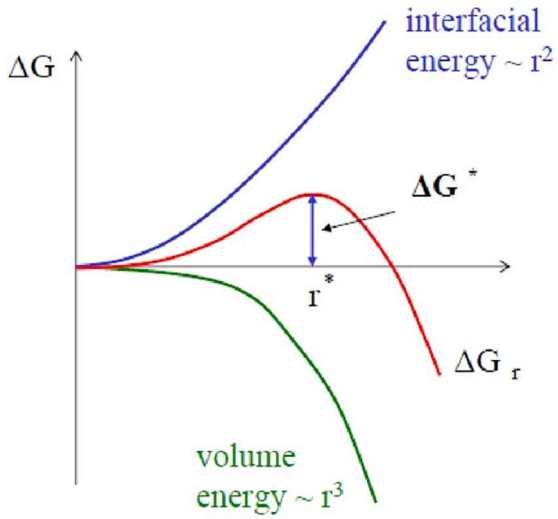

Figure 1-18-Evolution of the free enthalpy of nucleation (in red), and the two contributions: interfacial energy (blue) and the volume energy (green).

1.3.3.1.2 Heterogeneous nucleation

Heterogeneous nucleation differs from homogeneous nucleation by the fact that nuclei form unto foreign surfaces such as impurities, dusts, crystallizer walls, stirrer, etc. Nucleation unto such surfaces imply a lower interfacial energy since a smaller portion of the aggregate is in contact with the solution. The aggregate is no more spherical but form a contact angle θ with the foreign surface as shown in Figure 1-19. As a result, the energy barrier is lowered whereas the critical radius is unchanged. The energy of nuclei ΔG is calculated from homogeneous primary nucleation (Equation 1-5) with correction term Φ (function of the contact angle)(Equation 1-6 & 1-7[39]).

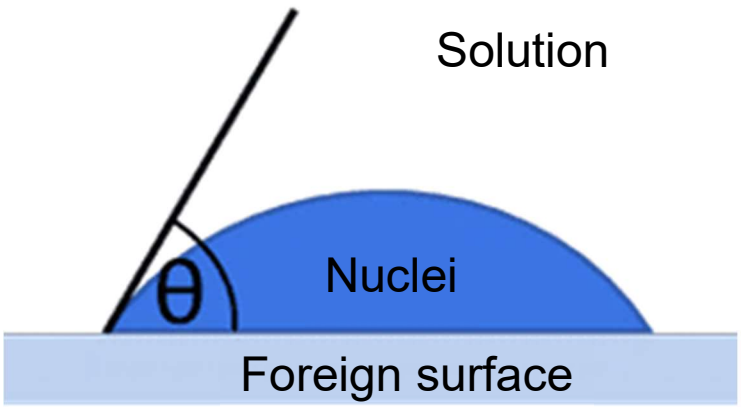

Figure 1-19-Interfacial energy between three phases (the solution, the foreign surface and the nuclei)

$$\Delta G_{het} = \Delta G_{homo} * \phi \qquad \textit{Equation 1-6}$$

$$\phi = \frac{(2+cos\theta)(1-cos\theta)^2}{4} \qquad \textit{Equation 1-7}$$

Therefore, the occurrence of heterogeneous nucleation is thermodynamically favoured compared to homogeneous nucleation provided foreign surfaces are present. The Ostwald zone for heterogeneous nucleation is narrower than for homogeneous nucleation[42]. Thus, voluntary addition of foreign particles has been used to reduce the induction time and control the nucleation. When the foreign particles have a structure similar to the one of the growing crystal the method is called templating, and help control the chirality[43], polymorphism[44,45] or morphology[46]. A proof of the initial presence of impurities in solution is the filtration that decreases the probability of nucleation and increases the MSZW[38,47]. Similarly, the addition of solid impurities decreases the MSZW[48].

1.3.3.2 Primary nucleation vs secondary

In supersaturated solutions, atoms (or molecules, or ions) are in movement, aggregates are forming, growing and dissolving. This causes the nucleation event to be stochastic. Eventually, few aggregates will grow to a sufficient size. As described above, homogeneous and heterogeneous nucleation are primary nucleation.

Secondary nucleation occurs from the supersaturated solution as a consequence of the presence of crystalline matter already existing in the solution. Such material can either originate from primary nucleation events or from seeding, which is the intentional addition of crystals. Two kind of secondary nucleation mechanisms can take place in the supersaturated solution: (i) the crystals already present in solution can act as heterogeneous surface to nucleate other nuclei. (ii) the agitation in the solution can induce collisions between crystals, crystals/stirrer or crystal/ crystallizer walls, causing small pieces of crystal to break off and creating tiny seed crystals.

The knowledge of the Ostwald limits allows to determine the best condition to seed the solution. The solution must be seeded in the metastable zone near the solubility curve[49]. Therefore, the seed will not dissolve. Under stagnant conditions, growth is promoted, which allow the formation of single-crystal whereas agitation will promote secondary nucleation.

1.3.3.3 Criticism of CNT

CNT makes some assumptions in order to simplify the model, but it also limits its applications[50]. The major assumptions are (i) the cluster is assimilated to a sphere (droplet model) with the same structure of the final crystal, (ii) the interfacial energy is supposed to be the same regardless of the size of the cluster and is independent of temperature (capillarity approximation[51]), (iii) growth and dissolution are viewed as addition or removal of one particle at a time. In particular, CNT has been criticised because of the difference observed between theory and experience[52]. Indeed, Yau and Vekilov[53] have shown, by AFM analysis, that cluster are composed of 50 apoferritin molecules maximum, and that the molecular arrangement gives to nuclei not a spherical shape but a planar one. Moreover, they also showed that surface tension is ill-defined for cluster inferior to 100 molecules. The surface tension value should not be considered as a constant but as a variable value temperature dependent [54]. Furthermore, the growth of cluster is made by addition of growth unit (i.e., pre-assemblies such as dimers)[55] or merge of clusters[56]. This led to reconsider the CNT and develop modern and more complex theories of nucleation such as the two-step nucleation model.

1.3.4 **Two step nucleation (TSN)**

Also called non classical nucleation or *PNC for prenucleation cluster*, the two-step nucleation theory (TSN) was developed first to describe protein nucleation. Through computational simulations, it has been shown that in the presence of a liquid-liquid phase separation, the solution close to the critical point exhibit large density fluctuations which led to the formation of dense liquid-like cluster (1st step) in which crystal nucleates (2nd step)[57]. Several simulations have shown the existence of either liquid like cluster or micelle[58], colloidal droplet[59], dense liquid droplet[60] and conclude that this sort of molecular aggregation is the first step toward crystal nucleation in solution. Compared to CNT, there is a barrier to overcome for each step (formation of dense clusters and crystal nucleation) and the barrier of energy is decreased for nucleation with reference to CNT due to a reduction of the interfacial energy.

Vekilov and co-workers[61] have proposed a model for the two-step nucleation theory, illustrated in Figure 1-20, in which the second step (i.e., the nucleation of the ordered structure in the dense liquid) is the rate determining step. TSN could be a generic phenomenon[62], but the

metastable phase of cluster can have a too short life-time that hindered its observation.

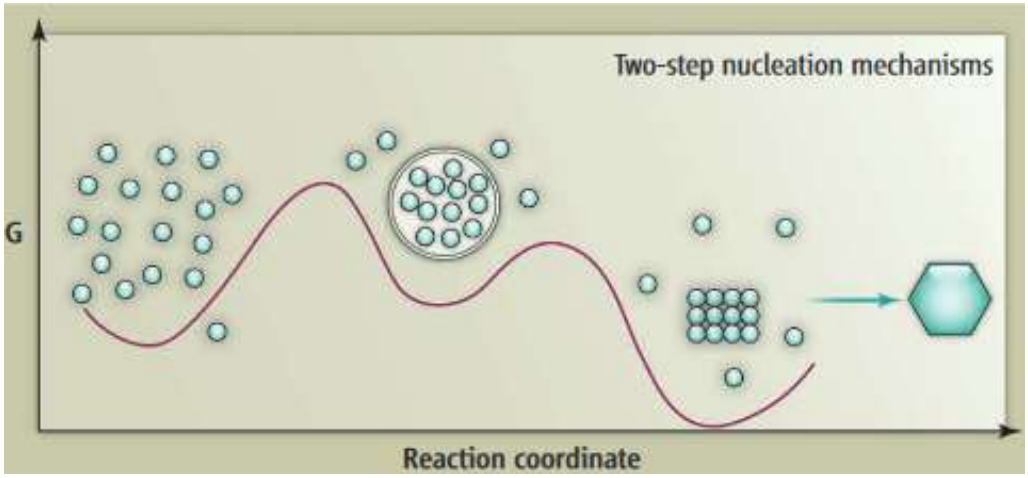

Figure 1-20-Schematic representation of the nucleation mechanism according to the two-step nucleation theory (from Myerson[41])

Experimental study has been conducted to prove the existence of such cluster. The use of Dynamic light scattering revealed the aggregation of protein in clusters[63]. Scanning electron microscopy, cryo-transmission electron microscopy[64] and atomic force microscopy[53] also highlighted the presence of such cluster.

Regarding the phenomenon of liquid-liquid phase separation as described in protein nucleation [57,65], Hans *et al.*[66] stated that in the presence of the phenomenon, nucleation proceeds by TSN whereas if there is no liquid-liquid phase separation the nucleation should occurs by one step nucleation process as in CNT. However, Davey *et al.* [67] differentiate the TSN from liquid-liquid phase separation and write: “the drops of concentrated liquid phase are not pre-nuclei, they are another bulk phase”.

Scientific community still works to understand the nucleation process, CNT is still under consideration for its simplicity of analysis. In the case of non-classical theory, the researchers do not agree about the intermediate phase. Figure 1-21 presents a review of the different non-classical nucleation theories suggested by different authors[68]. Figure 1-21,b is the TSN model described above. Figure 1-21,c is the case where the nucleus is represented by only one atom or molecule, thus the process is a barrier-free nucleation. Figure 1-21,d represent the case where the nucleus adopts the same structure as the final crystals but have a shape that do not allow a minimisation of ΔG such as the sphere in CNT. Figure 1-21,e

considers a rough nucleus interface with a variation over time of the structure in relation to the size.

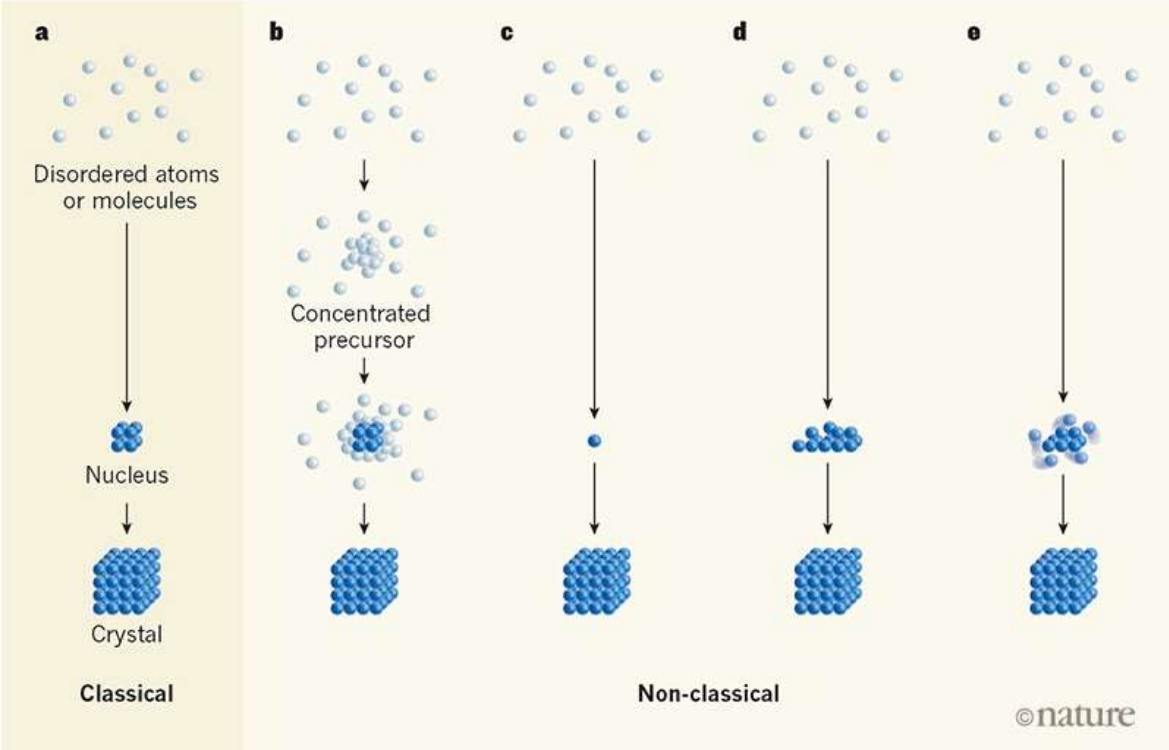

Figure 1-21-Classical Nucleation theory (a) and Non-classical nucleation theories: TSN (b), one atom as a nucleus (c), nuclei with the same final structure but a non-equilibrium shape (d) and nuclei with diffuse shape and size that vary with time (e). (adapted from Vekilov 2019[68])

1.3.5 **Kinetics of nucleation**

As discussed in §1.3.3.1.1, nucleation is an energy activated process: spontaneous crystallization of a supersaturated solution occurs if the system reaches the Ostwald limit (Figure 1-14). However, If the supersaturation ratio is insufficient (below the Ostwald limit) the supersaturated solution may remain in a metastable state and nucleation is only detected after an induction time that is inversely proportional to supersaturation. Induction times can be extremely long so that no nucleation is observed within the timeframe of months (or years) and it is necessary to seed such solution to promote crystallization. Obviously, the detection of newly formed nuclei is impossible due to their extremely small size, the nuclei is detected after growth to sufficient size according to the method of detection.

However due to the stochasticity of the nucleation process, the same set of experimental parameters performed at the scale of 50, 100 or more

experiments can lead to a distribution of induction times. For example, the induction time measurement of isonicotinamide in ethanol shows a variation ranging from 114s to 3h [38]. The same variability of induction time is found for other compounds in other solvents.[69–72] This implies that the collection of statistical data is required to thoroughly describe the nucleation behaviour.

Provided a sufficient number of identical experiments has been performed, the probability of nucleation as a function of time ($P_n(t)$) [69] can be measured. It is expressed as the number of experiments in which crystal are detected after a time t ($N_{cryst}(t)$) over the total number of experiments (N_{total}). (Equation 1-8). The probability of nucleation follows the Poisson distribution (Equation 1-9)[69]. Even if this model was designed for nucleation in agitated solutions while NPLIN occurs in stagnant conditions, it is believed that Poisson distribution can be applied as the influence of stirring or an external field is considered in the induction time (t). Figure 1-22 shows an example of a given set of probability of nucleation over time for potassium sulfate. The experimental data are represented by blue dot and the fit to Poisson distribution is represented by the solid line. It represents the likeliness to find crystals after a time t, for example, in Figure 1-22, the likeliness to find a crystal after 60 minutes is superior to 72%.

$$P_n(t) = \frac{N_{cryst}(t)}{N_{total}} \qquad \textit{Equation 1-8}$$

$$P_n(t) = 1 - e^{-JVt} \qquad \textit{Equation 1-9}$$

J: nucleation rate , V: volume of solution, t : induction time

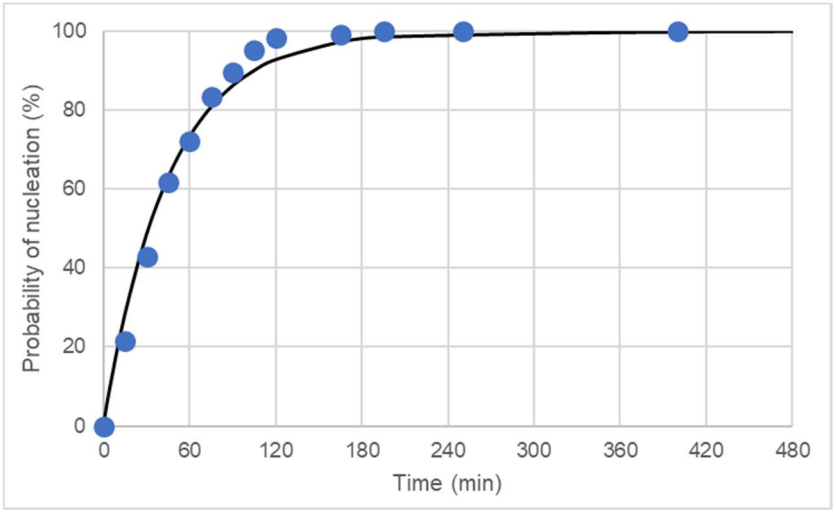

Figure 1-22-Experimental probability of nucleation for a given compound. (blue point). The solid line represents the fit of Equation 1-9. (J= 0.02202mL^{-1}min^{-1} or J=367m^{-3}s^{-1}).

Nucleation Rate (J) is defined as the number of nuclei appearing during a certain time, within a given volume of solution. The value is determined using the Poisson distribution to fit the experimental data and expressed in $m^{-3}s^{-1}$. The Nucleation rate can also be calculated from Equation 1-10, where A and B are kinetic and thermodynamic factors and β is the supersaturation.[69,73]

$$J_{homo} = A\beta e^{-\frac{B}{ln^2\beta}} \qquad \textit{Equation 1-10}$$

In the case of heterogeneous nucleation, the nucleation rate J can be calculated by Equation 1-11 where the factor C is the concentration of active centers presents in the solution due to heterogeneous particles[38].

$$J_{het} = CJ_{homo} \qquad \textit{Equation 1-11}$$

1.3.6 **Nucleation of gas – Cavitation**

Cavitation is the appearance of a gaseous phase in a liquid phase. The gaseous phase is called a cavity or a bubble and is composed of either dissolved gas or vapor or both. Bubble nucleation can be explained by different mechanisms based on classical nucleation or non-classical nucleation[74] in a similar way to nucleation of solid presented above.

Gas nucleation is commonly seen in sparkling drinks, where the liquid phase is in equilibrium with carbon dioxide gas. When opening a bottle, the pressure fails, and the solution becomes supersaturated in CO_2 with respect to the atmospheric pressure. This lead to spontaneous nucleation of gas[75]. Gas are also affected by temperature due to their retrograde solubility[76]. The increase in temperature will degas the solution. Knott *et al.* have shown that nucleation of CO_2 bubbles from supersaturated carbonated water can be induced by laser pulse[77]. Moreover, cavitation can be produced by ultrasound[78].

Vapor cavities are a result of a decrease of pressure below the vapor pressure, such depression can be found in fluid shear of a rotating blade. It can also result of a significant heating as in exposure to laser. Soare *et al.*[79] state that the absorbed laser pulse superheats the liquid which finally evaporates and produce vapor bubble.

Cavitation can promote crystals nucleation by generation of high pressure when the bubble collapse[80], by acting as heterogeneous surface[77], mechanical shock[81] or even scratching the wall of the vessels[39].

1.4 LASER AND LIGHT-MATTER INTERACTION

1.4.1 Introduction

LASER is an acronym for Light Amplification by Stimulated Emission of Radiation. A laser emits a coherent and monochromatic light of a defined wavelength, energy and direction. Since the invention of laser, a multitude of lasers have been developed always trying to change the wavelength, increase the power, reduce the pulse duration. Thus, lasers are now capable of generating pulses in the nanosecond, picosecond or femtosecond range, high energy and a large choice of wavelength from ultraviolet to infrared.

One of the most important elements of the laser is the gain medium or amplifying medium (see Figure 1-23), it dictates the properties of the beam such as the wavelength and power maximum. The gain medium is the source of the laser where photons are produced, those photons have the same properties due to the phenomenon of stimulated emission. The gain medium can be liquid (dye laser), gas (excimer laser, CO_2 laser) or solid (Nd-YAG).

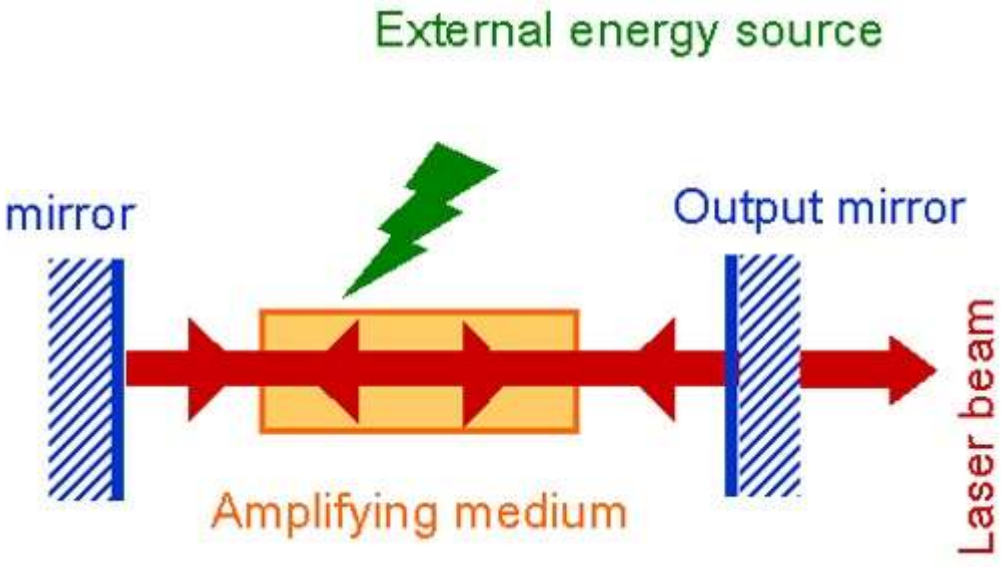

Figure 1-23-Formation of the laser beam (adapted from : laser fundamentals [82])

1.4.2 **Beam type: Continuous wave and pulsed**

Among the laser developed, two kinds of laser are emerging: continuous wave (CW) and pulsed laser. The continuous wave lasers are the first kind of laser invented. They produce a continuous wave light at a constant intensity. Whereas, pulsed lasers concentrate the intensity in a very short period of time (i.e., the pulse duration). Therefore, the shorter the pulse duration, the lower the pulse energy and mean power but the higher the intensity. The difference is shown in Figure 1-24, where power in function of time is represented for each laser.

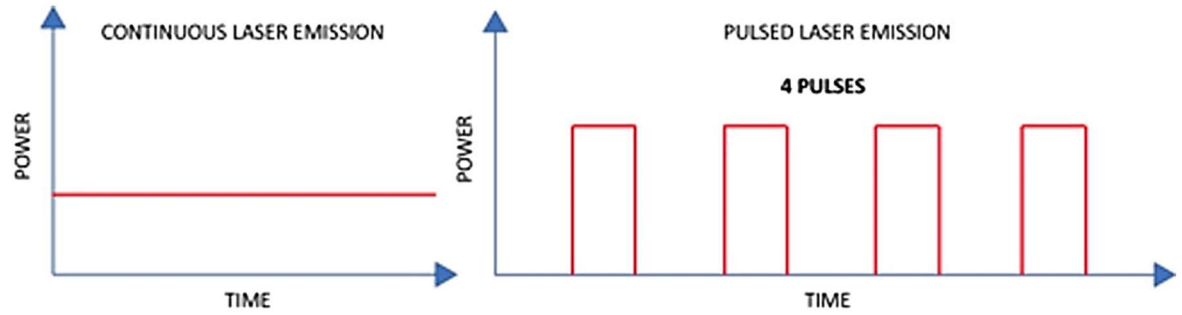

Figure 1-24-Difference between continuous and pulsed laser (adapted from [83])

There is different technology to produce pulses, one of them is the Q-switched. The Q-switched laser uses a Pokels cell (DKDP crystal) whose index of refraction is changed when variables voltage is applied. When high voltage is applied, the Q-switched is closed that is to say that the light undergoes a retardation and energy losses. Then, when no voltage is applied the Q-switched is opened (i.e., the light passes without loss) and the laser pulse is delivered.

1.4.3 **Laser beam characterisation**

A laser system produces a laser beam characterised by different physical parameters. Pulsed lasers are characterized via the pulse duration or pulse width (τ) and the repetition rate (f_{rep}) which is the frequency of the pulse (Figure 1-25). The power of the laser describes the amount of energy delivered over time, it is expressed in Watt (W) or in Joule per second ($J.s^{-1}$).

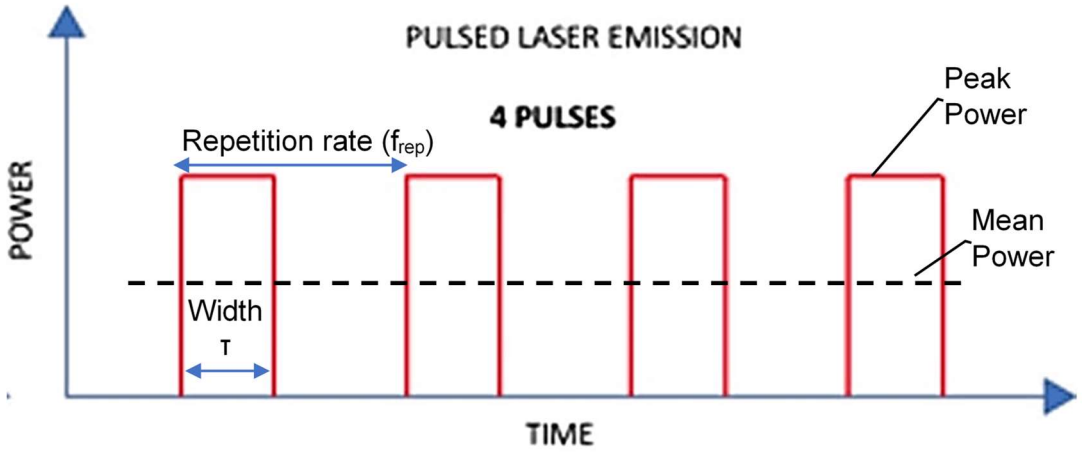

Figure 1-25-Schematic representation of the Laser pulses parameters

In the case of pulsed laser, it is important to differentiate the mean power and the peak power. The mean power of a pulsed laser is the power if the emission were continuous, i.e the energy of the pulse is spread uniformly across the period. The Peak Power is the maximum power emitted. Equation 1-12 allows to switch from peak power to mean power and inversely.

$$P_{peak} = \frac{P_{mean}}{f_{rep} * \tau} \Leftrightarrow P_{mean} = P_{peak} * f_{rep} * \tau \qquad \text{Equation 1-12}$$

A common used value for laser is its intensity expressed in W.cm^{-2}. It is sometimes called power density or pulse power. The intensity corresponds to the power applied by surface unit. The surface unit is the surface irradiated, related to the radius (r) of the laser beam. Pulsed laser can also be quantified by the energy per pulse. Energy is expressed in Joules (J) and measured for one pulse.

Knowing the characteristic of the laser system such as the repetition rate (f_{rep}), pulse duration (τ), diameter of the beam (or surface of the beam) calculation can be made to switch from measured energy (E_{pulse}) to power (P_{peak}) (Equation 1-13) or to intensity (I) (Equation 1-14).

$$P_{peak} = \frac{E_{pulse}}{\tau} \qquad \text{Equation 1-13}$$

$$I = \frac{P_{peak}}{\pi\, r^2} \qquad \text{Equation 1-14}$$

1.4.4 **Changing the wavelength**

The wavelength of the laser beam can be changed using the principle of second harmonic generation (SHG). The incident laser beam at frequency ω and wavelength λ goes through a non-linear crystal (non-centrosymmetric, see §1.2.2.1) and is converted into a laser beam of doubled frequency (2ω) and half wavelength (Figure 1-26). For example, the 1064nm laser beam will converts into a 532nm laser beam.

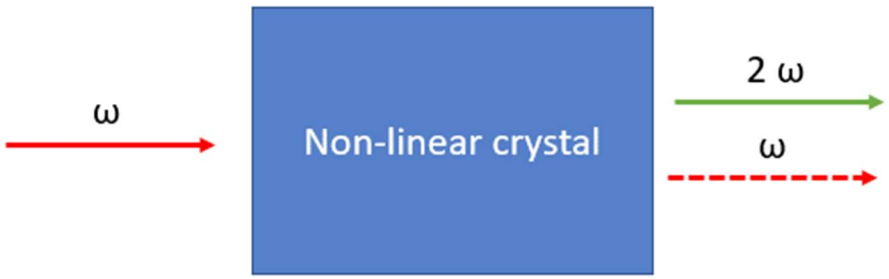

Figure 1-26-Illustration of the second harmonic generation

1.4.5 **Polarization**

The light produced by a laser can be described as electromagnetic waves (i.e., electric and magnetic field). Natural light is not polarized, the electric field oscillates in all directions in a plane perpendicular to the light propagation direction. The polarization is defined as the orientation of the electric field (Figure 1-27). Thus, if the electric field keeps the same direction during the propagation then the light is said linearly polarized. If the direction of the electric field describes a circle over time, then the light is said circularly polarized. According to the direction of rotation there are two types of circular polarization : left-handed or right handed.[84]

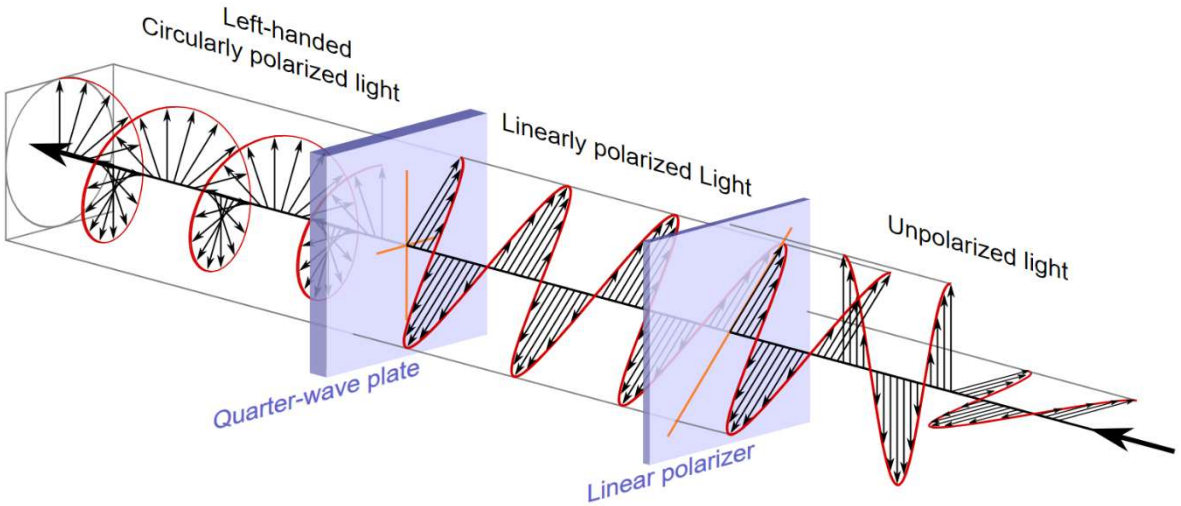

Figure 1-27-Description of polarized light

The polarization geometry of the laser light is often linear at the output [85]. In order to control the polarization, optical elements called waveplate are used. The half waveplate (λ/2) is used to change the direction of polarization of linearly polarized light. If the polarization of the light is aligned with the waveplate axis, there is no change of polarization, but if the polarization direction is 45° to the waveplate axis, then a left circular polarization becomes right circular and vice-versa and a linear polarized light stay linear but with a rotation of 90° of the plane. Similarly, when there is a 45° angle between the incident polarization and the axis, the quarter waveplate (λ/4) can convert linear to left or right circular polarization by rotating the waveplate 45° or -45° and vice versa.

1.4.6 **Interactions light-matter**

When a laser beam (or any light beam) encounters a surface, a particle or an interface between two media, different physical phenomena can occur. These phenomena are shown in Figure 1-28 and are detailed in the following sections.

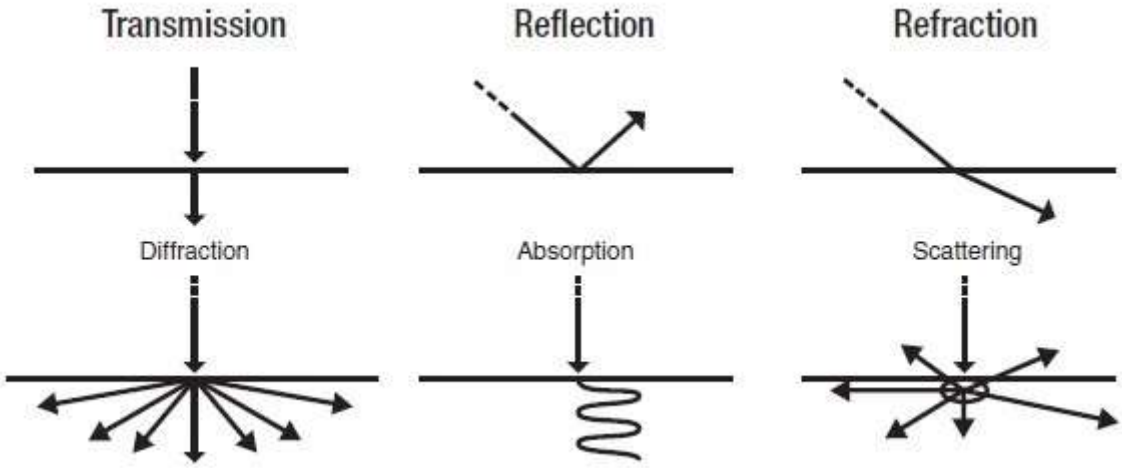

Figure 1-28-Different possible interaction between light and matter

1.4.6.1 Reflection and refraction

At the interface between two media of different refractive indices (i.e., speed of light in the medium), the reflection is the beam that will propagate in the same medium than the incident beam but with a certain angle. In the case of refraction, the refracted beam will go through the second medium with a change of the direction of propagation. The angles can be calculated by the Snell-Descartes' laws. A particular case of refraction is the double refraction or birefringence, it occurs when the medium is

anisotropic (i.e., variations of optical properties depending on the direction of propagation and polarization).

1.4.6.2 Light scattering

Also called diffusion or diffuse reflection, light scattering is the phenomenon where the beam is deviated from its trajectory in all the directions around the scattering center. This phenomenon occurs when small particles or rough surface are present in the trajectory of the light beam.

1.4.6.3 Absorption and transmission

When light beam enters the matter, it can go through it without losing any energy, the light is entirely transmitted by the medium. The medium is said transparent to the beam. Often, a part or the beam is absorbed by the matter. This absorption leads to a transformation of the electromagnetic energy into internal energy. The energy is absorbed by the atoms constituting the matter. It can either bring the atom to an excited state and produce photons by return to initial state (stimulated emission) or disturb the electronic cloud and/or produce thermal energy.

1.4.7 **Applications**

Due to the properties of laser light and the physical phenomenon involved, the interactions between the laser beam and the matters are numerous and lead to plenty of applications. Laser was created without a specific application and was described as "a solution looking for a problem"[86]. Nowadays, lasers are everywhere in our daily-lives but also for specific applications in areas such as medicine, industry, military and science.

Those applications are separated in two categories according to the type of light matter interaction occurring: reflection or the absorption. Applications based on reflections are non-destructive and concern communications, imaging and measurement. Application which resides in absorption of the matter can produce thermal effect such as melting or vaporization, formation of plasma, ablation and photochemical reactions.

Moreover, the use of high energy laser can induce phenomenon such as non-linear optics. Non-linear optics describes all the phenomena in which the response of the illuminated medium is not proportional to the electric field. For example, generation of second harmonic (SHG) is a phenomenon in which the light-matter interaction leads to doubling the frequency of the initial light.

Recently, lasers have started to be used for crystallization process such as photochemical light induced nucleation (PLIN) and Non-photochemical laser induced nucleation (NPLIN). In PLIN, the molecule that nucleate is different from the initial molecule in solution, i.e., photochemical reaction occurs. In 2004, Okutsu *et al.*[87] demonstrated the nucleation of benzopinacol from benzophenone solution after irradiation by a 355nm pulsed laser. Veesler *et al.*[88] also demonstrated the photochemical nucleation of lysozyme. They proposed a mechanism in which laser exposure produce a photochemical intermediate that leads to a denaturated species if irradiated or the intermediate relax to initial lysozyme and nucleate. In the case of NPLIN, the compound that nucleates has the same chemical structure that the one in solution at the beginning. Moreover, the formation of photochemical intermediates is not likely as the compound does not absorbs light at the working wavelength. The mechanism of NPLIN is not fully understood but it is certainly photophysical. Chapter 2 will present the state of the art of the NPLIN phenomenon.

1.5 REFERENCES

(1) Glusker, J. P.; Lewis, M.; Rossi, M. *Crystal Structure Analysis for Chemists and Biologists*; John Wiley & Sons, 1996.

(2) Dougherty, J. P.; Kurtz, S. K. A Second Harmonic Analyzer for the Detection of Non-Centrosymmetry. *J Appl Cryst* **1976**, *9* (2), 145–158. https://doi.org/10.1107/S0021889876010789.

(3) Kleinman, D. A. Theory of Second Harmonic Generation of Light. *Phys. Rev.* **1962**, *128* (4), 1761–1775. https://doi.org/10.1103/PhysRev.128.1761.

(4) Flack, H. D. Chiral and Achiral Crystal Structures. *HCA* **2003**, *86* (4), 905–921. https://doi.org/10.1002/hlca.200390109.

(5) *Sohncke groups - Online Dictionary of Crystallography*. https://dictionary.iucr.org/Sohncke_groups (accessed 2022-04-19).

(6) Threlfall, T. L. Analysis of Organic Polymorphs. A Review. *Analyst* **1995**, *120* (10), 2435–2460. https://doi.org/10.1039/AN9952002435.

(7) Domingos, S.; Andre, V.; Quaresma, S.; Martins, I.; Piedade, M.; Duarte, T. New Forms of Old Drugs: Improving without Changing. *The Journal of pharmacy and pharmacology* **2015**, *67*. https://doi.org/10.1111/jphp.12384.

(8) Burger, A.; Ramberger, R. On the Polymorphism of Pharmaceuticals and Other Molecular Crystals. I. *Mikrochim Acta* **1979**, *72* (3–4), 259–271. https://doi.org/10.1007/BF01197379.

(9) Haüy, R.-J. *Traite de Mineralogie*; Louis Librairie: Paris, 1801.

(10) Biot, J.-B. Phénomènes de Polarisation Successive, Observés Dans Des Fluides Homogènes. *Bull. Soc. Philomath* **1815**, 190.

(11) Herschel, J. F. W. *On the Rotation Impressed by Plates of Rock Crystal on the Planes of Polarization of the Rays of Light, as Connected with Certain Peculiarities in Its Crystallization*, Transactions of the Cambridge Philosophical Society.; J.Smith, 1820.

(12) Pasteur, L. *Researches on the Molecular Asymmetry of Natural Organic Products*; 1860.

(13) Kelvin, L. W. T. *Baltimore Lectures on Molecular Dynamics and the Wave Theory of Light*; CUP Archive, 1904.

(14) Curie, P. Sur la symétrie dans les phénomènes physiques, symétrie d'un champ électrique et d'un champ magnétique. *J. Phys. Theor. Appl.* **1894**, *3* (1), 393–415. https://doi.org/10.1051/jphystap:018940030039300.

(15) Van't Hoff, J. H. On Structural Formulas in Space. *Archives néerlandaises des sciences exactes et naturelles.* **1874**, 445–454.

(16) Le Bel, J. A. On the Relations That Exist between the Atomic Formulas of Organic Substances and the Rotatory Power of Their Solutions. *Bull. Société Chim.* **1874**, 337–347.

(17) Allinger, N. L.; Eliel, E. L.; Wilen, S. H. Recent Advances in Atropisomerism. In *Topics in Stereochemistry*; Ōki, M., Ed.; John Wiley & Sons, Inc.: Hoboken, NJ, USA, 2007; Vol. 14, pp 1–81. https://doi.org/10.1002/9780470147238.ch1.

(18) Prelog, V. Chirality in Chemistry. *Science* **1976**, *193* (4247), 17–24. https://doi.org/10.1126/science.935852.

(19) Kipping, F. S.; Pope, W. J. LXIII.—Enantiomorphism. *J. Chem. Soc., Trans.* **1898**, *73* (0), 606–617. https://doi.org/10.1039/CT8987300606.

(20) Suárez, M.; Branda, N.; Lehn, J.-M.; Decian, A.; Fischer, J. Supramolecular Chirality: Chiral Hydrogen-Bonded Supermolecules from Achiral Molecular Components. *Helvetica Chimica Acta* **1998**, *81* (1), 1–13. https://doi.org/10.1002/hlca.19980810102.

(21) Matsuura, T.; Koshima, H. Introduction to Chiral Crystallization of Achiral Organic Compounds: Spontaneous Generation of Chirality. *Journal of Photochemistry and Photobiology C: Photochemistry Reviews* **2005**, *6* (1), 7–24. https://doi.org/10.1016/j.jphotochemrev.2005.02.002.

(22) Matsumoto, A.; Kaimori, Y.; Kawasaki, T.; Soai, K. Asymmetric Autocatalysis Initiated by Crystal Chirality of Achiral Compounds. In *Advances in Asymmetric Autocatalysis and Related Topics*; Elsevier, 2017; pp 337–355. https://doi.org/10.1016/B978-0-12-812824-4.00018-6.

(23) Wright, A. F.; Lehmann, M. S. The Structure of Quartz at 25 and 590°C Determined by Neutron Diffraction. *Journal of Solid State Chemistry* **1981**, *36* (3), 371–380. https://doi.org/10.1016/0022-4596(81)90449-7.

(24) Lee, C.; Weber, J. M.; Rodriguez, L. E.; Sheppard, R. Y.; Barge, L. M.; Berger, E. L.; Burton, A. S. Chirality in Organic and Mineral Systems: A Review of Reactivity and Alteration Processes Relevant to Prebiotic Chemistry and Life Detection Missions. *Symmetry* **2022**, *14* (3), 460. https://doi.org/10.3390/sym14030460.

(25) Zachariasen, W. H. XXVIII. The Crystal Structure of Sodium Chlorate. *Zeitschrift für Kristallographie - Crystalline Materials* **1929**, *71* (1–6), 517–529. https://doi.org/10.1524/zkri.1929.71.1.517.

(26) Abrahams, S. C.; Bernstein, J. L. Remeasurement of Optically Active NaClO3 and NaBrO3. *Acta Crystallographica Section B* **1977**, *33* (11), 3601–3604. https://doi.org/10.1107/S0567740877011637.

(27) Viedma, C. Chiral Symmetry Breaking During Crystallization: Complete Chiral Purity Induced by Nonlinear Autocatalysis and Recycling. *Phys. Rev. Lett.* **2005**, *94* (6), 065504. https://doi.org/10.1103/PhysRevLett.94.065504.

(28) Kondepudi, D. K.; Kaufman, R. J.; Singh, N. Chiral Symmetry Breaking in Sodium Chlorate Crystallizaton. *Science* **1990**, *250* (4983), 975–976. https://doi.org/10.1126/science.250.4983.975.

(29) Schindler, M. Deracemization of Sodium Chlorate with or without the Influence of Sodium Dithionate, Rouen-Normandie, 2020.

(30) Matsumoto, A.; Ide, T.; Kaimori, Y.; Fujiwara, S.; Soai, K. Asymmetric Autocatalysis Triggered by Chiral Crystal of Achiral Ethylenediamine Sulfate. *Chem. Lett.* **2015**, *44* (5), 688–690. https://doi.org/10.1246/cl.150052.

(31) Nguyen, T. P. T.; Cheung, P. S. M.; Werber, L.; Gagnon, J.; Sivakumar, R.; Lennox, C.; Sossin, A.; Mastai, Y.; Cuccia, L. A. Directing the Viedma Ripening of Ethylenediammonium Sulfate Using “Tailor-Made” Chiral Additives. *Chem. Commun.* **2016**, *52* (85), 12626–12629. https://doi.org/10.1039/C6CC06534A.

(32) Ostwald, W. Studien über die Bildung und Umwandlung fester Körper: 1. Abhandlung: Übersättigung und Überkaltung. *Zeitschrift für Physikalische Chemie* **1897**, *22U* (1), 289–330. https://doi.org/10.1515/zpch-1897-2233.

(33) Kadam, S. S.; Kulkarni, S. A.; Coloma Ribera, R.; Stankiewicz, A. I.; ter Horst, J. H.; Kramer, H. J. M. A New View on the Metastable Zone Width during Cooling Crystallization. *Chemical Engineering Science* **2012**, *72*, 10–19. https://doi.org/10.1016/j.ces.2012.01.002.

(34) Bian, C.; Chen, H.; Song, X.; Yu, J. Metastable Zone Width and the Primary Nucleation Kinetics for Cooling Crystallization of NaNO3 from NaCl-NaNO3-H2O System. *Journal of Crystal Growth* **2019**, *518*, 5–13. https://doi.org/10.1016/j.jcrysgro.2019.04.013.

(35) Groen, H.; Roberts, K. J. An Examination of the Crystallization of Urea from Supersaturated Aqueous and Aqueous−Methanol Solutions as Monitored In-Process Using ATR FTIR Spectroscopy. *Crystal Growth & Design* **2004**, *4* (5), 930–936. https://doi.org/10.1021/cg030038y.

(36) Nemdili, L.; Koutchoukali, O.; Mameri, F.; Gouaou, I.; Koutchoukali, M. S.; Ulrich, J. Crystallization Study of Potassium Sulfate-Water System, Metastable Zone Width and Induction Time Measurements Using Ultrasonic, Turbidity and 3D-ORM Techniques. *Journal of Crystal Growth* **2018**, *500*, 44–51. https://doi.org/10.1016/j.jcrysgro.2018.08.009.

(37) Luo, M.; Liu, C.; Xue, J.; Li, P.; Yu, J. Determination of Metastable Zone Width of Potassium Sulfate in Aqueous Solution by Ultrasonic Sensor and FBRM. *Journal of Crystal Growth* **2017**, *469*, 144–153. https://doi.org/10.1016/j.jcrysgro.2016.09.006.

(38) Kulkarni, S. A.; Kadam, S. S.; Meekes, H.; Stankiewicz, A. I.; ter Horst, J. H. Crystal Nucleation Kinetics from Induction Times and Metastable Zone Widths. *Crystal Growth & Design* **2013**, *13* (6), 2435–2440. https://doi.org/10.1021/cg400139t.

(39) Mullin, J. W. *Crystallization*, 4th ed.; Butterworth-Heinemann: Oxford ; Boston, 2001.

(40) Volmer, M.; Weber, A. Keimbildung in übersättigten Gebilden. *Zeitschrift für Physikalische Chemie* **1926**, *119U* (1), 277–301. https://doi.org/10.1515/zpch-1926-11927.

(41) Myerson, A. S.; Trout, B. L. Nucleation from Solution. *Science* **2013**, *341*, 855–856. https://doi.org/10.1126/science.1243022.

(42) Kashchiev, D.; van Rosmalen, G. M. Review: Nucleation in Solutions Revisited. *Crystal Research and Technology* **2003**, *38* (7–8), 555–574. https://doi.org/10.1002/crat.200310070.

(43) Kavasmaneck, P. R.; Bonner, W. A. Adsorption of Amino Acid Derivatives by D- and l-Quartz. *J. Am. Chem. Soc.* **1977**, *99* (1), 44–50. https://doi.org/10.1021/ja00443a011.

(44) Carter, P. W.; Ward, M. D. Directing Polymorph Selectivity During Nucleation of Anthranilic Acid on Molecular Substrates. *J. Am. Chem. Soc.* **1994**, *116* (2), 769–770. https://doi.org/10.1021/ja00081a048.

(45) Caridi, A.; Kulkarni, S. A.; Di Profio, G.; Curcio, E.; ter Horst, J. H. Template-Induced Nucleation of Isonicotinamide Polymorphs. *Crystal Growth & Design* **2014**, *14* (3), 1135–1141. https://doi.org/10.1021/cg401605m.

(46) Heywood, B. R.; Mann, S. Template-Directed Nucleation and Growth of Inorganic Materials. *Advanced Materials* **1994**, *6* (1), 9–20. https://doi.org/10.1002/adma.19940060103.

(47) Javid, N.; Kendall, T.; Burns, I. S.; Sefcik, J. Filtration Suppresses Laser-Induced Nucleation of Glycine in Aqueous Solutions. *Crystal Growth & Design* **2016**, *16* (8), 4196–4202. https://doi.org/10.1021/acs.cgd.6b00046.

(48) Dwyer, L.; Kulkarni, S.; Ruelas, L.; Myerson, A. Two-Stage Crystallizer Design for High Loading of Poorly Water-Soluble Pharmaceuticals in Porous Silica Matrices. **2017**, 14.

(49) Zhang, F.; Shan, B.; Wang, Y.; Zhu, Z.; Yu, Z.-Q.; Ma, C. Y. Progress and Opportunities for Utilizing Seeding Techniques in Crystallization Processes. *Org. Process Res. Dev.* **2021**, *25* (7), 1496–1511. https://doi.org/10.1021/acs.oprd.1c00103.

(50) Erdemir, D.; Lee, A. Y.; Myerson, A. S. Nucleation of Crystals from Solution: Classical and Two-Step Models. *Acc. Chem. Res.* **2009**, *42* (5), 621–629. https://doi.org/10.1021/ar800217x.

(51) Laaksonen, A.; Napari, I. Breakdown of the Capillarity Approximation in Binary Nucleation: A Density Functional Study. *J. Phys. Chem. B* **2001**, *105* (47), 11678–11682. https://doi.org/10.1021/jp0116454.

(52) Merikanto, J.; Zapadinsky, E.; Lauri, A.; Vehkamäki, H. Origin of the Failure of Classical Nucleation Theory: Incorrect Description of the Smallest Clusters. *Phys. Rev. Lett.* **2007**, *98* (14), 145702. https://doi.org/10.1103/PhysRevLett.98.145702.

(53) Yau, S.-T.; Vekilov, P. G. Direct Observation of Nucleus Structure and Nucleation Pathways in Apoferritin Crystallization. *J. Am. Chem. Soc.* **2001**, *123* (6), 1080–1089. https://doi.org/10.1021/ja003039c.

(54) Gránásy, L.; Iglói, F. Comparison of Experiments and Modern Theories of Crystal Nucleation. *The Journal of Chemical Physics* **1997**, *107* (9), 3634–3644. https://doi.org/10.1063/1.474721.

(55) Davey, R. J.; Allen, K.; Blagden, N.; Cross, W. I.; Lieberman, H. F.; Quayle, M. J.; Righini, S.; Seton, L.; Tiddy, G. J. T. Crystal Engineering – Nucleation, the Key Step. *CrystEngComm* **2002**, *4* (47), 257–264. https://doi.org/10.1039/B203521A.

(56) Zurek, W. H.; Schieve, W. C. Multistep Clustering and Nucleation. *J. Phys. Chem.* **1980**, *84* (12), 1479–1482. https://doi.org/10.1021/j100449a010.

(57) Wolde, P. R. ten; Frenkel, D. Enhancement of Protein Crystal Nucleation by Critical Density Fluctuations. *Science* **1997**, *277* (5334), 1975–1978. https://doi.org/10.1126/science.277.5334.1975.

(58) Gavezzotti, A. Molecular Aggregation of Acetic Acid in a Carbon Tetrachloride Solution: A Molecular Dynamics Study with a View to Crystal Nucleation. *Chemistry – A European Journal* **1999**, *5* (2), 567–576.

https://doi.org/10.1002/(SICI)1521-3765(19990201)5:2<567::AID-CHEM567>3.0.CO;2-6.

(59) Soga, K. G.; Melrose, J. R.; Ball, R. C. Metastable States and the Kinetics of Colloid Phase Separation. *J. Chem. Phys.* **1999**, *110* (4), 2280–2288. https://doi.org/10.1063/1.477881.

(60) Wallace, A. F.; Hedges, L. O.; Fernandez-Martinez, A.; Raiteri, P.; Gale, J. D.; Waychunas, G. A.; Whitelam, S.; Banfield, J. F.; De Yoreo, J. J. Microscopic Evidence for Liquid-Liquid Separation in Supersaturated CaCO3 Solutions. *Science* **2013**, *341* (6148), 885–889. https://doi.org/10.1126/science.1230915.

(61) Pan, W.; Kolomeisky, A. B.; Vekilov, P. G. Nucleation of Ordered Solid Phases of Proteins via a Disordered High-Density State: Phenomenological Approach. *J. Chem. Phys.* **2005**, *122* (17), 174905. https://doi.org/10.1063/1.1887168.

(62) Lutsko, J. F.; Nicolis, G. Theoretical Evidence for a Dense Fluid Precursor to Crystallization. *Phys Rev Lett* **2006**, *96* (4), 046102. https://doi.org/10.1103/PhysRevLett.96.046102.

(63) Georgalis, Y.; Umbach, P.; Raptis, J.; Saenger, W. Lysozyme Aggregation Studied by Light Scattering. I. Influence of Concentration and Nature of Electrolytes. *Acta Crystallogr D Biol Crystallogr* **1997**, *53* (Pt 6), 691–702. https://doi.org/10.1107/S0907444997006847.

(64) Gebauer, D.; Cölfen, H. Prenucleation Clusters and Non-Classical Nucleation. *Nano Today* **2011**, *6* (6), 564–584. https://doi.org/10.1016/j.nantod.2011.10.005.

(65) Vekilov, P. G. Dense Liquid Precursor for the Nucleation of Ordered Solid Phases from Solution. *Crystal Growth & Design* **2004**, *4* (4), 671–685. https://doi.org/10.1021/cg049977w.

(66) Haas, C. The Interface between a Protein Crystal and an Aqueous Solution and Its Effects on Nucleation and Crystal Growth. *J. Phys. Chem. B* **2000**, *104* (2), 368–377. https://doi.org/10.1021/jp993210a.

(67) Davey, R. J.; Schroeder, S. L. M.; ter Horst, J. H. Nucleation of Organic Crystals—A Molecular Perspective. *Angewandte Chemie International Edition* **2013**, *52* (8), 2166–2179. https://doi.org/10.1002/anie.201204824.

(68) Vekilov, P. G. Crystallization Tracked Atom by Atom. *Nature* **2019**, *570* (7762), 450–452. https://doi.org/10.1038/d41586-019-01965-2.

(69) Jiang, S.; ter Horst, J. H. Crystal Nucleation Rates from Probability Distributions of Induction Times. *Crystal Growth & Design* **2011**, *11* (1), 256–261. https://doi.org/10.1021/cg101213q.

(70) Shiau, L.-D. Determination of the Nucleation and Growth Kinetics for Aqueous L-Glycine Solutions from the Turbidity Induction Time Data. *Crystals* **2018**, *8* (11), 403. https://doi.org/10.3390/cryst8110403.

(71) Lyczko, N.; Espitalier, F.; Louisnard, O.; Schwartzentruber, J. Effect of Ultrasound on the Induction Time and the Metastable Zone Widths of Potassium Sulphate. *Chemical Engineering Journal* **2002**, *86* (3), 233–241. https://doi.org/10.1016/S1385-8947(01)00164-4.

(72) Brandel, C.; ter Horst, J. H. Measuring Induction Times and Crystal Nucleation Rates. *Faraday Discuss.* **2015**, *179*, 199–214. https://doi.org/10.1039/C4FD00230J.

(73) Kashchiev, D. *Nucleation: Basic Theory with Applications*; Elsevier, 2000.

(74) Vachaparambil, K. J.; Einarsrud, K. E. Explanation of Bubble Nucleation Mechanisms: A Gradient Theory Approach. *J. Electrochem. Soc.* **2018**, *165* (10), E504. https://doi.org/10.1149/2.1031810jes.

(75) Liger-Belair, G.; Marchal, R.; Robillard, B.; Vignes-Adler, M.; Maujean, A.; Jeandet, P. Study of Effervescence in a Glass of Champagne: Frequencies of Bubble Formation, Growth Rates, and Velocities of Rising Bubbles. *American Journal of Enology and Viticulture* **1999**, *50*, 317–323.

(76) Henry, W.; Banks, J. III. Experiments on the Quantity of Gases Absorbed by Water, at Different Temperatures, and under Different Pressures. *Philosophical Transactions of the Royal Society of London* **1803**, *93*, 29–274. https://doi.org/10.1098/rstl.1803.0004.

(77) Knott, B. C.; LaRue, J. L.; Wodtke, A. M.; Doherty, M. F.; Peters, B. Communication: Bubbles, Crystals, and Laser-Induced Nucleation. *J. Chem. Phys.* **2011**, *134* (17), 171102. https://doi.org/10.1063/1.3582897.

(78) Noltingk, B. E.; Neppiras, E. A. Cavitation Produced by Ultrasonics. *Proc. Phys. Soc. B* **1950**, *63* (9), 674–685. https://doi.org/10.1088/0370-1301/63/9/305.

(79) Soare, A.; Dijkink, R.; Pascual, M. R.; Sun, C.; Cains, P. W.; Lohse, D.; Stankiewicz, A. I.; Kramer, H. J. M. Crystal Nucleation by Laser-Induced Cavitation. *Crystal Growth & Design* **2011**, *11* (6), 2311–2316. https://doi.org/10.1021/cg2000014.

(80) Hunt, J. D.; Jackson, K. A. Nucleation of the Solid Phase by Cavitation in an Undercooled Liquid Which Expands on Freezing. *Nature* **1966**, *211* (5053), 1080–1081. https://doi.org/10.1038/2111080b0.

(81) Liu, Y.; van den Berg, M. H.; Alexander, A. J. Supersaturation Dependence of Glycine Polymorphism Using Laser-Induced Nucleation, Sonocrystallization and Nucleation by Mechanical Shock. *Phys. Chem. Chem. Phys.* **2017**, *19* (29), 19386–19392. https://doi.org/10.1039/C7CP03146G.

(82) *Laser :Fundamentals*. http://www.optique-ingenieur.org/en/courses/OPI_ang_M01_C01/co/OPI_ang_M01_C01_web.html (accessed 2022-03-11).

(83) Panthier, F.; Doizi, S.; Corrales, M.; Traxer, O. Pulsed Lasers and Endocorporeal Laser Lithotripsy. *Progrès en Urologie* **2021**, *31* (8), 451–457. https://doi.org/10.1016/j.purol.2020.11.008.

(84) Born, M.; Wolf, E. *Principles of Optics: Electromagnetic Theory of Propagation, Interference and Diffraction of Light*; Elsevier, 2013.

(85) Paschotta, D. R. *Polarization of Light*. RP Photonics Encyclopedia. https://www.rp-photonics.com/polarization_of_light.html (accessed 2022-08-25).

(86) Garwin, L.; Lincoln, T. *A Century of Nature : Twenty-One Discoveries That Changed Science and the World*; Chicago : University of Chicago Press, 2003.

(87) Okutsu, T.; Nakamura, K.; Haneda, H.; Hiratsuka, H. Laser-Induced Crystal Growth and Morphology Control of Benzopinacol Produced from Benzophenone in Ethanol/Water Mixed Solution. *Crystal Growth & Design* **2004**, *4* (1), 113–115. https://doi.org/10.1021/cg0340493.

(88) Veesler, S.; Furuta, K.; Horiuchi, H.; Hiratsuka, H.; Ferté, N.; Okutsu, T. Crystals from Light: Photochemically Induced Nucleation of Hen Egg-White Lysozyme. *Crystal Growth & Design* **2006**, *6* (7), 1631–1635. https://doi.org/10.1021/cg0506424.

Chapter 2. NON-PHOTOCHEMICAL LASER INDUCED NUCLEATION: STATE OF THE ART

2.1 INTRODUCTION

This chapter is dedicated to the description of the non-photochemical laser induced nucleation (NPLIN) process: from its discovery to the current research. A review of the previous studies will be presented, and each proposed hypothesis of mechanism will be detailed and discussed.

2.2 DISCOVERY OF NPLIN

In 1996, Garetz et al[1] found that exposition of supersaturated solutions of urea to light from a high energy pulsed laser, initially to measure a second harmonic generation (SHG) response, resulted in the nucleation of needle-like crystals of urea. They called this phenomenon Non-Photochemical Laser Induced Nucleation (NPLIN). Laser induced nucleation (LIN) techniques were already known since the work of Tyndall in 1896[2], but implied photochemical reaction. In the NPLIN process, the non-photochemical characteristic is important as it allows to nucleate crystals of the same chemical composition of the initial solvated molecules. This requires that neither the solute nor the solvents absorbs the laser energy at the wavelength used.

Since this discovery, the possibility to nucleate through the use of laser has developed and has interested many scientists. Indeed, the process allows temporal and spatial control of nucleation without seeding the solution. The number of publications on the topic has increased and various compounds with various laser set-up have been studied. NPLIN is a broad term that can refer to different experimental techniques. Indeed, studies using continuous laser or pulsed laser from nanosecond to femtosecond in which laser induces nucleation without photochemical damage of the compound are considered as NPLIN. In this study, the NPLIN phenomenon is restricted to nanosecond laser pulses since it is possible that the mechanism behind the different laser sources used is different.

Table 2-1 reviews the researches done on NPLIN using a nanosecond laser and lists the molecules studied, laser wavelengths and energies, alongside the mechanisms proposed, from 1996 to 2021 (42 *articles*). The general trend is as follows: small organics molecules were the first cases considered. Glycine received special attention due to its polymorphic behaviour. Then, NPLIN phenomena of some proteins were studied, but most of them were crystallized using femtosecond pulses laser. And then,

NPLIN studies focused on inorganic salts. The last column in Table 2-1, referring to the proposed mechanisms, will be regarded later during this chapter.

*Table 2-1- List of compounds used in NPLIN studies , the parameters of the laser and the proposed mechanism involved according to the authors. (ns: nanosecond laser; fs: femtosecond laser; ps: picosecond laser; f: focussed; *Intensity given is the maximum used in the study, all intensity values are given in GW/cm² to unify the units and compare more easily, energy value in J/pulse is given when intensity value was not available) [OKE : Optical Kerr Effect , DP: Dielectric polarization]*

Compound/ solvent	**Reference**	**Laser**	**λ (nm)**	**Intensity* (max)**	**Mechanism**
Urea/ H_2O	*Garetz, 1996*[1]	ns	1064	0.25 GW/cm²	**OKE**
	Matic, 2005[3]	ns	1064 532	0.35 GW/cm²	**OKE**
	Liu, 2017[4]	ns	1064 532	0.20 GW/cm²	
Glycine/ H_2O (D_2O)	*Zaccaro, 2001*[5]	ns	1064	0.70 GW/cm²	**OKE**
	Garetz, 2002[6]	ns	1064	0.70 GW/cm²	**OKE**
	Sun, 2006[7]	ns	1064 532	0.46 GW/cm²	**OKE**
	Clair, 2014[8]	ns	532	0.70 GW/cm²	
	Javid, 2016[9]	ns	1064	0.47 GW/cm²	
	Liu, 2017[10]	ns	1064	0.50 GW/cm²	**Cavitation**
	Tasnim, 2018[11]	ns	1064	0.50 GW/cm²	
	Gowayed, 2019[12]	ns	1064	0.40 GW/cm²	
	Hua, 2020[13]	ns	1064	0.20 GW/cm²	**DP**
	Irimia, 2020[14]	ns	1064 532	0.22 GW/cm²	
DAST	*Tsunesada,2002*[15]	ns,f	1064	/	
4,4'-dimethyl-chalcone / ethyl acetate	*Murphy, 2007*[16]	ns	1064	0.01 GW/cm²	**OKE**
Ice	*Lindinger, 2007*[17]	ns,f	1064	1mJ/pulse	
	Nevo,2020[18]	ns	532	0.01GW/cm²	
L-histidine/ H_2O	*Sun, 2008*[19]	ns	532	0.24 GW/cm²	**OKE**
Lysozyme/ H_2O	*Lee, 2008*[20]	ns, ps	1064 532	0.12 GW/cm²	

5CB (supercooled)	*Sun, 2009*[21]	ps	532	0.003GW/cm²	**OKE**
KCl/ H_2O (KBr)	*Alexander, 2009*[22]	ns	1064	0.04 GW/cm²	**DP**
	Duffus, 2009[23]	ns	1064	0.06 GW/cm²	
	Ward, 2009[24]	ns	1064	2 MW/cm²	
	Ward, 2012[25]	ns	1064 532	0.04 GW/cm²	**DP**
	Fang, 2014[26]	ns, f	532	0.05 GW/cm²	
	Kacker, 2018[27]	ns	1064 532 355	0.05 GW/cm²	
	Hua, 2019[28]	ns	1064	0.10 GW/cm²	**DP**
$(NH_4)_2SO_4$/ methanol/ethanol	*Soare,2011*[29]	ns, f	532	0.5 mJ	**Cavitation**
$NaClO_3$ molten	*Ward, 2011*[30]	ns	1064	0.14 GW/cm²	**DP**
$NaClO_3$/ H_2O	*Barber, 2019*[31]	ns, f	1064 532	87 TW/cm²	**Cavitation**
CO_2 / H_2O	*Knott, 2011*[32]	ns	1064 532 355	50 mJ/pulse	**Cavitation**
	Ward, 2015[33]	ns fs	532 800	0.03 GW/cm² 11 GW/cm²	**Nanoparticle heating**
Acetic acid	*Ward, 2012*[34]	ns	1064	5.85 MW/cm²	**DP**
KNO_3 / H_2O	*Jacob, 2012*[35]	ns, f	532	0.06 GW/cm²	
	Gharib, 2021	ns, f	532	250mJ/pulse	
Carbamazepine/ Acetonitrile / methanol	*Ikni, 2014*[36]	ns	532	0.35 GW/cm²	**OKE**
Sulfathiazole / H_2O-ethanol	*Li, 2016*[37]	ns	532	0.30 GW/cm²	**OKE**
NH_4Cl / H_2O	*Ward, 2016*[38]	ns	1064	0.01 GW/cm²	**Nanoparticle heating**
NaCl, $NaBrO_3$, tartaric acid / H_2O	*Mirsaleh-kohan, 2017*[39]	ns, f	1064	1.90 TW/cm²	
CsCl/water +polymers	*Liu, 2021*[40]	ns	532	0.016GW/cm²	
Sodium acetate/ water + polymers	*Liu, 2021*[41]	ns	1064	0.016GW/cm²	
NaBr / H_2O	*Barber, 2021*[42] *11*	ns	1064 532	0.30 GW/cm²	

2.3 PRINCIPLE

The NPLIN process, represented in Figure 2-1, uses a high energy (from MW/cm² to TW/cm²) short pulsed laser to induce the nucleation of a supersaturated solution (or a supercooled liquid). The process allows temporal control of nucleation: laser irradiation strongly reduces the induction time (t_{ind}) for nucleation compared to a non-irradiated sample where spontaneous nucleation takes place. Calculating the probability of nucleation and plotting the curves $P_n(t)=f(t)$ (Chapter1- 1.3.5) for irradiated samples compared to non-irradiated samples allows to visualize the NPLIN effect. As seen in Figure 2-2, at a given time, the probability of nucleation is much higher for NPLIN sample than for control samples (non-irradiated) (Figure 2-2, 1) and also a much longer time to reach the same probability of nucleation is needed for control samples (Figure 2-2,2).

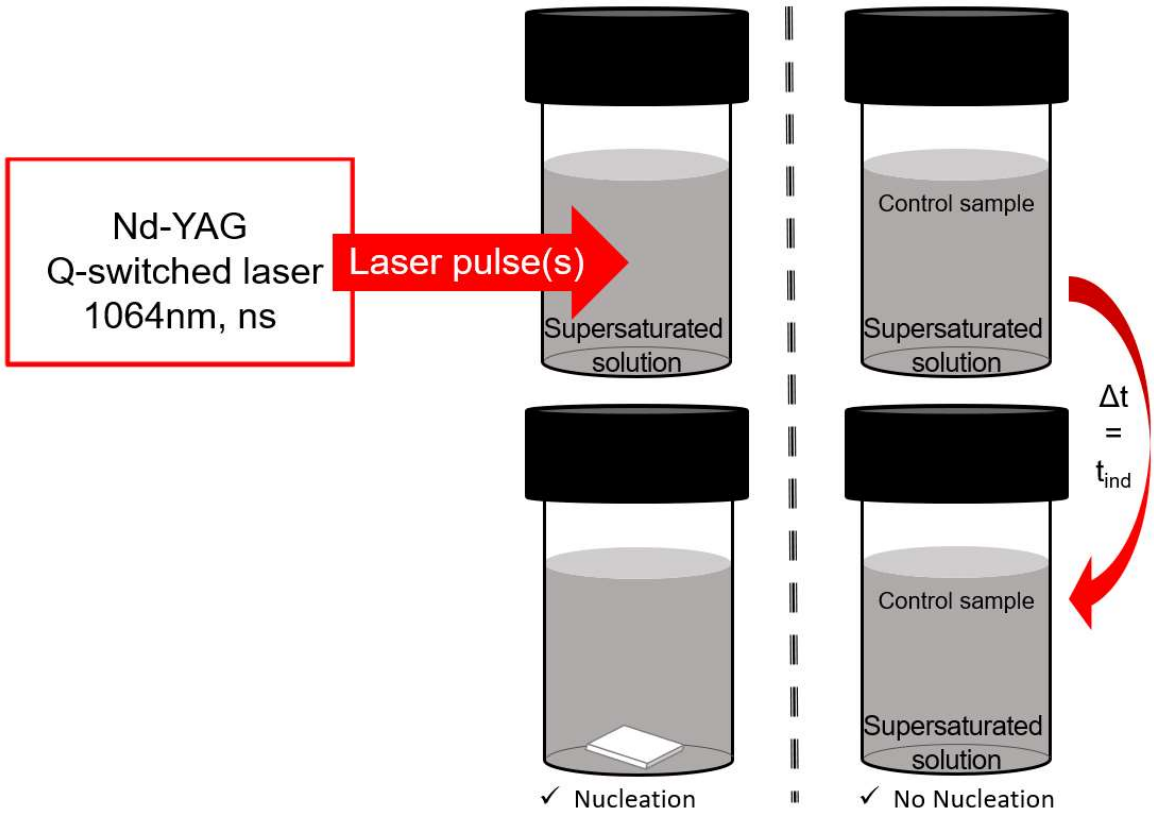

Figure 2-1 Representation of the NPLIN principle, with the set-up used in this study. Although nucleation occurred within the volume irradiated by the beam path, the formed crystal has sedimented.

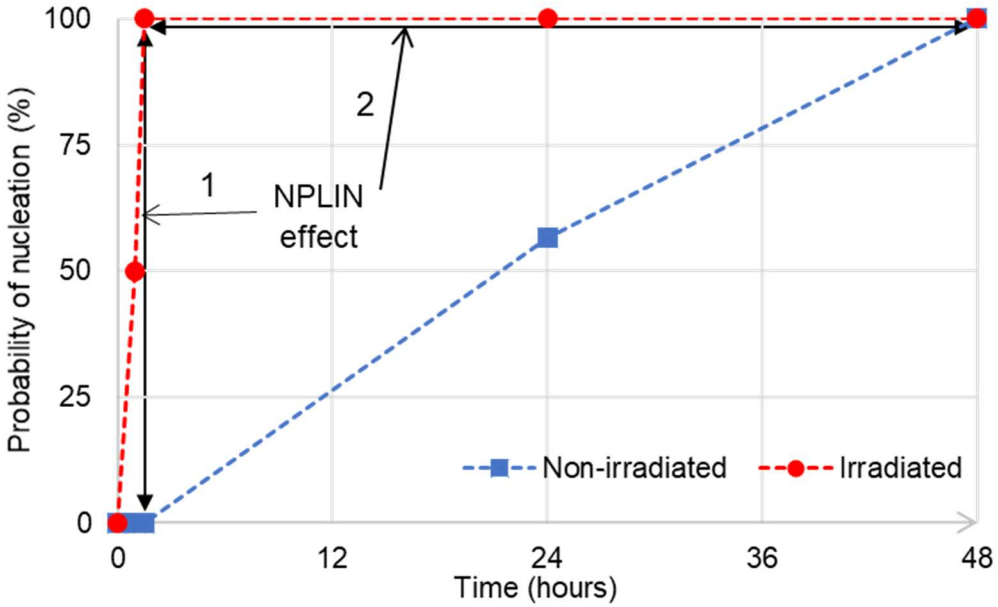

Figure 2-2- $P_n(t) = f(t)$ curves for irradiated samples (red) and non-irradiated samples (blue).The NPLIN efficiency is measured by (1)-the gap between probability of nucleation at a given time and (2)-the gap between time to reach a given probability of nucleation.

It also allows spatial control of the nucleation as the nuclei primarily form in the volume irradiated by the laser beam path, thus offering the possibility to trigger nucleation at a given spot as demonstrated by Duffus et al[23] (see Figure 2-3). On the contrary, spontaneous nucleation in non-irradiated sample can occurs anywhere in the solution volume.

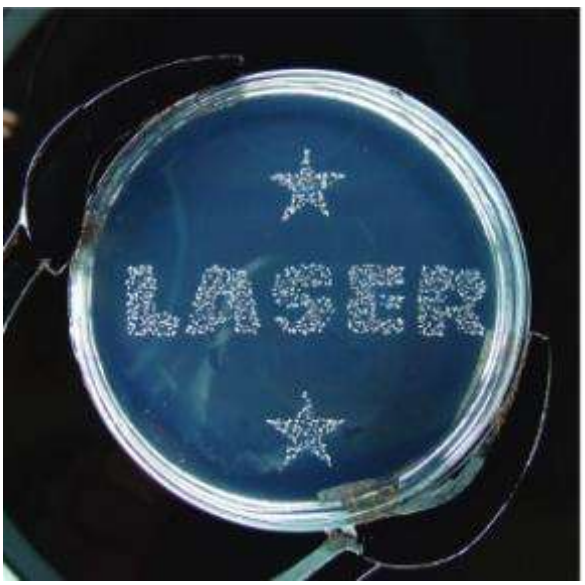

Figure 2-3- Spatial control of KCl nucleation in agarose gel using an optical mask (Adapted from Duffus et al)

Moreover, NPLIN process can lead to different number of crystals from one single crystal[22] to a multitude of crystals resulting in different sizes of crystals.[28,37,38] Thus, the NPLIN technique could be a good way to control Crystal size distribution (CSD) just by varying laser parameters.

In principle, NPLIN does not induce photochemical damage: the initial solvated compound is the same that crystallizes. However, NPLIN is limited by the fact that the molecules studied (crystallizing compound and solvent) must have no or low optical absorbance at the irradiation wavelength. It must also be underlined that the NPLIN process is not observed for every compound. Further, the mechanisms behind the laser interaction with the solution which trigger nucleation is not fully understood despite the proposed hypotheses. Several parameters have been reported to influence the NPLIN process and it is important to identify them and their influence on the process to help to understand the mechanism.

First, each mechanism proposed to explain NPLIN will be defined and discussed. Then, the parameters, divided in two categories : (i) the parameters related to the solution and (ii) the ones related to the laser will be listed and presented individually.

2.4 MECHANISM HYPOTHESES

2.4.1 The Optical Kerr Effect: OKE

2.4.1.1 Definition

The Optical Kerr Effect (OKE) is a nonlinear optics phenomenon induced by an electric field such as the one produced by a high energy laser light. It causes a change in the refraction index of the materials which induces birefringence (OKE is also called light induced birefringence[43]). At a molecular level, if one considers a group of anisotropic polarizable molecules in solution, the electric field induces a dipole moment inside the molecule, which results in an alignment of all the molecules in the same direction than that of the electromagnetic field of the laser. (Figure 2-4).

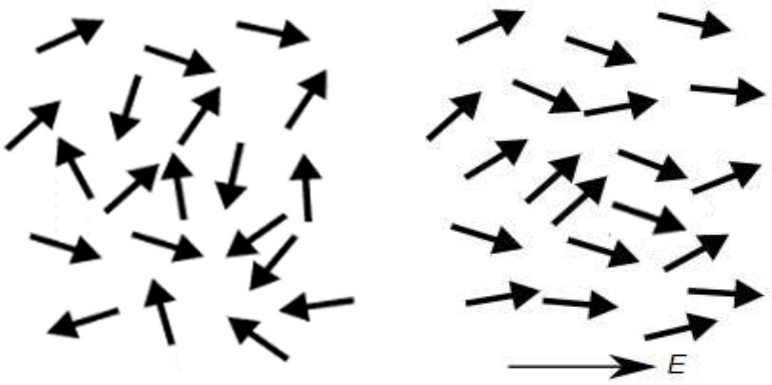

Figure 2-4- Orientation of the dipole in presence of an electric field. Arrow are representing the dipole of the molecules, on the left no electric field is applied and on the right with an electric field.

In the context of an NPLIN experiment, the alignment of the molecules contributes to form an ordered critical nucleus (as in the CNT model [1.3.3.1]) or to arrange the molecules inside the PNC (as in TSN model [1.3.4]).

2.4.1.2 Argument in favour of OKE mechanism, polarization switching

This section describes the different factors that lead to consider OKE as a possible hypothesis to explain the NPLIN mechanism.

OKE was first mentioned to explain NPLIN by Garetz et al[1] when they discovered the NPLIN phenomenon in the case of urea supersaturated solutions. They observed an alignment of urea crystalline needles axis with the direction of the electric field of their linearly polarized laser beam. They explained this observation by the facts that:

(i) urea molecule has an anisotropic polarizability,
(ii) interaction of the laser with the solution results in a cooperative polarization of the urea molecules in the “dense liquid precursors” which eventually leads to their alignment with the direction of polarization of the linearly polarized light,
(iii) the most polarizable direction of urea corresponds to the main axis of the crystalline needles,
(iv) such laser light induces organization of the “dense liquid precursors” results in the crystal nucleation of the needles parallel to the polarized light direction.

The main experimental support for OKE mechanism came from a NPLIN study on the polymorphism of glycine[6], in which the polarization geometry of the laser light (i.e circular or linear) was reported to induce different

polymorphs. Indeed, in the case of glycine, three polymorphs are reported α, β and γ-glycine but only two polymorphs can nucleate via NPLIN: α-glycine or γ-glycine. In solution, there are assemblies of glycine molecules forming dimers (or n-mers) and according to the geometry of the solvated dimer, a cyclic dimer has disk-like polarizabilities and lead to α-glycine whereas a helical dimer has rod-like polarizabilities and lead to γ-glycine. In their study, the authors claimed that linear polarization was more effective at aligning rod-like polarized clusters, thus resulting in the NPLIN induced crystallization of γ-glycine, whereas circular polarization was more effective at aligning disk-like polarized clusters, thus resulting in the NPLIN induced crystallization of α-glycine (see Figure 2-5). This phenomenon was called polarization switching as, for the same ratio of supersaturation, the polarization of the incident light seems to control the polymorph produced. In contrast, spontaneous nucleation of a glycine supersaturated solution produces α-glycine at low supersaturation and γ-glycine at high supersaturation[44].

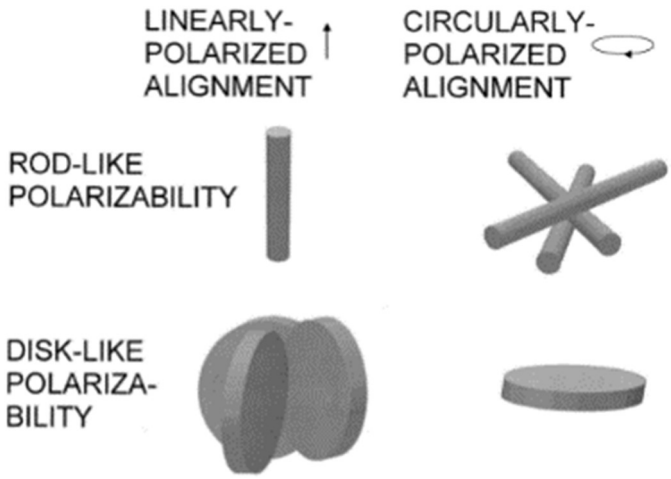

Figure 2-5- Alignment of the polarizabilities according to the polarization of the laser (adapted from Garetz et al[6])

Studies about others molecules such as Carbamazepine[36] and Sulfathiazole[37], which exhibit both polymorphism, seem in agreement with the fact that the geometry of molecule polarizabilities interacts differently according to the polarization geometry and direction of light. In addition, molecules that does not exhibit polymorphism seems also impacted by the polarization since they either present rod-like or disk-like polarizabilities[7]. For instance, it has been shown that urea exhibits rod-like polarizabilities and thus nucleate more easily with linear polarized light[3].

The OKE mechanism has also been considered in the case of compounds exhibiting supramolecular chirality. In order to induce chiral symmetry breaking, Murphy *et al.*[16] exposed solutions of 4-4'-dimethylchalcone to different radiation. They found that linearly polarized light leads to a larger distribution of (+) and (-) optical rotations compared to circularly polarized light or stirred crystallization (Figure 2-6). Although there is no preferred enantiomorph formed, they have highlighted an influence of the polarization on chiral distributions which they attribute to the ability of linearly polarized light to more efficiently align the rod-like cluster of 4-4'-dimethylchalcone.

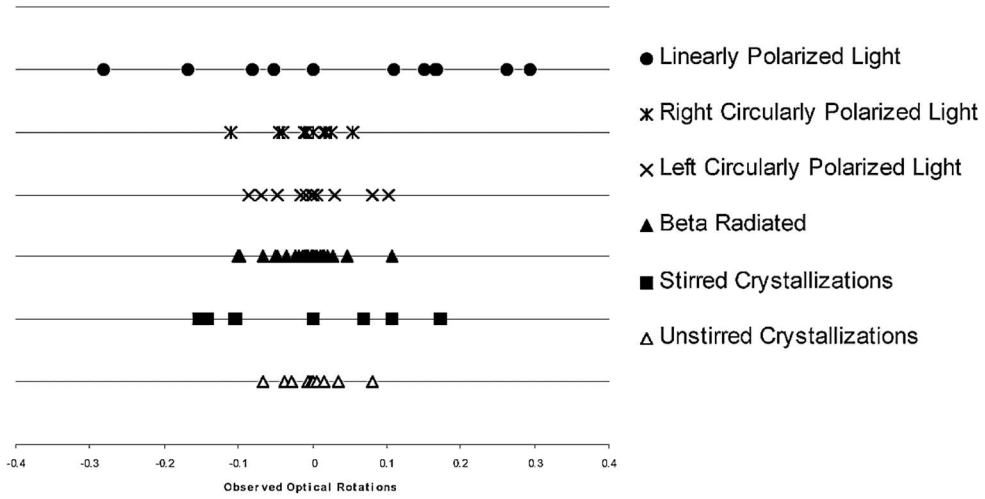

Figure 2-6- Observed optical rotations for 4-4'-dimethylchalcone exposed to different conditions (from Murphy et al)

2.4.1.3 Limits of the OKE mechanism

Recently, the OKE mechanism have been criticized since the results reported by Garetz et al. regarding Urea and Glycine could not be reproduced. Indeed, Liu *et al*[4] used digital imaging to measure the angle of the urea crystal (needle-like) compared to the direction of polarization of the laser. They showed that there is no correlation between the orientations of the freshly nucleated crystalline needle and that of the plan of polarized light of the laser. This, in addition to other recently reported results, questions the OKE theory. Further to this, theoretical calculations made by Knott *et al*[45] *using* Monte Carlo simulations showed that the energy required to align the dipole along the electromagnetic field of the laser should be much higher than the energy provided by the laser. They concluded that the electromagnetic field of the laser cannot change the orientation of the solute molecules in the solvent.

Moreover, the phenomenon of polarization switching of Glycine described by Garetz et al.[6] was found to be poorly reproducible by Sun *et al*[7]*, who* described the phenomenon as possible only over a reduced supersaturation range. Others authors interested in the polymorphic behaviour of glycine did not observed the polarization switching phenomenon[10,13,14,46]. Finally, it seems that the polarization of the light does not have an influence on the polymorphism of the crystal produced in the case of glycine. In the case of carbamazepine and sulfathiazole, there are no other studies investigating the influence of the polarized light on the resulting polymorphs. But, Yu *et al*[47] used femtosecond laser and showed the influence of laser power on the ratio of polymorphic form obtained. In addition, polarization geometry had no effect on the NPLIN behaviour of several inorganic salts such as KCl[22] or $NaClO_3$[30]. In fact, the OKE mechanism is not applicable to explain NPLIN of molecules with isotropic polarizabilities.

2.4.2 **The dielectric polarization (DP)**

2.4.2.1 Definition

The dielectric polarization (DP) or isotropic electronic polarizability refers to the electronic polarization of isotropic compounds (i.e without preferential polarization axis). In this mechanism, the laser electromagnetic field shifts the electrons of the atom and deforms the electronic cloud as seen in Figure 2-7. Alexander and Camp[22] claimed that the pre-critical solid cluster free energy decreases when exposed to an electromagnetic field if the relative permittivity of the pre-critical solid cluster (ε_p) is superior to the one of the medium (solution) (ε_s): $\varepsilon_p > \varepsilon_s$. Thus, the dielectric free energy is added to the free energy equation (Chapter 1-Equation 1-6) to give Equation 2-1 with E the electric field strength and a, a function of the dielectric permittivity (a>0 when $\varepsilon_p > \varepsilon_s$).

$$\Delta G = 4\pi r^2\gamma - \frac{4}{3}\pi r^3(\Delta Gv + aE^2) \qquad \textit{Equation 2-1}$$

It results in the stabilization of the critical nucleus at smaller size and lower free energy barrier(ΔG) (Figure 2-8). The DP mechanism has been studied in the context of both the CNT[22] and TSN theories[13].

The DP mechanism does not rule out the OKE mechanism. DP mechanism can be seen as an extension of the OKE mechanism since OKE is restricted to anisotropic polarizabilities, DP brings an explanation for isotropic polarizabilities and compounds with no preferred polarization axis in the structure.

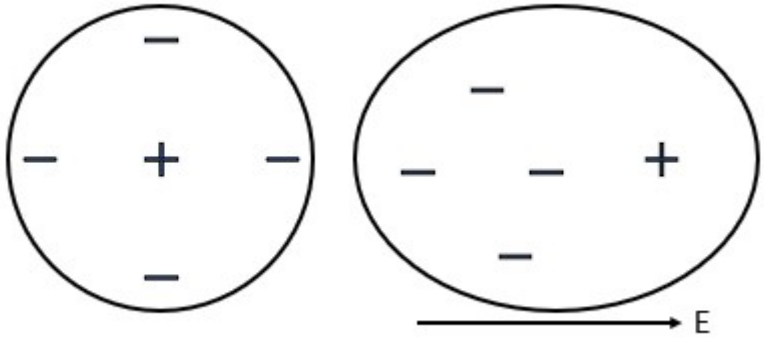

Figure 2-7- Deformation of the electronic cloud of an atom when an electric field is applied on the right. (without electric field on the left)

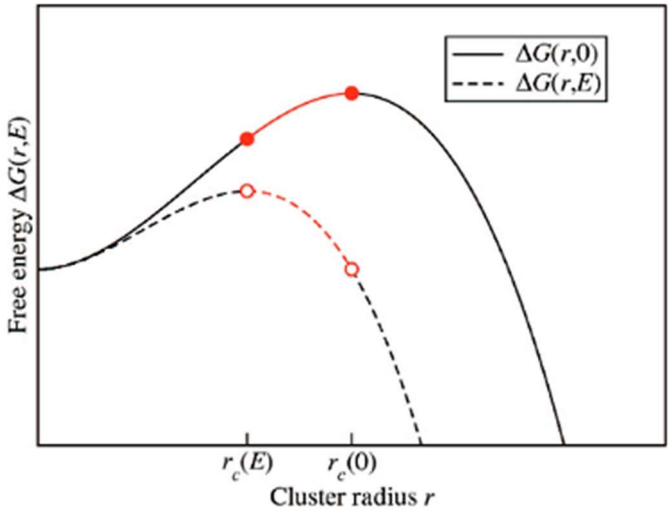

Figure 2-8- Lowering of the energy barrier in the presence of an electric field, adapted from Alexander and Camp[22]

2.4.2.2 Argument in favour of DP mechanism

The DP mechanism hypothesis arises from the observation of NPLIN for potassium chloride (KCl) aqueous solution[22]. KCl crystallizes in a cubic space group and has no preferential polarization axis and no dipole to align with the electromagnetic field of the laser (no OKE mechanism possible). The DP model using CNT predicts a linear dependence of the probability of nucleation to laser intensity which match their experimental data. Then, the DP mechanism was used to explain NPLIN of (i) potassium

bromide in the study of Ward et al[25] in which they observed a higher lability of KBr compared to KCl due to the higher relative permittivity of KBr, and (ii) supercooled acetic acid[34] in which calculation showed that the free energy of the clusters is lowered with an applied electric field.

The modelisation of DP mechanism offers good fit with experimental data and explain the variation of probability of nucleation with temperature, supersaturation, intensity and wavelength.[48] Moreover, the small influence of wavelength on NPLIN could be explained by the wavelength-dependent value of permittivity (ε).

2.4.2.3 Limits of DP mechanism

In the context of the CNT, Hua et al[13] showed that the DP mechanism is not in agreement with the experimental results for glycine. Indeed, the calculated lability (i.e susceptibility of a solution to nucleate) from the DP model is 15 orders of magnitude larger than the one obtained from experimental data. It is however more efficient in the context of the TSN nucleation where the theory and experiment coincide better. Considering polarization switching, the theory of the DP mechanism has no explanations for this phenomenon.

Moreover, the initial DP model predicts a zero threshold laser intensity, the model has to be shifted to account for the threshold value and fit the experimental data[22]. Also, according to Ward *et al* [34], as in the case of the OKE model, the laser energy involved in the DP model is too low to permit nucleation of the critical cluster even if their size is reduced by the electromagnetic field.

2.4.3 **Cavitation**

2.4.3.1 Definition

Cavitation is defined as the formation of bubbles of gas or vapor of solvent inside the solutions (Chapter 1- 1.3.6). Those bubble could collapse and lead to nucleation or act as a foreign particle and lead to heterogeneous nucleation. Crystallization induced by cavitation occurs during sonocrystallization (i.e ultrasound induced crystallization) or during mechanical shocks applied to the solution.

2.4.3.2 Argument in favour of cavitation

A first set of studies related to the formation of gaseous bubbles under laser irradiation lead the community to focus on the interconnections between laser induced gas cavitation and crystal nucleation. The NPLIN of CO_2 bubbles observed by Knott *et al*[32] was the first step towards the development of this cavitation mechanism. Given that CO_2 bubble has a smaller relative permittivity ($\varepsilon_p<\varepsilon_s$), the DP mechanism cannot stabilize the nucleus and the OKE mechanism is also not applicable since the nucleation of gas bubble would not be enhanced by an alignment of the molecules. Moreover, these authors also showed that gently shaking a co-supersaturating aqueous solution with glycine and argon, allows to release argon bubbles and lead to the crystallisation of glycine without the use of laser which evidences a link between bubble and nucleation. In addition, Alexander *et al*[49] have demonstrated the cavitation induced nucleation of ammonium chloride after mechanical shock.

Cavitation is the most popular mechanism when dealing with focused femtosecond laser pulse. Indeed, bubbles are observed in several system exposed to femtosecond laser as for example the case of anthracene[50], protein[51], acetaminophen[52] or sulfathiazole[47]. The only example of cavitation using a nanosecond laser is the study of Soare et al, yet they used focused laser beam and the solution were doped with ink to facilitate absorption and formation of bubble.

2.4.3.3 Limits of cavitation

Given that our study discusses the mechanism of NPLIN regarding nanosecond laser only, the cavitation mechanism as it is depicted for femtosecond laser may be not valid in the case of nanosecond laser. There is no evidence of bubble nucleation in the case of NPLIN studies using nanosecond, non-focused laser pulses, even though those bubbles could be short-lived and too small to be detected[32].

In addition, Kacker *et al*[27] measured the pressure variations after irradiation (1pulse at 80MW/cm², unfocused nanosecond laser) in masked vial and unmasked vial filled with the same solution. They observed a much higher peak pressure signal in masked vial but no nucleation and a lower peak pressure signal in unmasked vial but with nucleation. They concluded that the pressure measured was too low to influence nucleation kinetics and the cavitation by means of shock waves induced by the laser was unlikely.

Soare et al[29] stated however that ultrasonic cavitation differs from laser induced cavitation as ultrasound bubble are made of gas and laser bubble of vapor. Although cavitation is involved in both cases, the nucleation mechanism of the bubble and then the crystal may differ.

2.4.4 **Nanoparticle heating**

2.4.4.1 Definition

The nanoparticle heating mechanism implies the presence of nanoparticle in the solution that act in some handover process between laser irradiation and nucleation. When the supersaturated solution is exposed to laser pulses, various hypotheses regarding the behaviour of the nanoparticles upon irradiation and its consequence on solution nucleation have been proposed. The first step of this mechanism relies on the absorption of the laser energy by a solid impurity particle (Figure 2-9 a). Then the particle releases heat energy and triggers the nucleation of a short-lived cavity composed of gaseous matter or solvent vapor. It has been proposed that: (i) the gas bubbles formation could lead to a local and sudden increase in concentration resulting in heterogeneous nucleation (Figure 2-9 b), or (ii) the collapse of the bubble could produce a pressure wave that will induce the nucleation such as in sonocrystallization (i.e nucleation assisted by ultrasound) (Figure 2-9 c). It has also been proposed that, provided enough energy, the particle can be destroyed by the laser - in this case, the nucleation can occur due to the resulting shock or due to new heterogeneous interfaces. (Figure 2-9 d)

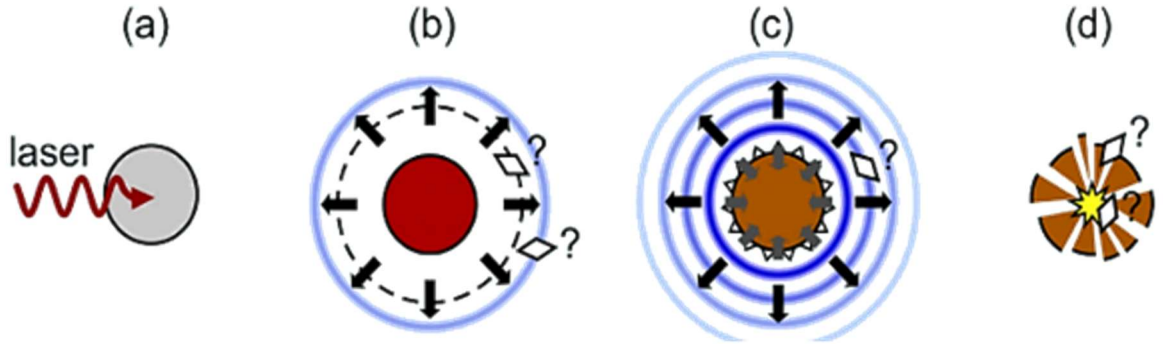

Figure 2-9- Possible behaviour of the nanoparticle regarding NPLIN induction. a) absorption/diffusion of the laser pulse by a particle b) heating of the surrounding solution and formation of gaseous/ vapor cavities. b) Collapsing of the cavity causes pressure wave d) destruction of the particle. Adapted from Alexander et al[48]

2.4.4.2 Argument in favour of nanoparticle heating mechanism

Ward *et al*[33] investigated the NPLIN of CO_2 gas bubbles from aqueous solutions doped with sucrose. Sucrose was used as an impurity, with concentration much lower than saturation. They have observed that the addition of sucrose increases the probability to nucleate CO_2 bubbles but that filtering the supersaturated solution induces a strong decrease of CO_2 nucleation rate. This lead to consider that some insoluble impurity particles coming from the sucrose lots must be present in solution prior to filtration, enhancing the NPLIN efficiency on CO_2. Several researches reported similar behaviors during their NPLIN studies: solution filtration most often results in a strong decrease of the NPLIN rate[9,22,27]. Ward *et al*[38] investigated the chemical nature of such impurity nanoparticles and found that they are composed mainly of iron and phosphorus. These impurities originate from ammonium chloride, but the impurity composition and size may differ from one compound to another. Moreover, Alexander *et al*[49] conducted a study on nucleation of ammonium chloride by mechanical shock and observe no influence of filtration nor doping of solution, which suggest a particular interaction between nanoparticle and the laser.

More hypotheses have been drawn out of these experimental observations[48]. (i) The systematic existence of an intensity threshold during NPLIN experiments could be due to the need of sufficient energy to heat the nanoparticles up to a level at which it can trigger nucleation of the solution. (ii) The different results observed in NPLIN experiments for the same compound could be due to differences in concentration and nature of the impurities. (iii) the polarization switching phenomenon could be explained by the difference of optical properties of the nanoparticles upon irradiation with linearly or circularly polarized light.

2.4.4.3 Limits of the nanoparticle heating mechanism

The cavitation mechanism describes the formation of bubbles induced by the laser which then induce the nucleation of the supersaturated compound. However, the mechanism by which bubble formation triggers the nucleation is not clear (Figure 2-9).

One should first question the energy required to heat a single nanoparticle in solution. Irimia *et al*[14] showed an elevation of temperature of only 0.6K for 600 pulses at 532nm and 4.5K for 600 pulses at 1064nm in supersaturated solutions. Yet, it is known that NPLIN can occur even if only one pulse is applied, while the temperature elevation for one single

pulse would be negligible, Irimia showed that one single pulse enables higher probability of nucleation than 600 pulses. Moreover, the probability of nucleation is also higher with the use of 532nm than 1064nm[7]. Thus, NPLIN is favoured when conditions minimize the temperature increase. So, is the energy of a single pulse at 532nm sufficient to generate a vapor bubble? Nevertheless, it should be noted that the temperature elevation measurement concerns the global temperature of the solution, the nanoparticle heating mechanism might involve a significant local temperature increase around the nanoparticle. For example, the exposition of gold nanoparticle solution to nanosecond laser pulse causes the nanoparticle to heat up to 700K[53], this heat is dissipated into the surrounding water, above a certain distance from the particle, the temperature of the solution is unchanged.[54]

Besides, the presence of bubbles is necessary but not sufficient to induce nucleation. A study shows that even in degassed solution there is still gas bubbles remaining in the solution with a concentration of 4.10^7/mL and a mean diameter of 250nm.[55]

2.5 SOLUTION PARAMETERS

They are five parameters linked to the solution preparation that can influence the NPLIN phenomenon. They are summarized in Table 2-2 and presented in detail in the following paragraphs.

Table 2-2- Summary of the parameters related to the solution, their influence on NPLIN phenomenon, and references in which the related parameters have been investigated.

Parameters	Influence	References
Supersaturation	- Probability of nucleation - Induction time - Polymorphism	7,10,14,22,27
Aging	- Probability of nucleation (organic molecules) - No influence (for inorganic salt)	5,13 22
Impurities	- Probability of nucleation	9,27,38
Viscosity	- Spatial control - Polymorphism	11,23
Solvent	- Probability of nucleation - Induction time - Polymorphism	36

2.5.1 **Solution Supersaturation**

Supersaturation is the most important parameter of the solution when dealing with crystallization from solution, since the supersaturation is the driving force for nucleation (Chapter 1-1.3.1). For NPLIN experiments the supersaturation has to be chosen so that the system is in the metastable zone (Chapter 1-1.3.2) in order to strongly reduce the rate of primary nucleation and to assert that any nucleation event is triggered by the laser irradiation. Depending on the compound studied, the metastable zone can be quite large, therefore a range of supersaturation can be investigated. At high supersaturation, the system is more labile to nucleate, the induction time decreases and the probability of nucleation increases. In return, the laser intensity threshold (see 2.6.3) required to nucleate is decreased.[7,10,14,22,27] As for regular solution crystallization, in NPLIN process, supersaturation also affects polymorphism. For instance, in the case of glycine Sun *et al*[7] and Liu *et al*[11] have shown that high supersaturation lead to γ-glycine and low supersaturation lead to α-glycine (see 2.4.1.2).

2.5.2 **Solution Aging**

Aging of the solution refers to the delay time before irradiation of the supersaturated solution after its preparation. Aging of the solution is a parameter which was mainly explored for the study of organic molecules [1,5,20,36,37]. Some authors claimed that aging of solution helps increasing the probability of nucleation by the creation of clusters during aging[5,13]. This waiting time is indeed regarded as necessary for the establishment of the "dense liquid precursors" in the first step of the TSN (two step nucleation) model (Chapter1-1.3.4), and the laser would facilitate crystal nucleation during the second step. However, in the case of inorganic salts, the authors claimed that the aging period had no influence on the kinetics of NPLIN[22]. Overall, there is no consensus on the impact of solution ageing on NPLIN induction times[48], it might be compound-dependent.

2.5.3 **Presence of Impurities**

It has been shown that the preparation procedure of the supersaturated solutions has also an influence on the NPLIN behavior. In particular, if the supersaturated solutions are filtered (usually using 0.2 µm syringe filters), a process which is believed to remove insoluble dusts, then a drastic reduction or even suppression of the NPLIN phenomenon has been reported. It seems that the presence of solid impurities in the solution

enhances nucleation[9,27,38]. This is further developed in the section 2.4.3 about the nanoparticle heating mechanism.

2.5.4 **Viscosity of the medium**

The use of a gelling agent like agarose in solution increases the viscosity of the medium and seems to increase the nucleation rate (reduce the induction time) and increase the number of crystals produced.[23] It was also shown that NPLIN experiments performed using a supersaturated gel matrix could influence the polymorphism of glycine.[11]

2.5.5 **Solvent Nature**

As shown in Table 2-1, the studied solutions are mostly aqueous. Nevertheless, Ikni *et al*[36] compared the influence of acetonitrile and methanol on carbamazepine nucleation by NPLIN. As expected, the solvent in which the molecule is the more soluble gives higher probability of nucleation. Moreover, the choice of the solvent can influence the polymorphism. They have showed that spontaneous nucleation in both solvent leads to form III of carbamazepine whereas via NPLIN methanol lead to form III also, but acetonitrile can lead to the formation of a mix of form I, II and III with different proportion.

2.6 LASER PARAMETERS

The laser parameters which have been reported to impact the NPLIN behaviour are summarized in Table 2-3 and presented in detail in the following paragraphs.

Table 2-3- Summary of the parameters related to the laser, their influence on NPLIN phenomenon, and related literature.

Parameters	Influence	References
Wavelength	- Little or no influence	3,7,20,25 27,32,42
Polarisation	- Polymorphism ? - Probability of nucleation - No influence	7,19,36,37 3 22
Intensity	- Probability of nucleation - Induction time	22,27,28,37
Number of pulses	- Number of crystals - Probability of nucleation - Induction time	14,22,28,37,38
Pulse duration	- Different mechanism - Influence to confirm	20,24
Focusing	- Cavitation	29,31,39

2.6.1 **Wavelength**

In most NPLIN studies, the lasers used emit at a wavelength of 1064nm or 532nm (double frequency). Since the process is regarded as a non-photochemical phenomenon, the wavelength of the laser used should not have an influence on the process. However, it has been observed that NPLIN at 1064nm is less effective than at 532nm.[3,7,20,25] Indeed, changing the working wavelength and the absorbance of the solvent is different. In the case of aqueous solution, water has a higher absorption coefficient at 1064nm than 532nm. Moreover, Irimia *et al*[14] measured temperature increase in a solution exposed to 600 pulses of 1064nm laser of at least 4K whereas it is less than 1K with a 532nm laser (with the same pulse energy). It is well known that the temperature considerably affects the supersaturation of the solution (Chapter1-1.3.1) and affects NPLIN efficiency (see section 2.5.1). Matic *et al*[3] has already advised the use of 532nm instead of 1064nm to avoid heating of aqueous solution. Yet, the use of 1064nm wavelength seems more common (see Table 2-1) and some researchers claimed that NPLIN is wavelength independent.[27,32,42]

2.6.2 **Polarization**

The polarization of the laser was reported to control the polymorphism as in the “polarization switching” observation made in the case of glycine[7] and L-histidine[16] NPLIN, but also in the cases of sulfathiazole[37] and carbamazepine[36]. The handedness of the circular polarized light has no influence on the NPLIN of L-histidine, for the other molecules the handedness was not specified. The polarization of the laser light is also reported to affect the nucleation of compounds that do not exhibit polymorphism, for example Matic *et al*[3] showed that linear polarization gives higher probability of nucleation than circular polarization in the case of urea (see section 2.4.1.2). However, in the case of sodium chloride, Alexander *et al*[22] did not observe any influence of the polarization. Besides, the use of circular polarized light is expected to help control the chirality of resulting crystals, a possibility that is not yet confirmed[16,30,31].

2.6.3 **Laser Intensity**

Laser Intensity is one of the main parameters that influences NPLIN. Higher laser intensities seem to decrease the induction time and increase the probability of nucleation[22,27,28,37]. In NPLIN experiments, several authors report an energy threshold below which no nucleation

occurs[3,6,13,22]. This threshold appears to be dependent of the supersaturation of the solution.[27]

2.6.4 **Number of pulses**

The number of pulses is a parameter that is complementary to the intensity parameters and also helps increasing the NPLIN efficiency. In addition, the number of pulses imposes the number of crystals nucleated. For example, Alexander *et al*[22] demonstrated that one single pulse allows to nucleate a single crystal. Moreover, the increase in the number of pulses increases the number of crystals obtained[37] but Hua *et al*[28] stated that the number of crystals is independent of the number of laser pulses. Yet, there is a limit, too many pulses can have an inverse effect: a lower efficiency of NPLIN due to heating of solution which decreases the supersaturation[14] or maybe to the destruction of cluster or impurities[38].

2.6.5 **Pulse duration**

Pulse duration is the time width of the laser pulse (Chapter1-1.4.3). A pulse duration covers several orders of magnitude from nanosecond to picosecond or femtosecond depending of the type of laser used. Yet, even if only nanosecond lasers are relevant to the work presented in this manuscript, there are still differences in pulse duration from one laser to another. Typical pulse width is between 5ns and 9ns. Ward *et al*[24] compared the impact of two different pulse widths (a short pulse of 6ns and a long pulse of 200ns) for NPLIN of KCl. They found no correlation between the probability of nucleation and the pulse width. However, Lee *et al*[20] suggest to use shorter pulse durations to minimize the energy absorbed and increase NPLIN efficiency.

2.6.6 **Focusing**

Focusing of the laser beam results in higher intensity as the illuminated surface is reduced. Usually NPLIN studies do not use focused laser beams but a few articles report the use of focused beams. Most studies using focused laser report cavitation phenomenon[29,31] or shock-waves[35,39,56]. Barber et al[31] showed the formation of plasma in the irradiated solution with a single nanosecond focused laser pulse and giving mostly one or two crystals. No comparative studies on the behaviour of NPLIN between a focused and unfocused laser are available.

2.7 REFERENCES

(1) Garetz, B. A.; Aber, J. E.; Goddard, N. L.; Young, R. G.; Myerson, A. S. Nonphotochemical, Polarization-Dependent, Laser-Induced Nucleation in Supersaturated Aqueous Urea Solutions. *Physical review letters* **1996**, *77* (16), 3475.

(2) Tyndall, J. *Philos.Mag.* **1869**, *37*, 384.

(3) Matic, J.; Sun, X.; Garetz, B. A.; Myerson, A. S. Intensity, Wavelength, and Polarization Dependence of Nonphotochemical Laser-Induced Nucleation in Supersaturated Aqueous Urea Solutions. *Crystal Growth & Design* **2005**, *5* (4), 1565–1567. https://doi.org/10.1021/cg050041c.

(4) Liu, Y.; Ward, M. R.; Alexander, A. J. Polarization Independence of Laser-Induced Nucleation in Supersaturated Aqueous Urea Solutions. *Phys. Chem. Chem. Phys.* **2017**, *19* (5), 3464–3467. https://doi.org/10.1039/C6CP07997K.

(5) Zaccaro, J.; Matic, J.; Myerson, A. S.; Garetz, B. A. Nonphotochemical, Laser-Induced Nucleation of Supersaturated Aqueous Glycine Produces Unexpected γ-Polymorph. *Crystal Growth & Design* **2001**, *1* (1), 5–8. https://doi.org/10.1021/cg0055171.

(6) Garetz, B. A.; Matic, J.; Myerson, A. S. Polarization Switching of Crystal Structure in the Nonphotochemical Light-Induced Nucleation of Supersaturated Aqueous Glycine Solutions. *Physical Review Letters* **2002**, *89* (17). https://doi.org/10.1103/PhysRevLett.89.175501.

(7) Sun, X.; Garetz, B. A.; Myerson, A. S. Supersaturation and Polarization Dependence of Polymorph Control in the Nonphotochemical Laser-Induced Nucleation (NPLIN) of Aqueous Glycine Solutions. *Crystal growth & design* **2006**, *6* (3), 684–689.

(8) Clair, B.; Ikni, A.; Li, W.; Scouflaire, P.; Quemener, V.; Spasojević-de Biré, A. A New Experimental Setup for High-Throughput Controlled Non-Photochemical Laser-Induced Nucleation: Application to Glycine Crystallization. *J Appl Cryst* **2014**, *47* (4), 1252–1260. https://doi.org/10.1107/S160057671401098X.

(9) Javid, N.; Kendall, T.; Burns, I. S.; Sefcik, J. Filtration Suppresses Laser-Induced Nucleation of Glycine in Aqueous Solutions. *Crystal Growth & Design* **2016**, *16* (8), 4196–4202. https://doi.org/10.1021/acs.cgd.6b00046.

(10) Liu, Y.; van den Berg, M. H.; Alexander, A. J. Supersaturation Dependence of Glycine Polymorphism Using Laser-Induced Nucleation, Sonocrystallization and Nucleation by Mechanical Shock. *Phys. Chem. Chem. Phys.* **2017**, *19* (29), 19386–19392. https://doi.org/10.1039/C7CP03146G.

(11) Tasnim, T.; Goh, A.; Gowayed, O.; Hu, C. T.; Chen, T.-Y.; Aber, J. E.; Garetz, B. A. Dendritic Growth of Glycine from Nonphotochemical Laser-Induced Nucleation of Supersaturated Aqueous Solutions in Agarose Gels. *Crystal Growth & Design* **2018**, *18* (10), 5927–5933. https://doi.org/10.1021/acs.cgd.8b00688.

(12) Gowayed, O.; Tasnim, T.; Fuentes-Rivera, J. J.; Aber, J. E.; Garetz, B. A. Non-Photochemical Pulsed-Laser-Induced Nucleation in a Continuous-Wave-Laser-Induced Phase-Separated Solution Droplet of Aqueous Glycine Formed by

Optical Gradient Forces. *Crystal Growth & Design* **2019**, *19* (12), 7372–7379. https://doi.org/10.1021/acs.cgd.9b01255.

(13) Hua, T.; Valentín-Valentín, C.; Gowayed, O.; Lee, S.; Garetz, B. A.; Hartman, R. L. Microfluidic Laser-Induced Nucleation of Supersaturated Aqueous Glycine Solutions. *Crystal Growth & Design* **2020**, acs.cgd.0c00669. https://doi.org/10.1021/acs.cgd.0c00669.

(14) Irimia, D.; Jose Shirley, J.; Garg, A. S.; Nijland, D. P. A.; van der Heijden, A. E. D. M.; Kramer, H. J. M.; Eral, H. B. Influence of Laser Parameters and Experimental Conditions on Nonphotochemical Laser-Induced Nucleation of Glycine Polymorphs. *Crystal Growth & Design* **2020**, No. 21, 631–641. https://doi.org/10.1021/acs.cgd.0c01415.

(15) Tsunesada, F.; Iwai, T.; Watanabe, T.; Adachi, H.; Yoshimura, M.; Mori, Y.; Sasaki, T. High-Quality Crystal Growth of Organic Nonlinear Optical Crystal DAST. *Journal of Crystal Growth* **2002**, *237–239*, 2104–2106. https://doi.org/10.1016/S0022-0248(01)02266-7.

(16) Murphy, N. C.; Compton, R. N.; Pagni, R. M. Effect of Chiral and Achiral Perturbations on the Crystallization of 4,4‘-Dimethylchalcone from Ethyl Acetate. *Crystal Growth & Design* **2007**, *7* (2), 449–452. https://doi.org/10.1021/cg0680125.

(17) Lindinger, B.; Mettin, R.; Chow, R.; Lauterborn, W. Ice Crystallization Induced by Optical Breakdown. *Phys. Rev. Lett.* **2007**, *99* (4), 045701. https://doi.org/10.1103/PhysRevLett.99.045701.

(18) Nevo, I.; Jahn, S.; Kretzschmar, N.; Levantino, M.; Feldman, Y.; Naftali, N.; Wulff, M.; Oron, D.; Leiserowitz, L. Evidence for Laser-Induced Homogeneous Oriented Ice Nucleation Revealed via Pulsed x-Ray Diffraction. *J. Chem. Phys.* **2020**, *153* (2), 024504. https://doi.org/10.1063/5.0006100.

(19) Sun, X.; Garetz, B. A.; Myerson, A. S. Polarization Switching of Crystal Structure in the Nonphotochemical Laser-Induced Nucleation of Supersaturated Aqueous L -Histidine †. *Crystal Growth & Design* **2008**, *8* (5), 1720–1722. https://doi.org/10.1021/cg800028v.

(20) Lee, I. S.; Evans, J. M. B.; Erdemir, D.; Lee, A. Y.; Garetz, B. A.; Myerson, A. S. Nonphotochemical Laser Induced Nucleation of Hen Egg White Lysozyme Crystals. *Crystal Growth & Design* **2008**, *8* (12), 4255–4261. https://doi.org/10.1021/cg800696u.

(21) Sun, X.; Garetz, B. A.; Moreira, M. F.; Palffy-Muhoray, P. Nonphotochemical Laser-Induced Nucleation of Nematic Phase and Alignment of Nematic Director from a Supercooled Thermotropic Liquid Crystal. *Phys. Rev. E* **2009**, *79* (2), 021701. https://doi.org/10.1103/PhysRevE.79.021701.

(22) Alexander, A. J.; Camp, P. J. Single Pulse, Single Crystal Laser-Induced Nucleation of Potassium Chloride. *Crystal Growth & Design* **2009**, *9* (2), 958–963. https://doi.org/10.1021/cg8007415.

(23) Duffus, C.; Camp, P. J.; Alexander, A. J. Spatial Control of Crystal Nucleation in Agarose Gel. *J. Am. Chem. Soc.* **2009**, *131* (33), 11676–11677. https://doi.org/10.1021/ja905232m.

(24) Ward, M. R.; Ballingall, I.; Costen, M. L.; McKendrick, K. G.; Alexander, A. J. Nanosecond Pulse-Width Dependence of Nonphotochemical Laser- Induced Nucleation of Potassium Chloride*. *481*, 13.

(25) Ward, M. R.; Alexander, A. J. Nonphotochemical Laser-Induced Nucleation of Potassium Halides: Effects of Wavelength and Temperature. *Crystal Growth & Design* **2012**, *12* (9), 4554–4561. https://doi.org/10.1021/cg300750c.

(26) Fang, K.; Arnold, S.; Garetz, B. A. Nonphotochemical Laser-Induced Nucleation in Levitated Supersaturated Aqueous Potassium Chloride Microdroplets. *Crystal Growth & Design* **2014**, *14* (5), 2685–2688. https://doi.org/10.1021/cg5004319.

(27) Kacker, R.; Dhingra, S.; Irimia, D.; Ghatkesar, M. K.; Stankiewicz, A.; Kramer, H. J. M.; Eral, H. B. Multiparameter Investigation of Laser-Induced Nucleation of Supersaturated Aqueous KCl Solutions. *Crystal Growth & Design* **2018**, *18* (1), 312–317. https://doi.org/10.1021/acs.cgd.7b01277.

(28) Hua, T.; Gowayed, O.; Grey-Stewart, D.; Garetz, B. A.; Hartman, R. L. Microfluidic Laser-Induced Nucleation of Supersaturated Aqueous KCl Solutions. *Crystal Growth & Design* **2019**, *19* (6), 3491–3497. https://doi.org/10.1021/acs.cgd.9b00362.

(29) Soare, A.; Dijkink, R.; Pascual, M. R.; Sun, C.; Cains, P. W.; Lohse, D.; Stankiewicz, A. I.; Kramer, H. J. M. Crystal Nucleation by Laser-Induced Cavitation. *Crystal Growth & Design* **2011**, *11* (6), 2311–2316. https://doi.org/10.1021/cg2000014.

(30) Ward, M. R.; Copeland, G. W.; Alexander, A. J. Chiral Hide-and-Seek: Retention of Enantiomorphism in Laser-Induced Nucleation of Molten Sodium Chlorate. *The Journal of Chemical Physics* **2011**, *135* (11), 114508. https://doi.org/10.1063/1.3637946.

(31) Barber, E. R.; Kinney, N. L. H.; Alexander, A. J. Pulsed Laser-Induced Nucleation of Sodium Chlorate at High Energy Densities. *Crystal Growth & Design* **2019**, acs.cgd.9b00951. https://doi.org/10.1021/acs.cgd.9b00951.

(32) Knott, B. C.; LaRue, J. L.; Wodtke, A. M.; Doherty, M. F.; Peters, B. Communication: Bubbles, Crystals, and Laser-Induced Nucleation. *J. Chem. Phys.* **2011**, *134* (17), 171102. https://doi.org/10.1063/1.3582897.

(33) Ward, M. R.; Jamieson, W. J.; Leckey, C. A.; Alexander, A. J. Laser-Induced Nucleation of Carbon Dioxide Bubbles. *The Journal of Chemical Physics* **2015**, *142* (14), 144501. https://doi.org/10.1063/1.4917022.

(34) R. Ward, M.; McHugh, S.; J. Alexander, A. Non-Photochemical Laser-Induced Nucleation of Supercooled Glacial Acetic Acid. *Physical Chemistry Chemical Physics* **2012**, *14* (1), 90–93. https://doi.org/10.1039/C1CP22774B.

(35) Jacob, J. A.; Sorgues, S.; Dazzi, A.; Mostafavi, M.; Belloni, J. Homogeneous Nucleation-Growth Dynamics Induced by Single Laser Pulse in Supersaturated Solutions. *Crystal Growth & Design* **2012**, *12* (12), 5980–5985. https://doi.org/10.1021/cg301024t.

(36) Ikni, A.; Clair, B.; Scouflaire, P.; Veesler, S.; Gillet, J.-M.; El Hassan, N.; Dumas, F.; Spasojević-de Biré, A. Experimental Demonstration of the Carbamazepine Crystallization from Non-Photochemical Laser-Induced Nucleation in Acetonitrile

and Methanol. *Crystal Growth & Design* **2014**, *14* (7), 3286–3299. https://doi.org/10.1021/cg500163c.

(37) Li, W.; Ikni, A.; Scouflaire, P.; Shi, X.; El Hassan, N.; Gémeiner, P.; Gillet, J.-M.; Spasojević-de Biré, A. Non-Photochemical Laser-Induced Nucleation of Sulfathiazole in a Water/Ethanol Mixture. *Crystal Growth & Design* **2016**, *16* (5), 2514–2526. https://doi.org/10.1021/acs.cgd.5b01526.

(38) Ward, M. R.; Mackenzie, A. M.; Alexander, A. J. Role of Impurity Nanoparticles in Laser-Induced Nucleation of Ammonium Chloride. *Crystal Growth & Design* **2016**, *16* (12), 6790–6796. https://doi.org/10.1021/acs.cgd.6b00882.

(39) Mirsaleh-Kohan, N.; Fischer, A.; Graves, B.; Bolorizadeh, M.; Kondepudi, D.; Compton, R. N. Laser Shock Wave Induced Crystallization. *Crystal Growth & Design* **2017**, *17* (2), 576–581. https://doi.org/10.1021/acs.cgd.6b01437.

(40) Liu, Y.; Qiu, Q.; Ding, G.; You, W. Effect of Acidic Polymers on the Morphology of Laser-Induced Nucleation of Cesium Chloride. *ACS Omega* **2021**. https://doi.org/10.1021/acsomega.0c04902.

(41) Liu, Y.; He, H.; Liu, Y. Morphology Control of Laser-Induced Dandelion-like Crystals of Sodium Acetate through the Addition of Acidic Polymers. *J Appl Cryst* **2021**, *54* (4). https://doi.org/10.1107/S1600576721005409.

(42) Barber, E. R.; Ward, M. R.; Ward, A. D.; Alexander, A. J. Laser-Induced Nucleation Promotes Crystal Growth of Anhydrous Sodium Bromide. *CrystEngComm* **2021**. https://doi.org/10.1039/D1CE01180D.

(43) Garetz, B. A. The Kerr Effect. *Optics News* **1986**, *12* (10), 28. https://doi.org/10.1364/ON.12.10.000028.

(44) Aber, J. E.; Arnold, S.; Garetz, B. A.; Myerson, A. S. Strong Dc Electric Field Applied to Supersaturated Aqueous Glycine Solution Induces Nucleation of the γ Polymorph. *Phys. Rev. Lett.* **2005**, *94* (14), 145503. https://doi.org/10.1103/PhysRevLett.94.145503.

(45) Knott, B. C.; Doherty, M. F.; Peters, B. A Simulation Test of the Optical Kerr Mechanism for Laser-Induced Nucleation. *The Journal of Chemical Physics* **2011**, *134* (15), 154501. https://doi.org/10.1063/1.3574010.

(46) Liu, T.-H.; Uwada, T.; Sugiyama, T.; Usman, A.; Hosokawa, Y.; Masuhara, H.; Chiang, T.-W.; Chen, C.-J. Single Femtosecond Laser Pulse-Single Crystal Formation of Glycine at the Solution Surface. *Journal of Crystal Growth* **2013**, *366*, 101–106. https://doi.org/10.1016/j.jcrysgro.2012.11.018.

(47) Yu, J.; Yan, J.; Jiang, L. Crystallization of Polymorphic Sulfathiazole Controlled by Femtosecond Laser-Induced Cavitation Bubbles. *Crystal Growth & Design* **2021**. https://doi.org/10.1021/acs.cgd.0c01476.

(48) Alexander, A. J.; Camp, P. J. Non-Photochemical Laser-Induced Nucleation. *J. Chem. Phys.* **2019**, *150* (4), 040901. https://doi.org/10.1063/1.5079328.

(49) Sun, Y.; Alexander, A. J. Mechanical Shock-Induced Nucleation in Solution: Is Cavitation Necessary? *Journal of Crystal Growth* **2022**, 126786. https://doi.org/10.1016/j.jcrysgro.2022.126786.

(50) Nakamura, K.; Hosokawa, Y.; Masuhara, H. Anthracene Crystallization Induced by Single-Shot Femtosecond Laser Irradiation: Experimental Evidence for the

Important Role of Bubbles. *Crystal Growth & Design* **2007**, *7* (5), 885–889. https://doi.org/10.1021/cg060631q.

(51) Yoshikawa, H. Y.; Murai, R.; Sugiyama, S.; Sazaki, G.; Kitatani, T.; Takahashi, Y.; Adachi, H.; Matsumura, H.; Murakami, S.; Inoue, T.; Takano, K.; Mori, Y. Femtosecond Laser-Induced Nucleation of Protein in Agarose Gel. *Journal of Crystal Growth* **2009**, *311* (3), 956–959. https://doi.org/10.1016/j.jcrysgro.2008.09.137.

(52) Wang, S.; Wang, S.; Jiang, L.; Wang, M.; Wei, Y.; Sun, J.; Zhan, S.; Li, X.; Qu, L. Polymorph-Controlled Crystallization of Acetaminophen through Femtosecond Laser Irradiation. *Crystal Growth & Design* **2019**, *19* (6), 3265–3271. https://doi.org/10.1021/acs.cgd.9b00123.

(53) Letfullin, R. R.; George, T. F.; Duree, G. C.; Bollinger, B. M. Ultrashort Laser Pulse Heating of Nanoparticles: Comparison of Theoretical Approaches. *Advances in Optical Technologies* **2008**, *2008*, 1–8. https://doi.org/10.1155/2008/251718.

(54) Sassaroli, E.; Li, K. C. P.; O'Neill, B. E. Numerical Investigation of Heating of a Gold Nanoparticle and the Surrounding Microenvironment by Nanosecond Laser Pulses for Nanomedicine Applications. *Phys. Med. Biol.* **2009**, *54* (18), 5541–5560. https://doi.org/10.1088/0031-9155/54/18/013.

(55) Lee, J. I.; Yim, B.-S.; Kim, J.-M. Effect of Dissolved-Gas Concentration on Bulk Nanobubbles Generation Using Ultrasonication. *Sci Rep* **2020**, *10* (1), 18816. https://doi.org/10.1038/s41598-020-75818-8.

(56) Gharib, S. A.; El Omar, A. K.; Naja, A.; Deniset-Besseau, A.; Denisov, S. A.; Pernot, P.; Mostafavi, M.; Belloni, J. Anisotropic Time-Resolved Dynamics of Crystal Growth Induced by a Single Laser Pulse Nucleation. *Crystal Growth & Design* **2021**, *21* (2), 799–808. https://doi.org/10.1021/acs.cgd.0c01016.

Chapter 3. MATERIAL & METHODS

3.1 CHEMICAL MATERIALS

During this work, different compounds were studied. The compound used as well as purity and suppliers are listed in Table 3-1 and were used without any further purification. Solutions were prepared with demineralized water (2-8 µS.cm^{-1}) supplied by an osmosis unit water purification system from OSMOTECH (Buchelay, France).

Table 3-1-List of compounds used with purity and supplier

Name	Purity	Supplier
Potassium sulfate	99%	MERCK
EDS	≥ 97%	MERCK
Diprophylline	>98%	MERCK

3.2 MEASURE OF SOLUBILITY

All solubility values reported in this work have been evaluated by gravimetric measurements using the following procedure: A suspension of crystals (marketed solid form) in a given solvent has been stirred at least 12h at a given temperature. The saturated solution was then filtered and weighted ($m_{saturated\ solution}$). After evaporation of the solvent in an oven at 50°C, the dry residue corresponding to the dissolved compound has been weighted ($m_{dry\ residue}$). The ratio of the masses gives the solubility S at the chosen temperature (Equation 3-1)

$$S = \frac{m_{dry\ residue}}{m_{saturated\ solution}} \cdot 100 \qquad \textit{Equation 3-1}$$

In the context of NPLIN experiments, the solubility values are appropriate if: (i) the values are sufficiently sensitive to temperature to allow cooling crystallization (ii) the solubility is high enough to obtain crystals of a size that can be detected with the naked eye but (iii) not too high to avoid uncontrolled crystallization and caking.

3.3 PREPARATION OF SUPERSATURATED SOLUTION

A stock solution is prepared at the desired concentration in order to be supersaturated at the working temperature and in the MSZW (determined from control sample and spontaneous nucleation). To prepare the solution defined masses of compound and solvent are weighted. The solution is heated until a homogeneous solution is obtained. The hot solution is transferred in vials (borosilicate glass. dimensions: 1.2 cm diameter, 1 mm thickness, total height 2.6 cm) with a precision pipette set at 1mL, the cone is changed every 5 vials. Each vial is carefully closed with a screw cap equipped with a rubber seal to avoid evaporation. All the vials are placed

in the oven for at least 3 hours, the temperature of T=50°C was sufficient for all our experiments to ensure complete dissolution of the solute. It was confirmed that no solvent evaporation occurred during this step. Then the vials are placed in a thermostated room at 20°C to reach supersaturation at least 1h before irradiation. This 1h wait is the minimum aging time to ensure the solution is cooled and is in a quiescent state. (The time is counted from the moment the vials are removed from the oven)

3.3.1 **Filtration**

When required, filtration of the samples was performed with hot solution, either with syringe filters (PTFE) or membrane filter. In the case of syringe filters, two sizes were used, 0.2µm or 0.45µm. The hot solution was collected with a 1mL syringe and passed over the filter to fill the vial. This was repeated until all the stock solution was used. The syringe and filter used were changed every 5 vials. In the case of membrane filter, all the solutions were passed through the same membrane and collected in the flask before being distributed in the vials as described in section 3.3. (see Figure 3-1 for the set-up of the filtration process). Special care was taken to ensure that no nucleation occurred during filtration, that could change the supersaturation. The concentration of the filtered solution was checked by gravimetry.

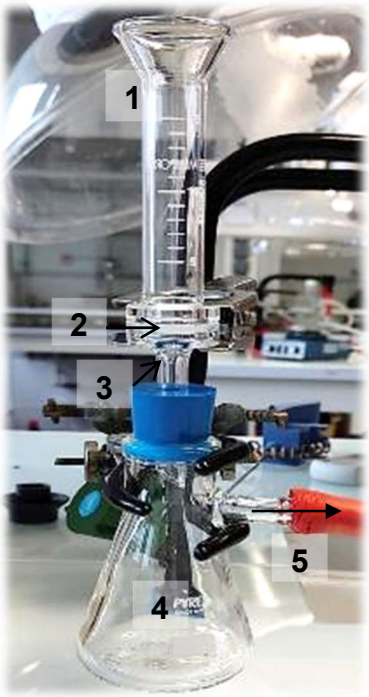

Figure 3-1-Membrane filtration set-up. 1)Funnel 2) membrane 3) Fritted glass support 4) flask 5) vacuum pump

3.3.2 **Doped solution**

To evaluate the influence of impurities, solutions were doped with known particles such as Gold nanoparticles aqueous solution stabilized with citrate buffer, Silver nanoparticles aqueous solution stabilized with citrate buffer, Stainless steel (316L) particle or rust (obtained from aqueous suspension of steel, when the solution turns orange-brown, the supernatant is filtered and the dry filter is gently scraped to recover the rust powder). The characteristics of the different particle used are detailed in Table 3-2.

Table 3-2-Characteristics of the particles used to dope solutions.

Nature of particle	Gold	Silver	Stainless Steel (316L)	Rust (“rouge”)
Supplier	MERCK	MERCK	GPM laboratory INSA	Produced from Stainless steel
Size	10nm	10nm	20-50µm	/
Appearance	Pink solution	Yellow solution	Grey powder (that settles)	Brown powder (suspension)
Concentration	0.06mg/mL	0.02mg/mL	/	/
λ_{max} (nm)	520	400	/	/

In the case of powder particles, they were added in the filtered stock solution. Stainless steel was added in higher quantity as the powder settles at the bottom of the vials. In the case of particles in aqueous suspension, the solution was prepared with an amount of water minus the amount of doping solution to add. The solution is filtered, and then the doping solution is added. Small amount of gold and silver solution were added in order to avoid the coloration of the solution.

Table 3-3-Concentration of the doping agent per gram of compound studied

	Gold[1]	Silver[1]	Stainless Steel (316L)	Rust
Volume or mass (for 15g EDS)	1.67mL	5mL	1g	2.5mg
Concentration mg/gEDS	0.006	0.006	60	0.16
Number of particles (in EDS solution)	$9.98.10^{12}$	$1.80.10^{13}$	/	/

3.3.3 **Gas saturation**

To study the influence of dissolved gas on the NPLIN behaviour of K_2SO_4, the above protocol was applied with the following modification. First, water was sonicated in an ultrasonic bath (VWR USC100T, 45KHz, 30W) for five minutes for degassing, then adequate amount of K_2SO_4 was added and the vessel containing the stock solution was rapidly sealed. While heating the stock solution, the selected gas was bubbled into the solution by using a gas filled balloon connected to a needle for at least 30 min. Nitrogen gas was purchased from Air liquide with a purity of 99.9999% (Alphagaz2). Carbon dioxide was produced by chemical reaction between calcium carbonate (RP Normapur 99%) and hydro-chloric acid 37% from VWR Chemicals. 1mL of solution is drawn out with a needle to fill the vials. At least 100 vials (4 sets of 25 vials) for each condition were exposed to laser as usual using one pulse at 85.6mJ.

3.4 LASER SET-UP

The laser used in this work is a nanosecond Q-switched Nd-YAG (NL300, EKSPLA, Vilnius, Lituania distributed by Opton Laser, France). This laser emits pulses at a wavelength of 1064nm, for a duration of 5.3ns with a pulse repetition frequency of 10Hz. With the addition of a module in front of the laser, the wavelength can be converted to 532nm (Chapter 1-1.4.4) as showed in the Figure 3-2,B.

The beam diameter at laser output is of 6mm (Figure 3-2 (1)). The polarization geometry of the laser light (linear or circular) was control by a quarter-wave plate placed on the beam path (Figure 3-2 (2)). The pulse energy was measured by means of a power meter NOVA II with a pyroelectric sensor (PE50BF-DIFH-C (OPHIR, Jerusalem, Israel distributed by MKS, Virigneux, France). Table 3-4 indicates the correspondence between measured energy and calculated intensity.

Table 3-4-Correspondence table between Energy and Intensity

Energy per pulse (mJ/pulse)	Intensity (MW/cm²)
18.0	12
34.8	23
51.5	34
68.4	46
85.6	57
102.4	68

As the vial containing the solution is cylindrical, it acts as a focusing lens thus the beam spot is reduced to an elliptical shape of 3x6mm at the exit of the vial. Therefore, the irradiated volume is considered as the one of a truncated cone, 0.20mL are irradiated corresponding to 20% of the total volume of solution in the vial (1mL). Moreover, it is considered that the vial surface is reflecting the laser light which reduces the energy received by the solution of an estimated value of circa 4% (the reflexion coefficient (R) is calculated with Equation 3-2, considering the indexes of refraction n_{air} = 1.0003; n_{glass} = 1.5066)

$$R = \frac{(n_{air} - n_{glass})^2}{(n_{air} + n_{glass})^2} = \frac{(1.0003 - 1.5066)^2}{(1.0003 + 1.5066)^2} = 0.04 \qquad \text{Equation 3-2}$$

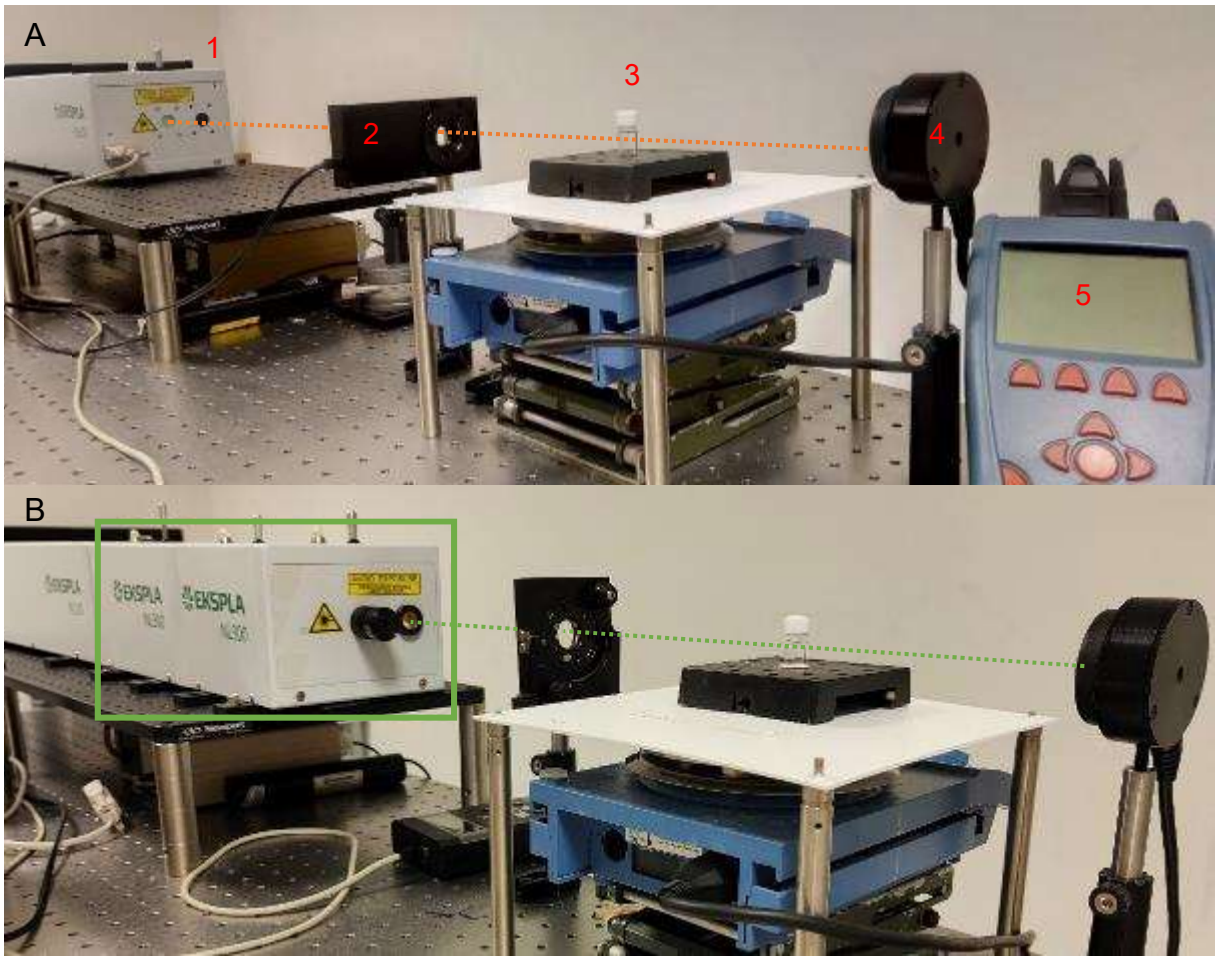

Figure 3-2-Set up of the irradiation of the supersaturated solutions. 1- Laser source 2- Quarter-wave plate 3- Vial containing supersaturated solution 4,5- Power meter. A- 1064nm set-up. B- 532nm set-up.

3.5 NPLIN EXPERIMENTS

3.5.1 Laser exposure

Vial containing supersaturated solutions were carefully and manually moved to be irradiated one by one (control sample were also moved in order to ensure nucleation is not due to the vials movement). To confirm that the nucleation is induced by the laser, at least 10% of the vials were not irradiated, they are hereafter called “control samples”. In some cases, in order to compare the spontaneous nucleation kinetics to the NPLIN kinetics, the number of control sample were the same that NPLIN sample. The number of pulses, intensity, polarization and wavelength were determined for each experiment before irradiation according to the compound studied and the desired objective.

3.5.2 **Collecting the results**

Nucleation via laser pulse is still a stochastic event that needs statistical data analysis. After irradiation of the samples, the nucleation was monitored visually by inspecting the vials with naked eyes. Three factors were used to evaluate the efficiency of NPLIN.

The first factor was the induction time (t_i) which is the time between laser exposure and the observed onset of nucleation. Obviously, the value is overestimated since it is impossible to observe the onset of nucleation, the crystal must grow to be detected.

The second factor was the probability of nucleation over time ($P_n(t)$). It represents the number of crystallized vials after a time t ($N_{cryst}(t)$) over the total number of irradiated vials (N_{vials}). (Equation 3-3)

$$P_n(t) = \frac{N_{cryst(t)}}{N_{vials}} * 100 \qquad \text{Equation 3-3}$$

The third factor focused on the crystals produced. The mean number of crystals per vial was determined for each set of experiments. In addition, crystals morphologies were observed via optical microscope.

Then, according to the compound studied, analytical techniques were used to check the polymorphism or the chirality.

3.6 ANALYTICAL TECHNIQUES

3.6.1 **X-Ray diffraction**

X-ray powder diffraction (XRPD) analyses were performed by D8-discover diffractometer (Bruker) equipped with a goniometer of geometry θ/θ, a copper anode (Kα 1.5418 Å) and a Lynx Eye linear detector.

Temperature resolved X-ray powder diffraction (TR-XRD) analyses were performed by D8 diffractometer (BRUKER) with a sample holder thermostated with a TTK 450 Anton parr heating chamber. Diffraction pattern of EDS were recorded during heating stage and cooling stage and at particular temperature of 240°C, over the 2θ range 4-80° by steps of 0.02° with 1s per step.

3.6.2 **Differential scanning calorimetry**

Differential scanning calorimetry was used to study the behaviour of the compound with temperature. The analyses were performed on a DSC 214 Polyma Netzsch apparatus, with aluminium pan closed or with pierced lid at rate of 2, 5 and 10K/min. Proteus software was used to analyses the data.

3.6.3 **Microscopy**

Microscope NIKON SMZ-10A equipped with a Sony DXC-950 3CCD Color Video Camera Power HAD was used to obtain pictures of crystals morphologies. Microscope NIKON Eclipse LV100 equipped with polarizer/analyser was used to identify the handedness of crystals of EDS. When the microscope is equipped with hot stage device (Linkam THMS 600), the behaviour of crystal with temperature can be observed.

3.6.4 **Second harmonic generation (SHG)**

SHG is a non-linear optical effect that occurs only in non-centrosymmetric crystals. It consists of an interaction between a laser light at wavelength λ and a solid crystalline material which results in the emission of a light with half wavelength ($\lambda/2$).

A femtosecond laser (Insight X3, spectaphysics) tunable over a range of wavelength from 680 to 1300nm coupled with a Leica SP8 confocal microscope was used to analyse the SHG response of the sample. The sample was exposed to a given wavelength and the detector used to collect intensity at half the excitation wavelength. SHG analyses were performed either on small single crystal or on powder. With a Linkam device, it was possible to perform the analyses at different temperatures and therefore follow the phase transitions of the sample.

3.6.5 **UV-visible spectroscopy**

Absorption spectra of saturated solutions were recorded using a lambda 35 UV/vis spectrophotometer from PerkinElmer. Sample were analysed in PMMA cell in the range of 400-1100nm with a resolution of 1nm. The blank reference was an empty cell.

3.6.6 **FTIR spectroscopy**

Infrared spectra were acquired using ATR-FTIR alpha-P spectrophotometer (Bruker). Samples were placed on the crystal of the ATR and spectra were recorded at room temperature, with 24 scans from 400 to 4000 cm^{-1} with a spectral resolution of 4 cm^{-1}.

3.6.7 **ICPE spectroscopy**

Inductively Coupled Plasma Emission (ICPE) Spectroscope (9800-Shimadzu) was used for elemental analysis of the remaining impurities after solution filtration. The PTFE filter membranes with impurities and without (control sample) were soak in hydrochloric acid (35%) for a day, and then the membrane was removed, and the solution diluted by 10 with water before analysis. The solution was injected into a plasma, which allows to ionize the sample which then emits a characteristic wavelength allowing the identification and an intensity proportional to the quantity. Three analyses were made for each sample in order to check the reproducibility of the results.

3.6.8 **Atomic force microscopy AFM**

AFM analysis allows to measure the roughness of a sample. In this work, the analysis was conducted in the Air contact mode, with a classic pyramid C-probe (0.38N/m), at scanning speed from 0.5 to 1Hz. Pictures are measured at different scales to get a global view of the sample and a more detailed view. The analysis gives results values such as the average roughness (Ra) and the maximum roughness (Rz).

3.6.9 **Scanning electron microscopy**

The SEM produce picture that shows the surface texture of the sample. The analysis was performed with a Jeol JCM 5000 NeoScope instrument. Glass vial samples were coated with gold layer prior to analysis. (Neo coater MP-19020NCTR).

Chapter 4. INVESTIGATING THE NPLIN BEHAVIOUR OF POTASSIUM SULFATE

4.1 INTRODUCTION

During this PhD work, the NPLIN phenomenon was studied through the case of potassium sulfate (K_2SO_4) in water. It is indeed a good candidate, since the K_2SO_4-H_2O system does not exhibit any hydrate and crystallizes from water as a single form at room temperature (i.e no concomitant polymorphism[1]) which facilitates the interpretation of the results. K_2SO_4 was found to be an interesting candidate to evaluate the influence of several parameters on the NPLIN kinetics such as the number of pulses and intensity, polarization, supersaturation, solvent, gelling, solution filtration. The nature and composition of the dissolved gas in solution and their impact on the NPLIN phenomenon was also examined.

4.1.1 Solid state

Under atmospheric pressure, K_2SO_4 crystallises in the orthorhombic space group *P*nam (n°62)[2] which is the stable polymorph (β-form) up to 583°C, above which it transforms into the α-form (*P*6$_3$/mmc (n°194))[3]. The crystallization of the high temperature polymorph (α-form) is not possible under the experimental conditions of our NPLIN study since the working temperature is of 20°C (Chapter 3- §3.3) and if heating occurs due to the laser pulses, the temperature of the aqueous solution cannot exceed 100°C (the boiling point) (Chapter 2-§2.4.4). There is also no hydrate of K_2SO_4 reported in literature and we did not observe any during our investigations. The study of the β-form crystal structure and birefringence values from literature[4] indicate that there is no strong polarization axis in the structure since the three refractive indices (one for each direction of the structure) are similar.

4.1.2 Solubility of Potassium sulfate

K_2SO_4 is an inorganic salt, principally soluble in water. First, it was important to measure the solubility in water in order to establish the crystallization conditions suitable for our nucleation study. The solubility in water was measured by the gravimetric method at two temperatures (Chapter 3- §3.2). The measured solubilities at 20 and 40°C are 10.05 and 12.81 %wt respectively. The solubility of K_2SO_4 in water is therefore said to be “normal” (Chapter 1- §1.3.1) and increases with temperature as opposed to the case of “retrograde” solubility, observed for instance in the case of sodium sulfate (Na_2SO_4[5]). The values are in good agreement with literature[6,7], as highlighted in Figure 4-1.

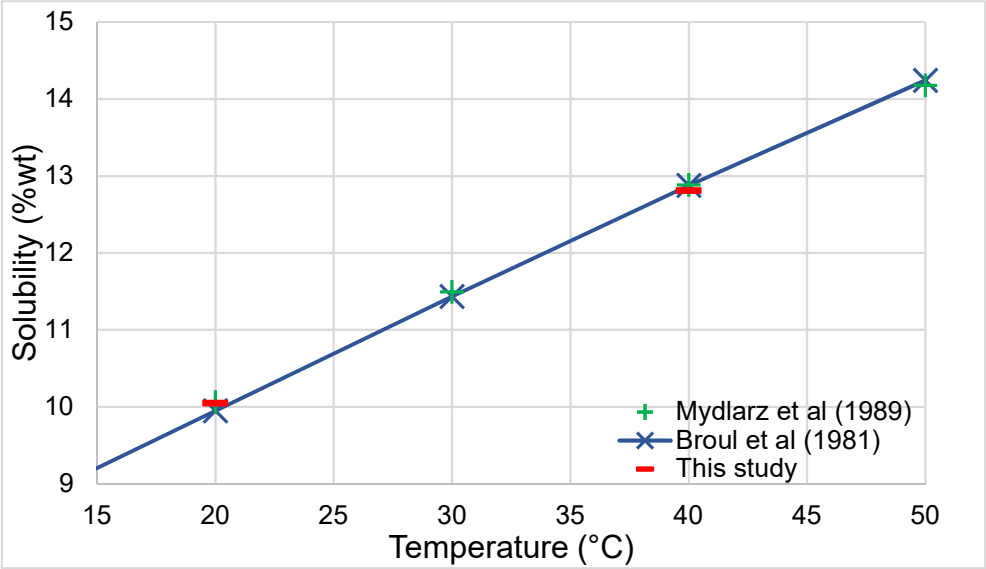

Figure 4-1-Representation of the experimentally measured aqueous solubility of K_2SO_4 as a function of temperature.

The solubility was also measured by gravimetry at 20°C in three aqueous-organic solvent mixtures: H_2O/Acetone, H_2O/Methanol and H_2O/Ethanol with a ratio of 10%wt of organic solvent in water. The solubility values obtained are presented in Table 4-1 and are in good agreement with those of Mydlarz *et al*.[8].

Table 4-1-Solubility values measured at 20°C for three water/organic solvent mixtures (10%wt). MeOH: methanol, EtOH: ethanol.

	H_2O/MeOH	H_2O/EtOH	H_2O/Acetone
Solubility (%wt)	4.5	4.2	4.7

The strong solubility decrease (of more than 50%) is obviously due to the fact that methanol, ethanol and acetone are very poor solvent for potassium sulfate.

4.1.3 **Spectroscopy UV-vis**

To design the NPLIN experiments, it was also necessary to confirm the absence of light absorption by the K_2SO_4 solutions in order to rule out any possibility of photochemical effects. The absorbances of a saturated solution of K_2SO_4 in demineralized water and that of pure demineralized water were measured by using UV-vis spectroscopy. The absorption spectra are shown in Figure 4-2. Pure water is known to absorb light at 980nm, and weaklier at 760nm and 840nm[9–11] and to exhibit higher absorbance in the NIR region at 1190, 1450 and 1940 nm[12]. At the working wavelength of 1064nm (represented by the vertical dashed line in Figure

4-2) there is little absorption of the K_2SO_4 solution, which is mainly due to the water absorption. This absorption is however very weak, and no photochemical reactions of K_2SO_4 are expected (nor was observed during this study). The negative absorption observed is due to the automatic suppression of the reference spectrum of the empty cell on the spectrum of the sample.

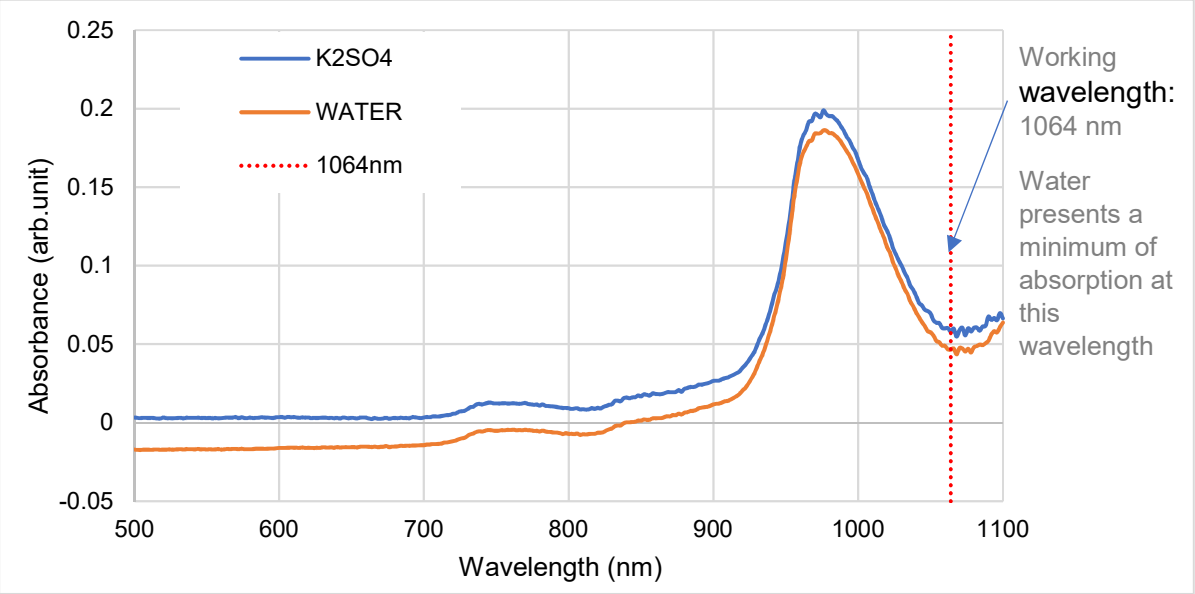

Figure 4-2-Absorption spectra of water and saturated aqueous solution of K_2SO_4.

4.1.4 Heating effect upon irradiation of a K_2SO_4 solution

The small absorption of water and aqueous solution of K_2SO_4 at 1064nm can however lead to heating of the solution exposed to the laser. In order to evaluate the temperature increase in the solution the temperature was measured with a thermocouple thermometer before and just after irradiation with a variable number of pulses with an energy of 85.6mJ/pulse.

Table 4-2 summarizes the temperature differences measured for different number of pulses on K_2SO_4 supersaturated solution at β=1.25. The temperature increase reaches almost 3 °C when 1200 pulses are used. In order to minimize the temperature increase, the parameters of irradiation will not exceed 100 pulses for the rest of the study. Using the same theoretical model developed and experimentally validated by Irimia *et al.*[13] the increase of temperature was calculated to be $2.4.10^{-3}$ K/pulse (with Cp=3.75 $J.g^{-1}K^{-1}$). Irimia *et al.*[13] also discussed the effect of an excessive number of pulses (over 600 pulses). They showed a decrease of the

probability of nucleation due to the overall temperature increase and associated supersaturation decrease of the solution.

Table 4-2-Measured temperature increases of K_2SO_4 solutions at β=1.25 as a function of the number of pulses (for an energy of 85.6mJ/pulse at 1064nm).

Number of pulses	ΔT (±0.1)
100	0.3
200	0.6
400	1.3
600	1.7
1200	2.7

4.2 STUDY OF THE NPLIN OF POTASSIUM SULFATE FROM WATER SOLUTION

This section reports the experimental results collected. The experimental set up and the methodology applied for statistical analyses of NPLIN induction times are fully described in Chapter 3. It is necessary to remind here that for every given NPLIN experimental set, at least 10% of the samples were not irradiated and serves as the reference to confirm the NPLIN effect.

4.2.1 Influence of supersaturation

As for regular crystallization process design, the first parameter that was investigated in this study was supersaturation. The range of investigated supersaturations should obviously be located in the MSZW of the compound (Chapter 2-§2.5.1). Indeed, supersaturation has to be sufficiently high for the nucleation kinetics (either spontaneous or NPLIN) to be measurable at reasonable time scale. Conversely, supersaturation has to be sufficiently low to avoid uncontrolled crystallization that would blur the limit between spontaneous crystallization and NPLIN. In the case of the K_2SO_4 water system, an adequate supersaturation range was therefore chosen via preliminary experiments. It was established that a $1.15<\beta<1.25$ supersaturation range fulfils the above criteria. The metastable zone limit was not determined but the supersaturation chosen are under this limit, which is confirmed by the control samples.

To study the influence of supersaturation on the NPLIN kinetics of K_2SO_4 at 20°C in water, vials containing the metastable solution of K_2SO_4 at supersaturation of β=1.25, 1.20 and 1.15 (at least 50 vials in each case) were exposed to one laser pulse with a pulse energy of 18 mJ at the entrance of the vial. The number of pulses was limited to a single shot in order to minimize the heating effect due to the water absorption at 1064 nm. In parallel, control samples (at least 10 vials for each value of β) prepared with the same procedure were not exposed to laser light to compare the kinetics of spontaneous crystallization with that of NPLIN experiments and thus confirm the presence of the NPLIN phenomenon.

The results, presented in Figure 4-3, highlight the presence of a NPLIN phenomenon in the K_2SO_4 – water system. Indeed, at each investigated β value, the irradiated samples have higher probability of nucleation and lower induction times than the control samples. For example, Figure 4-3 shows that 24h after irradiation, the probability of nucleation of all irradiated samples is doubled compared to the corresponding control samples. As expected, Figure 4-3 highlights that in the NPLIN process, the control of supersaturation is as important as in any nucleation process: the higher the supersaturation, the more labile to nucleation the system is, since higher supersaturations result in higher NPLIN probabilities. Although not shown in Figure 4-3, the probability of nucleation of β=1.20 and 1.15 samples both converge to a probability of nucleation of 100% after circa 72h.

Supersaturation of β=1.25 was chosen for the rest of the study as it offers the smallest induction time and the largest gap between NPLIN and spontaneous nucleation.

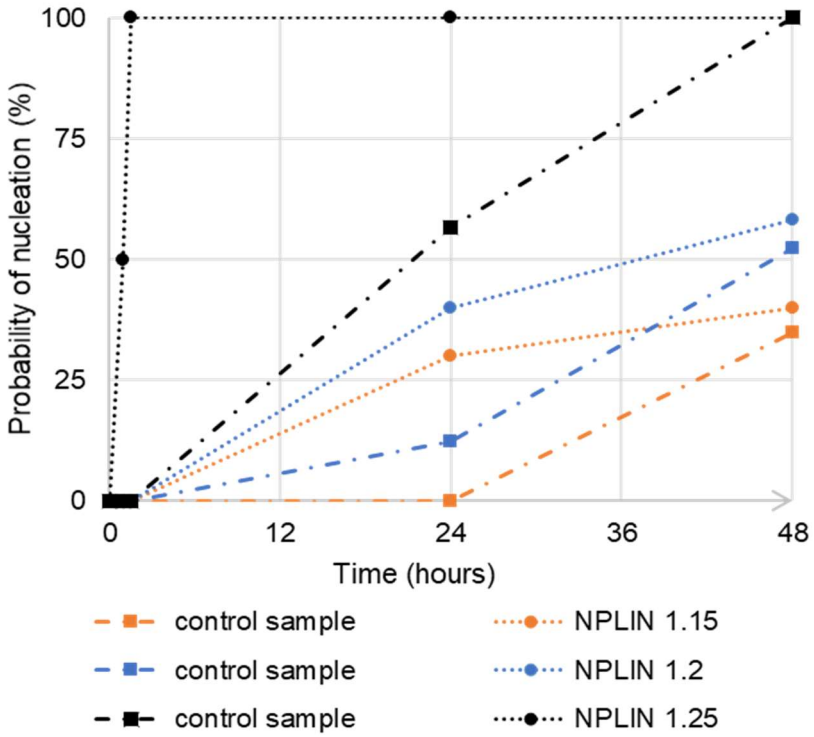

Figure 4-3-Evolution of the probability of nucleation as a function of time for different supersaturations. NPLIN samples were exposed to 1 pulse at 18mJ and control samples were not exposed to laser and nucleated spontaneously. (dashed lines are guides to the eye)

4.2.2 **Influence of the number of pulses and intensity**

In this section, the influence of the number of pulses and their intensity are investigated for K_2SO_4 (β=1.25) and compared with results obtained in literature, previously reviewed in Chapter 2 (§2.6.3 & §2.6.4). Table 4-3 shows the impact of these parameters on the minimum induction time, probability of nucleation and on the number of crystals produced during NPLIN experiments. It must be stressed that each row in Table 4-3 corresponds to a statistical analysis performed using at least 40 experiments (2 sets of 20) and the first visual inspection of the vials was made 30 minutes after irradiation. First, at constant laser intensity (first two rows in Table 3), there is a slight increase of the probability of nucleation at 1h30 upon increasing the number of pulses from 1 to 100. Second, when increasing the laser intensity from 18 to 85.6 mJ, the minimum induction time observed was reduced by half. Furthermore, there is an increase of the number of crystals produced which is actually dependent on both the number of pulses and the intensity of the laser suggesting a conjugated interaction on NPLIN results. Although we observed that a

single pulse of 18mJ is likely to induce the nucleation of an isolated crystal of K_2SO_4, it seems that the use of higher energy generates more crystals.

As seen in Chapter 2, our results agree with literature, particularly with Kacker *et al.*[14] who stated that the nucleation probability depends on the laser beam intensity. Moreover, concerning the number of crystals obtained, Alexander *et al.*[15] noticed that a single pulse gives a single crystal of potassium chloride, but the energy seems to affect the number of crystals as already discussed by Hua *et al.*[16].

Table 4-3-Influence of the number of pulse and its intensity on the nucleation behaviour of K_2SO_4 solutions at β =1.25. Np is the number of pulses; Ep is the intensity or pulse energy. The induction time represent the time at which the first crystal is detected after exposure to laser.

Np	Ep (mJ)	Induction time (min)	Probability of nucleation % (t=1h30)	Number of crystals per vial (min-max)
1	18	60	40	1-4
101	18	60	80	1-8
1	85.6	30	100	3-6
101	85.6	30	100	>30

4.2.3 **Polarization**

In order to evaluate the influence of polarization on the NPLIN behaviour of K_2SO_4 aqueous solutions, the impact of three types of polarization geometries, linear (LP), right circular (RCP) and left circular polarization (LCP), were compared by irradiation of solutions at the same supersaturated ratio of β=1.25. The same laser irradiation conditions (1 pulse at 85.6mJ) were used in each case. As discussed in Chapter 2, the influence of polarization on NPLIN behaviour is unclear. In the case of KCl[15] aqueous solutions, the polarization geometry of the laser has shown no incidence. It is worth noting that KCl crystallizes in a cubic space group and the structure has no preferential axis for polarization. K_2SO_4, however, is an orthorhombic salt, and polarization anisotropy could lead to different nucleation behaviour while using LP or CP, as it has been reported for urea[17] which crystallizes in a tetragonal structure. Table 4-4 shows the results obtained during this work. There is no difference observed for the three different polarization regarding the nucleation kinetics (i.e., minimum

induction time and probability of nucleation) or number and morphology of crystals produced.

Table 4-4-Influence of the type of polarization on the nucleation behaviour of K_2SO_4 solutions at β =1.25; LP (linear polarization), RCP (right circular polarization) and LCP (left circular polarization)

Polarization	Induction time (min)	Probability of nucleation % (t=1h30)	Number of crystals per vial (min-max)
LP	30	100	3-6
RCP	30	100	2-6
LCP	30	100	2-7

4.2.4 **Influence of solvent**

As K_2SO_4 is poorly soluble in other solvent than water, mixtures of solvent using acetone, methanol or ethanol at 10%wt in water were used to evaluate the influence of a change in solvent composition on NPLIN kinetics. The solubilities are given in Table 4-1. Two sets of 10 samples per conditions were performed. Table 4-5 shows the NPLIN kinetics for the different solvent compositions when supersaturated solutions at β=1.25 are exposed to one pulse of 18mJ. There is a clear increase of the minimum induction time and a marked decrease of the probabilities of nucleation when the solutions contain 10%wt organic solvent. However, since the solubility of K_2SO_4 is considerably reduced by the addition of organic solvents (Table 4-1), the concentration of K_2SO_4 is reduced and the chance that two entities join to crystallize also decreases. The composition of the solvent had the same impact on spontaneous nucleation and NPLIN.

Table 4-5-Influence of the composition of the solvent (β=1.25, 1pulse 18mJ)

	H_2O	H_2O/MeOH	H_2O/EtOH	H_2O/Acetone
Induction time (h)	1	3	3	4
Probability of nucleation (%) (t=4h)	100	30	30	30

4.2.5 **NPLIN in Gel**

NPLIN in gel has already been studied in the literature (Chapter 2-§2.5.4). In this study, the aim is to slow down the diffusivity of molecules and the sedimentation of the crystals after nucleation, in order to (i) locate the starting point of nucleation, (ii) observe a possible preferential orientation of the crystal expected from the OKE mechanism and (iii) possibly trap any cavitation bubble in the gel medium.

The first attempts to gel the K_2SO_4 aqueous solutions were made with agarose, however the high concentration of K_2SO_4 in the solution resulted in precipitation of agarose rather than gelling. To tackle this problem, tetramethoxysilane (TMOS) was used. TMOS is a chemical gelling agent, which means that the gelation is not reversible since it creates new Si-O-Si bond (Figure 4-4), contrary to agarose which forms physical gels reversible with temperature.

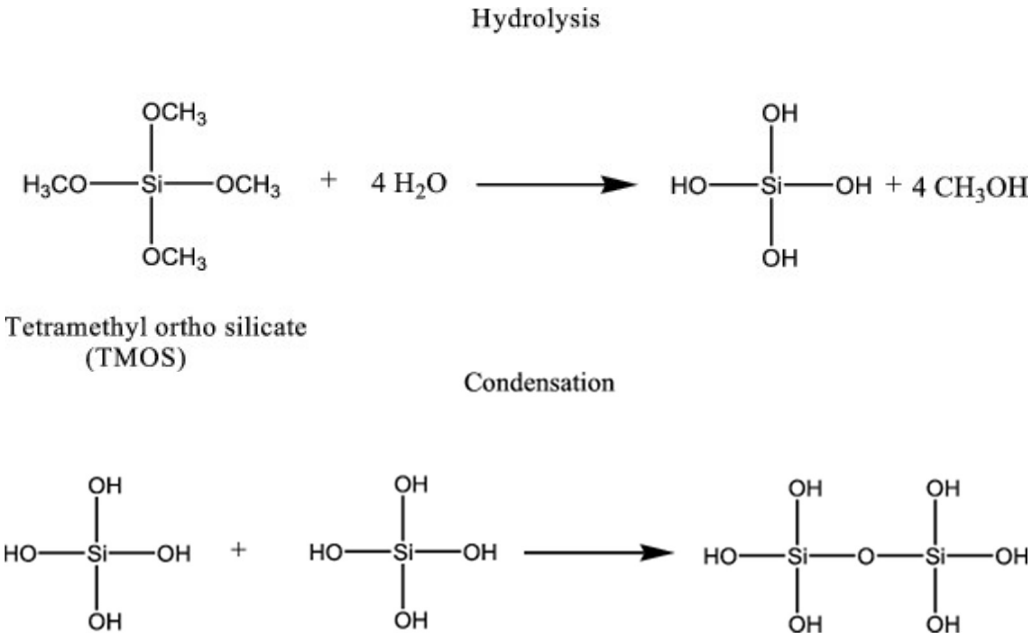

Figure 4-4-Schematic principle of the formation of a TMOS gel. First step (top) is the hydrolysis (which produces methanol), and the second step (bottom) is the condensation

TMOS gels supersaturated with K_2SO_4 were produced by addition of 10%vol of TMOS to a stock supersaturated solution at β=1.25. The solution was then transferred in the same vials as those used for typical NPLIN experiments (at least 10). The samples were left one night in the oven at 50°C to allow for the gel formation. After cooling down to room temperature, the vials were then irradiated with one pulse at 85.6mJ. Figure 4-5 shows typical optical microscopy pictures obtained by

observation of the irradiated TMOS gels (Figure 4-5, a-c). Figure 4-5,d presents a picture of a TMOS supersaturated gels that crystallized spontaneously (magnification is kept constant in Figure 4-5). Curiously, laser irradiation of the gel produces a multitude of K_2SO_4 crystals all along the beam path while only one was expected in comparison of non-viscous solution using the same laser parameters (Table 4-3). The gel matrix may promote the formation of more nucleation sites. Such behaviour allows to retrace the beam path inside the sample by looking at the location of the crystals: Figure 4-5,a highlights the circular section of the beam path at the entrance of the vials while Figure 4-5,c illustrates that the beam geometry becomes more elliptical at the exit due to the slight focusing of the laser beam through the vial. The results confirm the spatial control demonstrated by Duffus *et al.*[18] and that there is no shock-wave induced by the laser otherwise nucleation should also occur beyond the irradiated volume. These results indicate that in the case of a typical NPLIN experiment from a non-viscous solution, the first nucleus produced forms within the beam path and then either sediments in the bottom of the vials or, as observed, sometimes stay attached to the meniscus (meniscus might be in the beam path).

Moreover, while the first crystals are only detected 30min after irradiation in solution, kinetics of nucleation in gel are very fast. In gel, crystals are indeed visible a few minutes after irradiation and as there are plenty of crystals, they are more easily detected. The nucleation kinetics are also faster in the case of spontaneous nucleation in gel media. Nevertheless, it is suspected that TMOS gel reduces the solubility of K_2SO_4 as the hydrolysis reaction (Figure 4-4) produces methanol. The higher number of K_2SO_4 crystals and reduced induction times could indeed be a consequence of increased supersaturation due to the presence of methanol, although the results shown in 4.2.4. suggests that an increased content in methanol should give rise to shorter induction times.

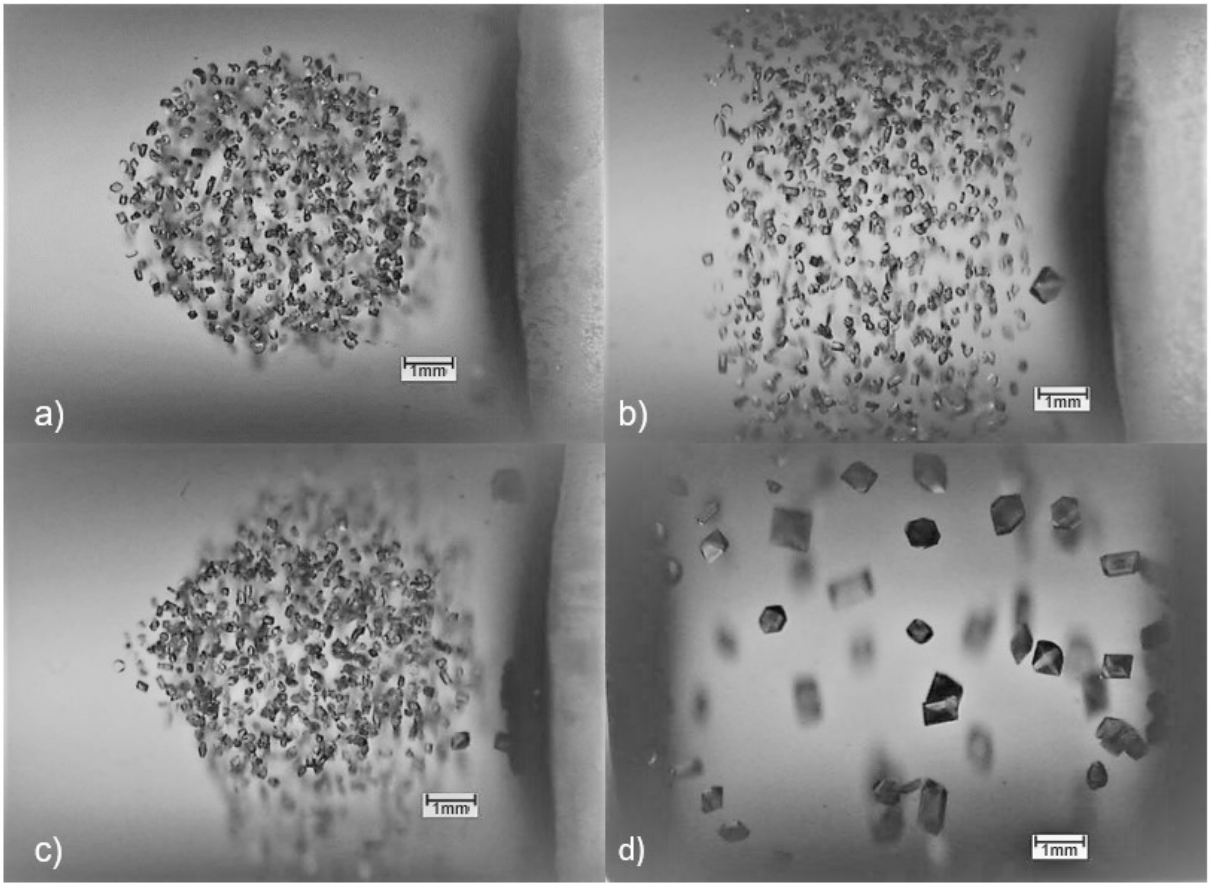

Figure 4-5-Pictures of K_2SO_4 crystals in TMOS gel matrix, a) view of laser beam entry b) view of the side of the vial c) view of laser beam exit d) control (sample spontaneous crystallization)

4.3 INFLUENCE OF GAS COMPOSITION AND NATURE

It is well known that gas nucleation in solution can be triggered by ultrasounds or mechanical shocks[19]. The retrograde solubilities of gas make gas nucleation in solutions also possible via local heating and it has been proposed that laser pulses can trigger bubble formation. Furthermore, some publications, reported and discussed in Chapter 2-§2.4.3.2, highlight a connexion between gas nucleation and crystal nucleation so that cavitation has been proposed as a possible mechanism for NPLIN.

The experiments reported in this section are based on the hypothesis that, since each gas has a different aqueous solubility, they should exhibit different nucleation behaviour under laser irradiation, which should in turn result in significantly different crystal-nucleation behaviours. The corollary of this is that if the solution is degassed prior to laser irradiation, no NPLIN effect should be observed. The methodology used in these experiments

was inspired by a crystal growth study performed in early 2010's at the SMS laboratory in which a systematic bubbling of saturated solutions with different gas was performed to evaluate the impact of gaseous matter on the formation of crystal defects[20].

To evaluate the incidence of gas on NPLIN kinetics, the presence of dissolved gas in K_2SO_4 supersaturated solutions (β=1.25) was controlled in term of composition (degassed by ultrasounds) and nature (N_2, CO_2, Ar) (Chapter 3- §3.3.3). The crystal nucleation probability of the irradiated solutions (and non-irradiated) as a function of time and gas composition is shown in Figure 4-6.

It should first be underlined that no macroscopic gas bubbles were observed during these experiments and that, if that occurred, the formed cavities were too small and/or short lived. Figure 4-6 shows that, although the presence of N_2 and CO_2 seems to slightly reduce the induction time, the five Pn(t) = f(t) curves remain quite similar: the kinetics of NPLIN of K_2SO_4 seems uncorrelated to the presence (or the absence) of dissolved gas, whatever the nature of the gas tested. In particular, the fact that CO_2 and N_2 saturated solutions gave the same NPLIN kinetics is a valuable information. Indeed, the solubility of these two gases in water are considerably different ($x(N_2)=0.1265.10^{-4}$ and $x(CO_2)=7.023.10^{-4}$ at 20°C express in mole fraction)[21] so that laser irradiation should produce significantly different amount of gas cavities and notable difference of NPLIN kinetics should have been observed for K_2SO_4. Degassed solutions also exhibited similar NPLIN regime to gas bubbled samples. Moreover, by comparing the shape of the NPLIN curves and the control sample curves, it seems that NPLIN shifts the minimal induction time but once the nucleation has started the evolution of both curves are similar.

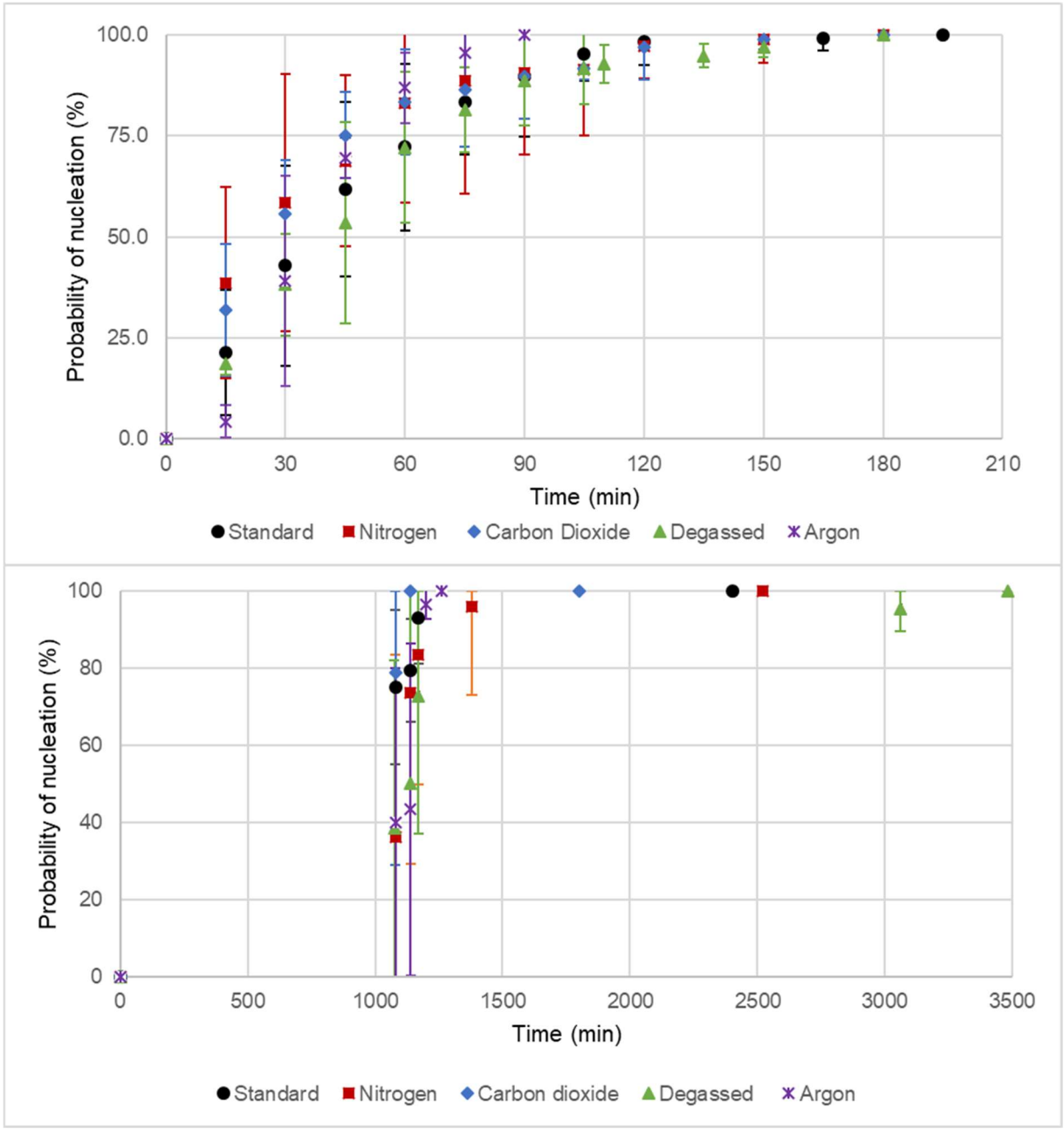

Figure 4-6-Influence of degassing and gas bubbling on the probability of NPLIN (at the top) and the probability of spontaneous nucleation (at the bottom) as a function of time (one pulse at 85.6mJ). "Standard" stands for no solution treatment, Nitrogen, Argon and Carbon dioxide are the gas used for bubbling, "Degassed" is solution degassed by ultrasounds

4.4 INFLUENCE OF FILTRATION

Filtration of solutions has already showed important decreases in the probability of nucleation during NPLIN experiments (Chapter 2- §2.5.3). It is suspected that filtration removes insoluble impurity particles that would be responsible for the nanoparticle heating mechanism (Chapter 2- §2.4.4). K_2SO_4 supersaturated solution was filtered to determine whether filtration had any influence on the NPLIN effect.

Filtered solutions of supersaturated K_2SO_4 solutions (β=1.25) were prepared as described in Chapter 3- §3.3.1. The solutions were then irradiated by a single pulse at 85.6mJ. The results are presented in Figure 4-7 and show a significant decrease of the probability of nucleation for NPLIN filtered solutions. There is also a slight influence of filtration on the control samples but limited compared to the irradiated samples. Moreover, it seems that filtration with smaller porosity (0.2µm) allows a more important decrease of the nucleation probability than with a porosity of 0.45µm for the irradiated sample. In comparison, for the control sample, the nucleation probability is lower for the 0.45µm filtered samples. However, considering a margin of error, the differences between the filtered control sample is small. An explanation could be the size of the impurities involved in the NPLIN phenomenon. Impurities contained in K_2SO_4 could have a wide range of size and some could be retained by the 0.45µm filter whereas the smallest ones go through. It is actually logical to suppose that some particles are smaller than 0.2µm since there is still a little NPLIN effect after 0.2µm filtration. These results confirm the presence of solid impurities in our solutions with a strong effect on the NPLIN phenomenon.

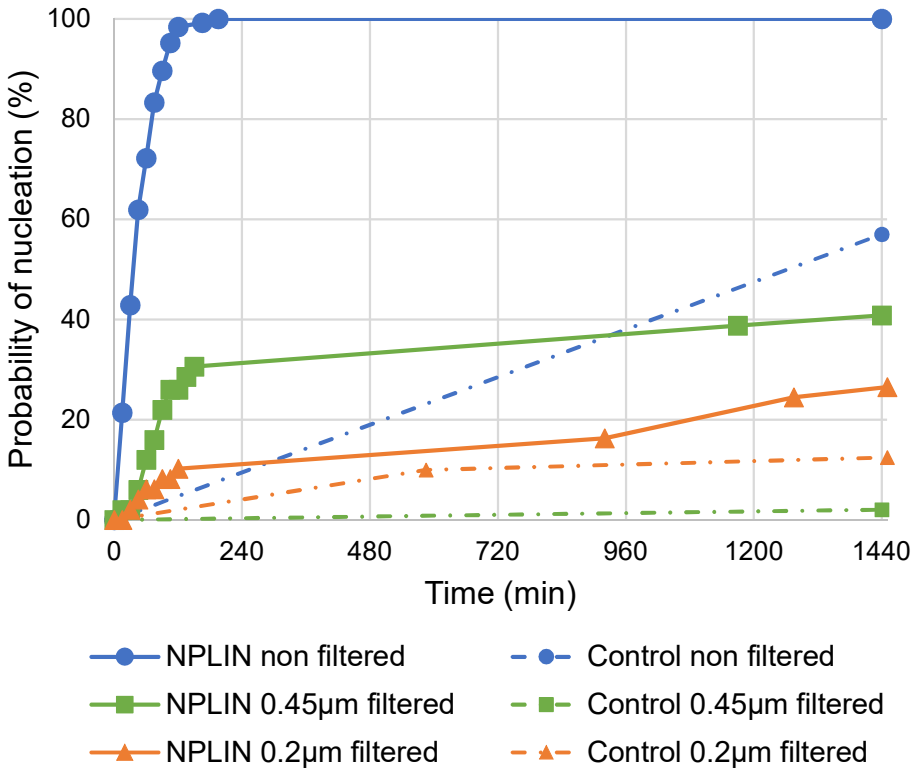

Figure 4-7-Influence of filtration on the nucleation kinetics of K_2SO_4. lines are guides to eye.

4.5 MEAN NUMBER OF CRYSTALS AND MORPHOLOGY

It is worth mentioning that no difference in the number of crystals has been detected when changing the supersaturation. The mean number of crystals per vial for the different nucleation conditions is summed up in Table 4-6. It has been observed to be circa 1.5 usually obtaining 1-2 crystals for each irradiated sample (1 pulse 18mJ); in some cases, up to 4 crystals were obtained. For control samples, the value is closer than 1.3. Also, almost no difference was observed when changing the gas content and nature for irradiated sample (1 pulse at 85.6mJ) since the mean number of crystals was close to 3. However, in the case of filtered solutions, the mean number of crystals per vial is reduced to 1.5. Ward *et al.*[22] also observed a decrease of the number of crystals produced by NPLIN in filtered solutions and an increase when solutions are doped with iron oxide and PEG. They attribute this trend to the decreases of nucleation sites due to filtration.

Table 4-6-Summary of the mean number of crystals obtained in different nucleation conditions

Nucleation Conditions	Control sample	1 pulse 18mJ	1 pulse 85.6mJ	Filtered 1pulse 85.6mJ
Mean number of crystals	1.3	1.5	3	1.5

Careful observations of the crystals produced either by spontaneous crystallization or by laser pulses showed constant crystal morphologies, various crystal shapes and the occasional occurrence of twinned crystals in both cases. No laser parameter was found to have an impact on the crystal facies. In Figure 4-8, the crystal displayed originates from several vials but have been grown in the same conditions.

Figure 4-8-K_2SO_4 crystals obtained from supersaturated solutions β=1.25: typical twin crystals observed in this study (left), crystals obtained by laser irradiation (middle) and crystals obtained by spontaneous nucleation (right). Pictures taken with a NIKON SMZ-10A microscope equipped with a Sony DXC-950 3CCD Color Video Camera Power HAD

4.6 DISCUSSION ON THE MECHANISM

In the following section, the different mechanisms proposed in the literature, which were detailed in Chapter 2, are discussed regarding the results obtained from all the experiments of NPLIN of K_2SO_4 presented above. The DP mechanism will not be discussed as no simulation of the model could be performed for K_2SO_4.

4.6.1 OKE mechanism

According to the OKE mechanism, the use of the appropriate polarization (linear, circular or elliptical) should result in an increase of the probability of nucleation, in a reduction of the induction time and/or in the control of

polymorphism, as discussed in Chapter 2 (§2.4.1.2). However, the results in Table 4-4 showed no influence of the laser polarization on the nucleation kinetics of K_2SO_4. Although the structure has very weak birefringence[4], and therefore no strong polarization axis that can interact with the electromagnetic field, the laser polarization geometry should at least affect the nucleation kinetics, especially considering the anisotropicity of the K_2SO_4 orthorhombic β-form. In addition, only β-form crystals were observed and no evidence of the presence of the α-form (nor any other polymorph or hydrate) were found, which is obviously not surprising considering the stability domain of the α-form being at T>583°C. The results shown in this chapter highlight that there is no evidence of the OKE mechanism occurring during the NPLIN of K_2SO_4 aqueous solutions.

4.6.2 **Cavitation mechanism**

In order to investigate the role of gas cavitation on the NPLIN mechanism, a set of crystallization experiments with controlled gas content was conducted. The formation of gas bubbles under laser irradiation implies (i) the formation of a heterogeneous surface which should favour heterogeneous nucleation and reduce induction time for crystallization, (ii) a localized mechanical stress which, as in sonocrystallization, could provoke faster nucleation. It was hypothesized in this work that different saturated gas should give rise to different gas cavitation behaviour and therefore, different NPLIN kinetics. The results of these experiments showed that saturating the supersaturated K_2SO_4 solution with a given gas (CO_2, N_2, Ar) had no impact on the NPLIN behaviour since no correlation between the NPLIN kinetics and the gas composition in solution was highlighted. One could question if cavitation occurred at all, but, although no gas bubble was visually observed in the course of our experiments, and although the gases were only saturated (and not supersaturated), it is possible that the experimental conditions used (unfocused nanosecond laser) can induce the formation of very small and short-lived gas cavities similarly to focused or femtosecond laser[23–25]. It should also be underlined that degassing the solution with ultrasound had also little to no impact on the NPLIN kinetics, but a recent study from Lee *et al*.[26] estimates that even in degassed water there is an average of 4.10^7 gas bubbles per mL with a diameter of circa 250nm. All these data suggest that if cavitation is involved during the NPLIN mechanism, the gas concentration and nature are not relevant criteria. The independence of NPLIN kinetics to various

gas bubbling also questions the chemical nature of the gas that cavitates: Is it gaseous matter resulting from matter exchange with the surrounding atmosphere prior to the experiment (O_2, N_2, CO_2…) or is it very short lived vaporized solvent resulting from the local temperature increase? Since no impact of gas bubbling on NPLIN was detected, our results tend to validate the second proposition. Moreover, if cavitation could indeed be a direct consequence of the interaction between the light and the solution, gases do not absorb at the wavelength used[27] and it is more likely that the light is absorbed by a solid colloidal particle and that such absorption provides suitable conditions for localized vapor formation. These considerations prompted us to design experiments focused on the nanoparticle heating mechanism.

4.6.3 **Nanoparticle heating mechanism**

The nanoparticle heating mechanism is based on the presence of solid colloidal particles that can absorbs sufficient energy under laser irradiation to induce a localized temperature increase, resulting in the formation of solvent vapor bubbles. As the bubble forms a pressure wave is produced and favour nucleation (sonocrystallization). It also envisaged that because of high energy absorption, the solid colloidal particles can be destroyed[28], thus providing fresh heterogeneous nucleation sites. In our experiments, the filtration of the supersaturated solution prior to irradiation resulted in the suppression (or at least to a decrease) of the NPLIN effect: Figure 4-7 shows indeed the decreases of the probability of nucleation in filtered solutions which supports the hypothesis of the presence of particles in solution that can be removed by filtration. This “filtration” effect has already been reported for other substances in the literature[15,22,29,30] and has become well known in the scientific community of NPLIN. The additional case of K_2SO_4 provides thus further evidences that the mechanism of NPLIN relies essentially on the presence of such insoluble particles.

It is therefore important to establish the nature of such solid colloidal impurities in order to understand how they can interact with the laser pulses. Ward *et al*.[22] brought a first answer by examining the influence of filtration of ammonium chloride solutions on the NPLIN kinetics. They evidenced that the impurities removed by filtration are mainly composed of iron and phosphates.

4.7 CONCLUSION

First of all, the results obtained demonstrate the possibility to nucleate K_2SO_4 via nanosecond pulsed NIR irradiation of aqueous supersaturated solutions and provide yet another NPLIN example to the scientific community via the publication of the results shown in this chapter in the journal Crystals[31]. Our results highlighted the impact of supersaturation, number of pulses and intensity that are predominant parameters for the control of NPLIN kinetics. As in numerous published NPLIN cases the nucleation of K_2SO_4 does not depends on the polarization geometry of the laser light which led us to set aside the OKE mechanism in the case of K_2SO_4. Moreover, there is no influence of changing the solvent on NPLIN of K_2SO_4. (i.e the influence is not specific to NPLIN as it is also observed for spontaneous nucleation). An important conclusion of this work is that bubbling the supersaturated solution with various gas prior to irradiation has almost no impact on the NPLIN kinetic. As discussed above, this is a proof that, if cavitation occurs during NPLIN of K_2SO_4, the concentration and nature of the dissolved gas play no role on the mechanism.

However, we have shown that the NPLIN of K_2SO_4 is linked to the presence of solid impurities and discussed the formation of vapor bubble through the nanoparticle heating mechanism. Further questions remain to be answered regarding this: (i) where does these impurities come from?, (ii) do they have the same chemical nature from one NPLIN case to another?, (iii) can we tailor made them to influence the process?, (iv) can we trigger nucleation by laser light in situations where NPLIN does not exists provided the systems are doped with such insoluble particles?

It is for instance worth mentioning that despite numerous efforts using different supersaturation ratio ($1.05 \leq \beta \leq 2$) and different laser parameters (from one to 600 pulses and from 85.6mJ to 175.2mJ) the NPLIN effect was not observed in the case of sodium sulfate (Na_2SO_4). Even if one could argue that this is due to a larger MSZW or to the presence of less soluble hydrates ($Na_2SO_4,7H_2O$ metastable and $Na_2SO_4,10H_2O$ for $T>32°C$[32]), it is also possible that the prepared supersaturated solutions do not contain the required impurities.

The second part of this work will examine this consideration using the case of another molecular compound, which allows to exclude any spontaneous nucleation in the NPLIN study.

4.8 REFERENCES

(1) Bernstein, J.; Davey, R. J.; Henck, J.-O. Concomitant Polymorphs. *Angewandte Chemie International Edition* **1999**, *38* (23), 3440–3461. https://doi.org/10.1002/(SICI)1521-3773(19991203)38:23<3440::AID-ANIE3440>3.0.CO;2-#.

(2) McGinnety, J. A. Redetermination of the Structures of Potassium Sulphate and Potassium Chromate: The Effect of Electrostatic Crystal Forces upon Observed Bond Lengths. *Acta Cryst B* **1972**, *28* (9), 2845–2852. https://doi.org/10.1107/S0567740872007022.

(3) Arnold, H.; Kurtz, W.; Richter-Zlnnius, A.; Bethke, J.; Heger, G. The Phase Transition of K2SO4 at about 850 K. *Acta Crystallographica Section B* **1981**, *37* (9), 1643–1651. https://doi.org/10.1107/S0567740881006808.

(4) Matviiv, R. B.; Rudysh, M. Ya.; Stadnyk, V. Yo.; Fedorchuk, A. O.; Shchepanskyi, P. A.; Brezvin, R. S.; Khyzhun, O. Y. Structure, Refractive and Electronic Properties of K2SO4:Cu2+ (3%) Crystals. *Current Applied Physics* **2021**, *21*, 80–88. https://doi.org/10.1016/j.cap.2020.09.015.

(5) Genkinger, S.; Putnis, A. Crystallisation of Sodium Sulfate: Supersaturation and Metastable Phases. *Environ Geol* **2007**, *52* (2), 329–337. https://doi.org/10.1007/s00254-006-0565-x.

(6) Broul, M.; Nývlt, J.; Söhnel, O. *Solubility in Inorganic Two-Component Systems*; Elsevier Science & Technology, 1981; Vol. 6.

(7) Mydlarz, J.; Jones, A. G.; Millan, A. Solubility and Density Isotherms for Potassium Sulfate-Water-2-Propanol. *J. Chem. Eng. Data* **1989**, *34* (1), 124–126. https://doi.org/10.1021/je00055a033.

(8) Mydlarz, J.; Jones, A. G. Potassium Sulfate Water-Alcohols Systems: Composition and Density of Saturated Solutions. *J. Chem. Eng. Data* **1990**, *35* (2), 214–216. https://doi.org/10.1021/je00060a036.

(9) Li, B.; Zhang, Y.; Zou, R.; Wang, Q.; Zhang, B.; An, L.; Yin, F.; Hua, Y.; Hu, J. Self-Assembled WO3−x Hierarchical Nanostructures for Photothermal Therapy with a 915 Nm Laser Rather than the Common 980 Nm Laser. *Dalton Transactions* **2014**.

(10) Curcio, J. A.; Petty, C. C. The Near Infrared Absorption Spectrum of Liquid Water. *J. Opt. Soc. Am.* **1951**, *41* (5), 302. https://doi.org/10.1364/JOSA.41.000302.

(11) Bakhsheshi, M.; Lee, T.-Y. Non-Invasive Monitoring of Brain Temperature by near-Infrared Spectroscopy. *Temperature* **2014**, *2*, 31–32. https://doi.org/10.4161/23328940.2014.967156.

(12) Muncan, J.; Tsenkova, R. Aquaphotomics—From Innovative Knowledge to Integrative Platform in Science and Technology. *Molecules* **2019**, *24* (15), 2742. https://doi.org/10.3390/molecules24152742.

(13) Irimia, D.; Jose Shirley, J.; Garg, A. S.; Nijland, D. P. A.; van der Heijden, A. E. D. M.; Kramer, H. J. M.; Eral, H. B. Influence of Laser Parameters and Experimental Conditions on Nonphotochemical Laser-Induced Nucleation of

Glycine Polymorphs. *Crystal Growth & Design* **2020**, No. 21, 631–641. https://doi.org/10.1021/acs.cgd.0c01415.

(14) Kacker, R.; Dhingra, S.; Irimia, D.; Ghatkesar, M. K.; Stankiewicz, A.; Kramer, H. J. M.; Eral, H. B. Multiparameter Investigation of Laser-Induced Nucleation of Supersaturated Aqueous KCl Solutions. *Crystal Growth & Design* **2018**, *18* (1), 312–317. https://doi.org/10.1021/acs.cgd.7b01277.

(15) Alexander, A. J.; Camp, P. J. Single Pulse, Single Crystal Laser-Induced Nucleation of Potassium Chloride. *Crystal Growth & Design* **2009**, *9* (2), 958–963. https://doi.org/10.1021/cg8007415.

(16) Hua, T.; Gowayed, O.; Grey-Stewart, D.; Garetz, B. A.; Hartman, R. L. Microfluidic Laser-Induced Nucleation of Supersaturated Aqueous KCl Solutions. *Crystal Growth & Design* **2019**, *19* (6), 3491–3497. https://doi.org/10.1021/acs.cgd.9b00362.

(17) Matic, J.; Sun, X.; Garetz, B. A.; Myerson, A. S. Intensity, Wavelength, and Polarization Dependence of Nonphotochemical Laser-Induced Nucleation in Supersaturated Aqueous Urea Solutions. *Crystal Growth & Design* **2005**, *5* (4), 1565–1567. https://doi.org/10.1021/cg050041c.

(18) Duffus, C.; Camp, P. J.; Alexander, A. J. Spatial Control of Crystal Nucleation in Agarose Gel. *J. Am. Chem. Soc.* **2009**, *131* (33), 11676–11677. https://doi.org/10.1021/ja905232m.

(19) Sun, Y.; Alexander, A. J. Mechanical Shock-Induced Nucleation in Solution: Is Cavitation Necessary? *Journal of Crystal Growth* **2022**, 126786. https://doi.org/10.1016/j.jcrysgro.2022.126786.

(20) Waldschmidt, A.; Couvrat, N.; Berton, B.; Dupray, V.; Morin, S.; Petit, S.; Coquerel, G. Impact of Gas Composition in the Mother Liquor on the Formation of Macroscopic Inclusions and Crystal Growth Rates. Case Study with Ciclopirox Crystals. *Crystal Growth & Design* **2011**, *11* (6), 2463–2470. https://doi.org/10.1021/cg200245m.

(21) Wilhelm, Emmerich.; Battino, Rubin.; Wilcock, R. J. Low-Pressure Solubility of Gases in Liquid Water. *Chem. Rev.* **1977**, *77* (2), 219–262. https://doi.org/10.1021/cr60306a003.

(22) Ward, M. R.; Mackenzie, A. M.; Alexander, A. J. Role of Impurity Nanoparticles in Laser-Induced Nucleation of Ammonium Chloride. *Crystal Growth & Design* **2016**, *16* (12), 6790–6796. https://doi.org/10.1021/acs.cgd.6b00882.

(23) Soare, A.; Dijkink, R.; Pascual, M. R.; Sun, C.; Cains, P. W.; Lohse, D.; Stankiewicz, A. I.; Kramer, H. J. M. Crystal Nucleation by Laser-Induced Cavitation. *Crystal Growth & Design* **2011**, *11* (6), 2311–2316. https://doi.org/10.1021/cg2000014.

(24) Nakamura, K.; Hosokawa, Y.; Masuhara, H. Anthracene Crystallization Induced by Single-Shot Femtosecond Laser Irradiation: Experimental Evidence for the Important Role of Bubbles. *Crystal Growth & Design* **2007**, *7* (5), 885–889. https://doi.org/10.1021/cg060631q.

(25) Yu, J.; Yan, J.; Jiang, L. Crystallization of Polymorphic Sulfathiazole Controlled by Femtosecond Laser-Induced Cavitation Bubbles. *Crystal Growth & Design* **2021**, *21* (6), 3202–3210. https://doi.org/10.1021/acs.cgd.0c01476.

(26) Lee, J. I.; Yim, B.-S.; Kim, J.-M. Effect of Dissolved-Gas Concentration on Bulk Nanobubbles Generation Using Ultrasonication. *Sci Rep* **2020**, *10* (1), 18816. https://doi.org/10.1038/s41598-020-75818-8.

(27) Horvath, H. Atmospheric Light Absorption—A Review. *Atmospheric Environment. Part A. General Topics* **1993**, *27* (3), 293–317. https://doi.org/10.1016/0960-1686(93)90104-7.

(28) Kurita, H.; Takami, A.; Koda, S. Size Reduction of Gold Particles in Aqueous Solution by Pulsed Laser Irradiation. *Appl. Phys. Lett.* **1998**, *72* (7), 789–791. https://doi.org/10.1063/1.120894.

(29) Javid, N.; Kendall, T.; Burns, I. S.; Sefcik, J. Filtration Suppresses Laser-Induced Nucleation of Glycine in Aqueous Solutions. *Crystal Growth & Design* **2016**, *16* (8), 4196–4202. https://doi.org/10.1021/acs.cgd.6b00046.

(30) Ward, M. R.; Jamieson, W. J.; Leckey, C. A.; Alexander, A. J. Laser-Induced Nucleation of Carbon Dioxide Bubbles. *The Journal of Chemical Physics* **2015**, *142* (14), 144501. https://doi.org/10.1063/1.4917022.

(31) Briard, M.; Brandel, C.; Morin-Grognet, S.; Coquerel, G.; Dupray, V. Potassium Sulfate: A New Candidate to Explore Non-Photochemical Laser-Induced Nucleation Mechanisms. *Crystals* **2021**, *11* (12), 1571. https://doi.org/10.3390/cryst11121571.

(32) Garrett, D. E. Phase Data and Physical Properties. In *Sodium Sulfate*; Elsevier, 2001; pp 317–351. https://doi.org/10.1016/B978-012276151-5/50008-5.

Chapter 5. INVESTIGATING NPLIN THROUGH ETHYLENE DIAMINE SULFATE

5.1 INTRODUCTION

It is remarkable how the filtration impacts the NPLIN process. Indeed, an important decrease of the probability of nucleation of irradiated filtered solutions is reported in the literature for several substances[1,2] and was confirmed in Chapter 4 (§4.4) for potassium sulfate. It is proposed that the insoluble solid impurities removed by filtration are responsible for the NPLIN process via the nanoparticle heating theory. In this chapter, the following questions will be explored: (i) where do these impurities come from? (ii) what is the chemical nature of these impurities? and (iii) can we tailor made them to influence the process?

To answer these questions, Ethylenediamine Sulfate (EDS), a molecular salt exhibiting supramolecular chirality was chosen to investigate further the NPLIN mechanism. At first, the solid landscape of EDS was investigated since only few data were available in the literature. EDS has proven to be a good candidate for NPLIN study due to the huge difference of nucleation kinetics between irradiated and non-irradiated solutions. It has to be highlighted that NPLIN of EDS was not reported prior to this work. Further, the impact of insoluble impurities on the NPLIN kinetics was investigated. In addition, the impact of the laser parameters on the produced crystal chirality was examined with the expectation of a stereoselective control using different polarization geometry.

5.2 SOLID STATE

EDS solid state remains quite unexplored in the literature: At ambient temperature, the crystals are reported as chiral and the structure was determined as tetragonal, either $P4_12_12$ (CSD refcode ETDAMS04) or $P4_32_12$ (CSD refcode ETDAMS05). Santhakumari *et al.*[3] reported the existence of a high temperature (T=209°C) form of EDS by using conductivity measurements. The crystal structure of HT-EDS is unknown.

5.2.1 Screening of EDS Polymorph

The solid state of EDS, which is relatively poorly known in the literature, was investigated by performing a polymorph screening in order to assess the presence of any polymorphs, hydrates or solvates. This is an important point to establish for a suitable interpretation of the experimental results presented in this chapter. EDS was crystallized by using several conventional methods, such as evaporation or cooling of aqueous solutions, but also anti-solvent addition (using methanol, ethanol or acetone). It has to be underlined that the choice of solvent was limited by

the poor solubility of EDS in solvents other than water. These experiments did not reveal the existence of additional polymorphs, hydrates or solvates of EDS. The polymorphic transition reported by Santhakumari *et al*.[3] was confirmed by heating the room temperature phase (RT-EDS, hereafter) to 228°C above which its transformation into the high temperature form (HT-EDS, hereafter) occurs. In order to further characterize the HT-EDS form and its relation to RT-EDS form, the RT-EDS will first be described and then the transformation into HT-EDS will be examined through different analytical techniques including DSC, TR-XRD, SHG and microscopy.

5.2.2 **Description of RT-EDS**

Achiral compounds exhibiting supramolecular chirality have been previously described in Chapter 1 (§1.2.4.3.3). RT-EDS crystals exhibits supramolecular chirality and can be either right or left handed: they are referred to as two enantiomorphs. RT-EDS structure has been reported by Sakurai *et al*.[4], then by Ghozlen *et al*.[5] and more recently by Matsumoto *et al*.[6] who reported the structure of both enantiomorphs ($P4_12_12$ and $P4_32_12$). The supramolecular chirality is due to the quaternary screw axis of the space group which can be either 4_1 or 4_3, as represented in Figure 5-1.

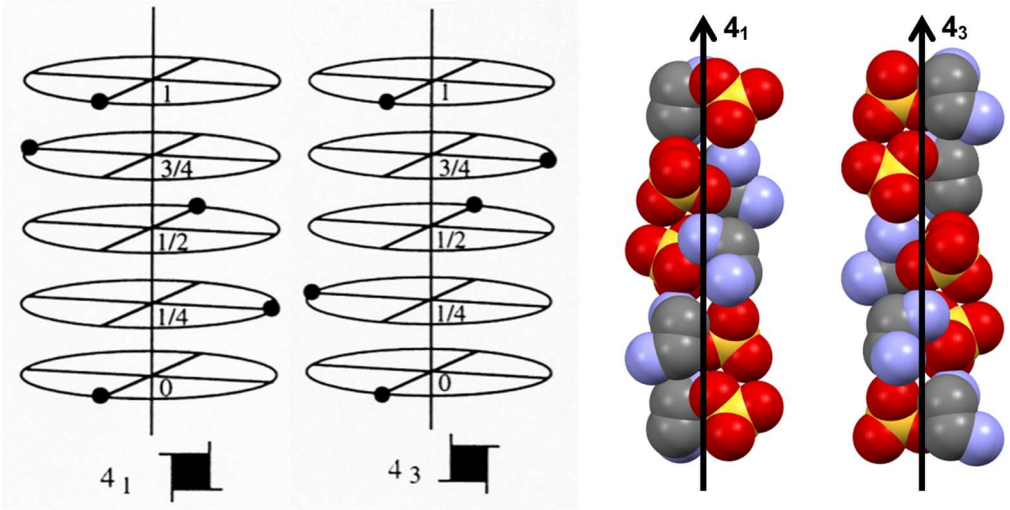

Figure 5-1-Representation of helical axes 4_1 and 4_3 in schematic (left) and in the EDS structure (hydrogen atoms omitted for clarity, right)

5.2.2.1 Determination of crystal chirality

A polarizing microscope (Chapter 3) was used to identify the handedness of the crystals of RT-EDS. As shown in Figure 5-2 the two enantiomorphs appear in different colour depending on the position of the polarizer in relation to the analyser of the microscope. When the polarizer is rotated anti-clockwise with respect to the analyser, l-crystals appear blue and d-

crystals appear light-brown (vice-versa if the polarizer is rotated clockwise). Most of RT-EDS crystals grow relatively flat, with the quaternary screw axis spreading perpendicularly to the highest morphological index faces. It is therefore easy to identify their chirality but sometimes, the handedness can be difficult to determine if the crystals are ill-shaped or if the quaternary screw axis is difficult to orientate. In such situation, the crystal was not counted in our experiments.

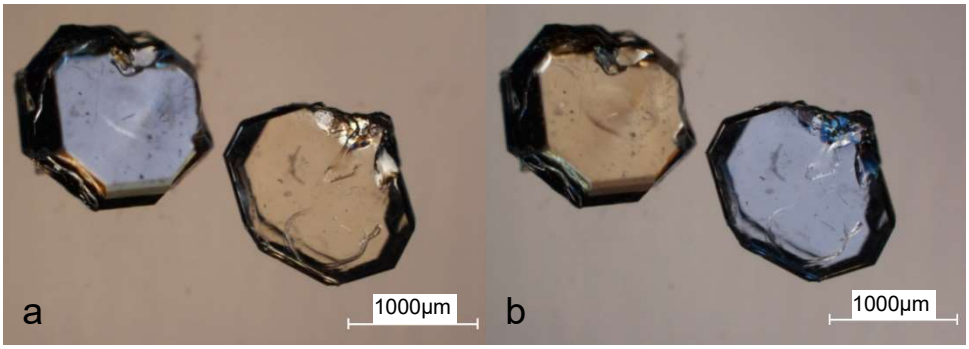

Figure 5-2-RT-EDS crystal observed with polarizing microscope. The picture shows the colour change of d-crystal (from blue (a) to brown (b)) and l-crystal (from brown (a) to blue (b)) when polarizer is rotated anti-clockwise with respect to analyser.

5.2.3 Description of HT-EDS

5.2.3.1 Differential scanning calorimetry (DSC)

10 mg of RT-EDS were loaded in a DSC crucible (sealed and pierced lid) and analysed by DSC. The result of the analysis is shown in Figure 5-3. Upon heating at 5 K/min from 20 to 220 °C, no thermal events could be observed. A single endothermic event was detected at T_{onset}= 228.5°C and attributed to the phase transition of RT-EDS into HT-EDS ($\Delta H_{transition}$=82.01 J/g). Upon cooling, two different exothermic peaks were detected at T_{onset}=224.4°C ($\Delta H_{transition}$=2.44 J/g) and T_{onset}=168.7 °C ($\Delta H_{transition}$=60.63 J/g). Both events were attributed to the reverse transformation HT-EDS→RT-EDS occurring with different degree of thermal hysteresis (almost 0°C of hysteresis for the first event and about 55°C for the second) into different particles[7],an interpretation that is further confirmed by the noisy appearance of the second event which was found reproducible during a second heating cycle. This thermal behaviour was found insensitive to heating and cooling rates of 2, 5 and 10 K/min. These data confirm the result of Santhakumari *et al.*[3] and no other polymorphic form of EDS was detected by thermal methods. From our results and those of Santhakumari *et al*., one can affirm that EDS polymorphs are enantiotrope, i.e., each polymorph has its own stability temperature range with a defined temperature of transition (See Chapter 1- §1.2.3).

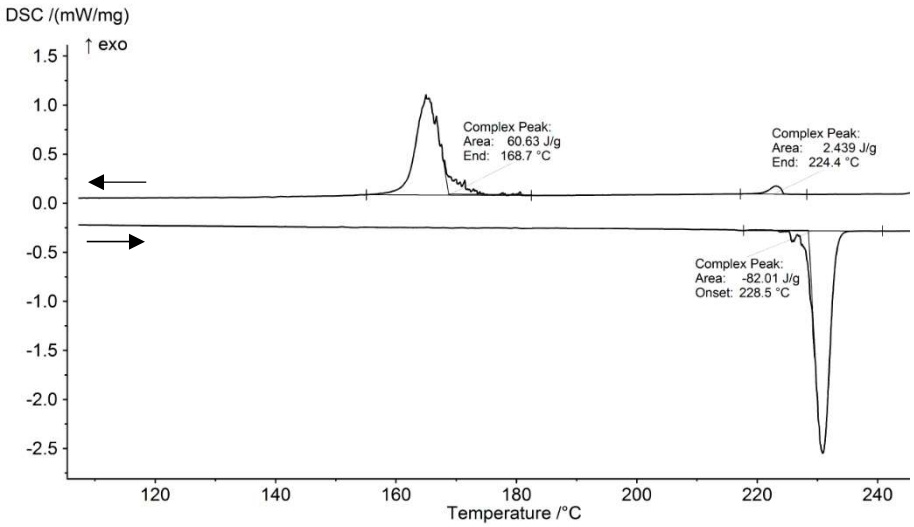

Figure 5-3-DSC analysis of RT-EDS powder. Heating and cooling rate are 5K/min

5.2.3.2 Temperature-resolved X-ray powder diffraction (TR-XRPD)

To further complement the results shown in section §5.2.3.1 a TR-XRD experiment was performed and the results are presented Figure 5-4. The XRPD pattern of the RT-EDS matches the calculated powder pattern of the structure described by Matsumoto *et al.*[6]. The XRPD pattern collected at 240°C confirms the formation of the high temperature form (HT-EDS), exhibiting significantly different diffraction peaks by comparison to those of the RT-EDS form. It has to be noticed that no XRPD pattern of the HT-EDS was reported by Santhakumari *et al.*[3] and thus, this is the first presentation of the XRPD pattern of HT-EDS. In accordance with our DSC experiments, this transition is reversible, and upon cooling, a mixture of the RT-EDS and HT-EDS was observed (at 220°C) which confirms our interpretation of the thermal behaviour. A full return to RT-EDS was observed below 180°C.

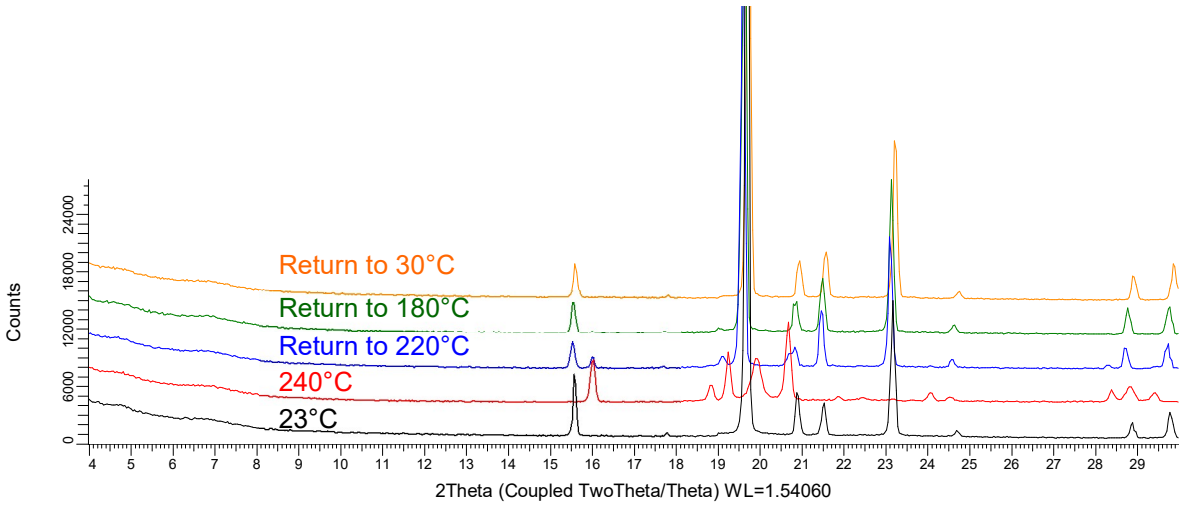

Figure 5-4-Diffractograms of EDS as a function of temperature

5.2.3.3 Second harmonic generation

Second Harmonic Generation (SHG) analysis was also used to gather information on the crystal structure of the two EDS solid forms. It was found that neither RT-EDS nor HT-EDS crystals exhibited a SHG signal. It should be underlined that Jayaraman[8] conducted SHG measurements on RT-EDS phase and reported a small SHG signal. However, the RT-EDS phase crystallizes in the quadratic chiral space group $P4_12_12$ which is indeed non-centrosymmetric, but its point group (422) is one of the point group for which the Kleinman's exclusion rules apply[9] (See Chapter 1-§1.2.2.1), meaning that no SHG signal is expected for this space group. It is thus not surprising that no SHG emission was observed for this polymorph. Concerning HT-EDS, the absence of signal implies that the space group is either centrosymmetric (HT-EDS crystals would be achiral) or belongs to the "Kleinman excluded" point group (HT-EDS would exhibit supramolecular chirality). Given that RT-EDS belongs to the 422 point group and present supramolecular chirality, it cannot be excluded that HT-EDS also presents that type of crystalline architecture.

5.2.3.4 Structural analysis of HT-EDS

Many attempts to grow single crystals of HT-EDS in view to solve the structure by SC-XRD were unfortunately unfruitful. It was also attempted to perform a single crystal to single crystal transition of a RT-EDS single crystal by slow heating of an individual crystal however these experiments systematically led to a polycrystal of HT-EDS as the single crystal nature of the particle was lost during the solid-solid transition. Appendix A.1 shows a typical hot-stage microscopy experiment with such a heating procedure and highlights the single crystal to polycrystal nature of the RT-EDS→HT-EDS transition. The unit cells dimensions and space group of HT-EDS were researched using the collected XRPD pattern of HT-EDS by using indexing procedures (TREOR, DICVOL or X-CELL programs) in the Material Studio suite[10]. Unfortunately, due to the low number of diffraction peaks in the HT-EDS XRPD pattern, it was not possible to establish any unit cell nor any space group with a good index of reliability.

To conclude on the screening of polymorphs, no hydrates nor solvates were found and only two polymorphs (HT-EDS and RT-EDS) which are enantiotropically related ($T_{transition}$= 220°C) and which were already discussed by Santhakumari, could be evidenced during this work. The structure of HT-EDS remains unsolved despite our efforts. In the context of NPLIN, it is however reasonable to assume that the HT-EDS form could

not crystallize in our aqueous solutions since its stability domain is above 220°C.

5.3 Discovery of a NPLIN phenomenon in EDS aqueous solution

First, it was necessary to determine the solubility behaviour of EDS in water and the absorption properties at the wavelength used.

5.3.1 Solubility of Ethylenediamine Sulfate

Figure 5-5 reports the evolution of RT-EDS solubility as a function of temperature in water as measured by gravimetry (§3.2). It can be observed that RT-EDS is highly soluble in water: at 20°C, the concentration of the saturated solution is as high as 35 %wt. No data were available in literature to compare these results.

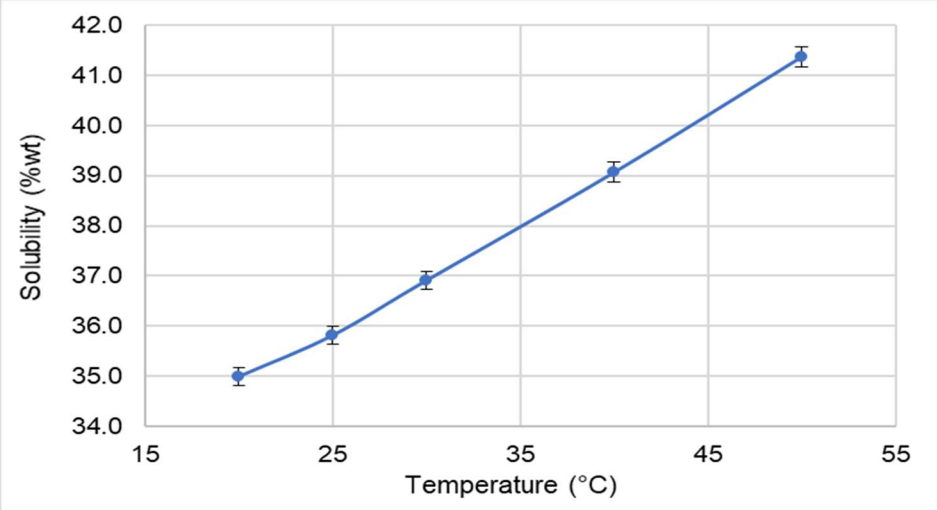

Figure 5-5-Experimentally measured aqueous solubility of RT-EDS as a function of temperature.

5.3.2 Spectroscopy UV-vis

Before starting the NPLIN experiments, it was necessary to confirm the absence of any unwanted light absorption by the EDS aqueous solutions. Figure 5-6 shows the measured absorption spectra of pure demineralized water and saturated solution of EDS (i.e., 35%wt), either non-filtered and filtered (syringe filter of 0.45µm). As explained in Chapter 4, pure water shows an absorption peak at 980nm, and absorbs weaklier at 760nm and 840nm. At the working wavelengths (i.e., 532nm and 1064nm) represented by vertical dashed lines in Figure 5-6, EDS solutions show a very small absorption compared to pure water. It can also be seen that non-filtered EDS solutions have slightly higher absorption than the filtered solutions. However, in both cases, the absorption is weak, and no photochemical reactions are expected nor have been observed.

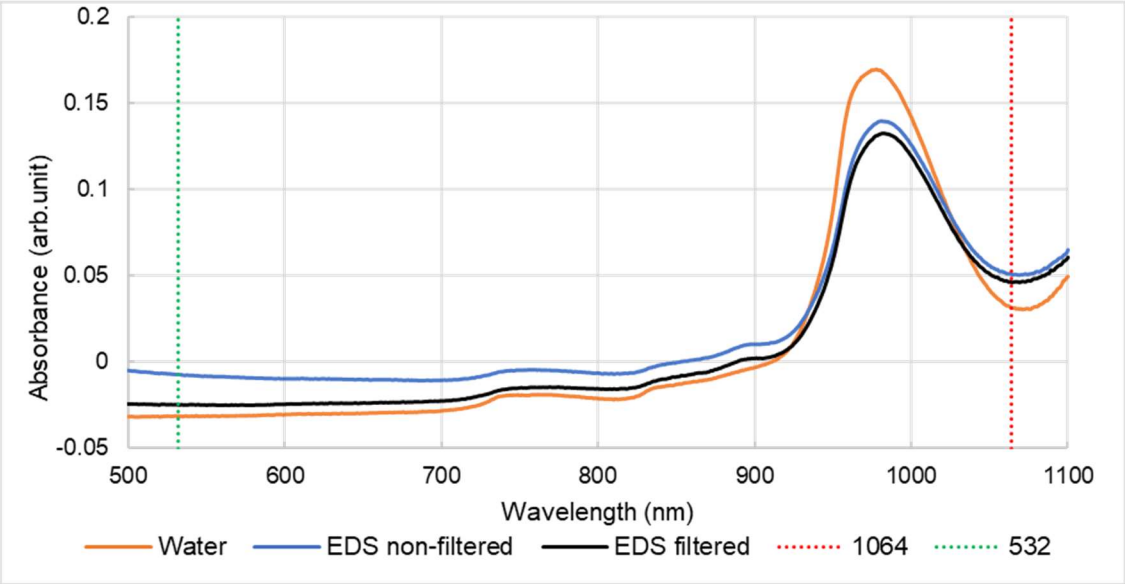

Figure 5-6-Absorption spectra of water and saturated aqueous solution of EDS

5.3.3 **The NPLIN phenomenon**

During this PhD work, we discovered that nucleation of supersaturated aqueous solutions of EDS could be triggered by laser pulses. Basing our methodology with reference to our experiments reported in Chapter 4, the first stage was to determine the conditions of irradiation and solution parameters for NPLIN phenomenon to occurs and to be measured with reasonable time scale. At first, a supersaturation of β=1.15 was used with different number of pulses (from 1 to 100) and energies (from 34.8 to 85.6mJ). All irradiated samples nucleated fast and gave rise to several crystals in each vial. In order to favour the nucleation of a single crystal per irradiated vial, supersaturation was decreased to β=1.10, as pulse number and energy could not be reduced. Like for K_2SO_4, a single pulse was found sufficient to favour the crystallization of a single individual crystal per vial. An energy of 34.8mJ was chosen as it allowed sufficiently fast nucleation kinetics so that the use of higher energies was not necessary. Figure 5-7 shows the typical NPLIN kinetics observed for EDS supersaturated solution β=1.10, 100 vials were exposed to 1 pulse at 34.8mJ.

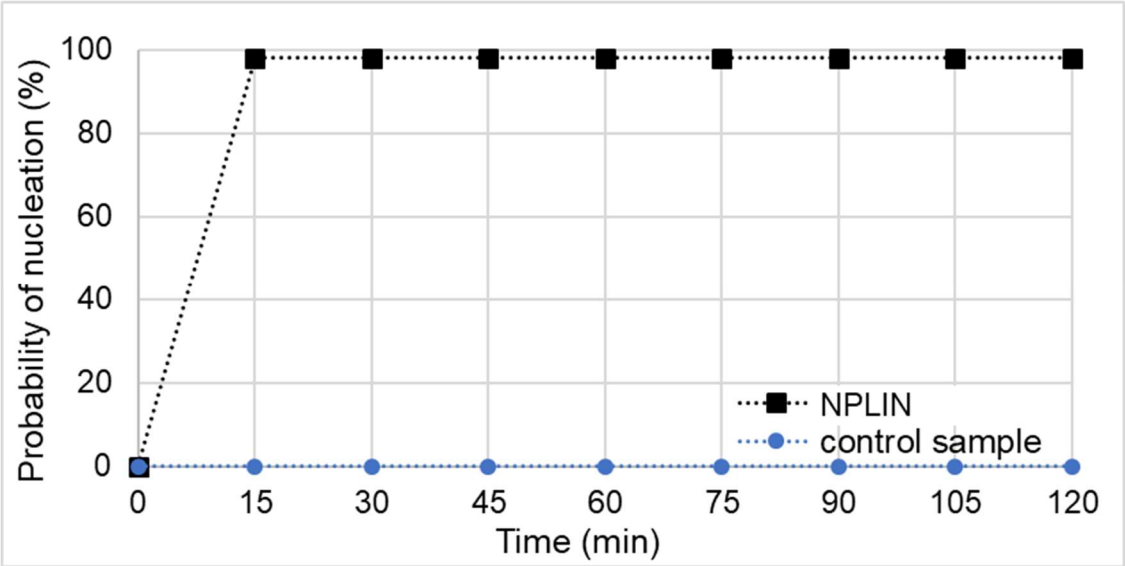

Figure 5-7-Probability of nucleation as a function of time for EDS supersaturated solution β=1.10 exposed to 1 pulse at 34.8mJ at 1064nm compared to non-exposed control samples. .

Regarding spontaneous nucleation of EDS supersaturated solution at β=1.10, the control samples did not nucleate during our NPLIN experiments. Actually, they remained supersaturated for at least 3 weeks and up to 2 years after the experiment, giving rise to only one single crystal per vial. The difference of induction time between spontaneous nucleation and NPLIN is striking. Thus, it cannot be denied that the exposure of the solution to laser light is responsible for nucleation.

5.4 Influence of impurities on NPLIN behaviour

As already discussed in Chapter 2-§2.5.3 and highlighted by our study concerning K_2SO_4 (Chapter 4- §4.4), the presence (or absence) of solid colloidal impurities plays a major role on the NPLIN mechanisms. The nature of these impurities as well as the nature of the light-matter interaction involved in the process remains to be fully understood. In this context, the aims of the experiments reported in this section were: (i) to confirm that the NPLIN kinetics of aqueous EDS solutions is also sensitive to the presence of such impurities, (ii) to identify their chemical nature, (iii) to replace the removed impurities by a given quantity of known particles for a better understanding of the influence of particle nature on NPLIN kinetics.

5.4.1 **Influence of filtration on EDS NPLIN kinetics**

The EDS supersaturated solutions (β=1.10) were filtered using either PTFE syringe filters or a Nylon membrane filter (Chapter 3- §3.3.1). Figure 5-8 shows the different nucleation probabilities as a function of time measured for the different sets (each set consists of at least 2 sets of 25 samples, with 10 control samples) irradiated with 1 pulse at 34.8mJ. As for the case of K_2SO_4 aqueous solutions (Chapter 4- §4.4), filtration induces a significant drop of the probability of nucleation. It can be seen that filtration with PTFE syringe filters gives rise to comparable probabilities of nucleation regardless of the pore size (i.e., 0.20µm and 0.45µm). Filtration with a Nylon membrane filter (0.45µm pore size) also gave a similar nucleation trend. This implies that most of the particles involved in the NPLIN process of EDS are larger than 0.45µm and have been removed by filtration, regardless of the method. Nevertheless, it cannot be excluded that particles smaller than 0.2 µm are still present in the solutions and still interact with the laser light after filtration. It has to be mentioned that, even to this day (i.e., more than 1 year after the experiment), the filtered control samples did not nucleate at all.

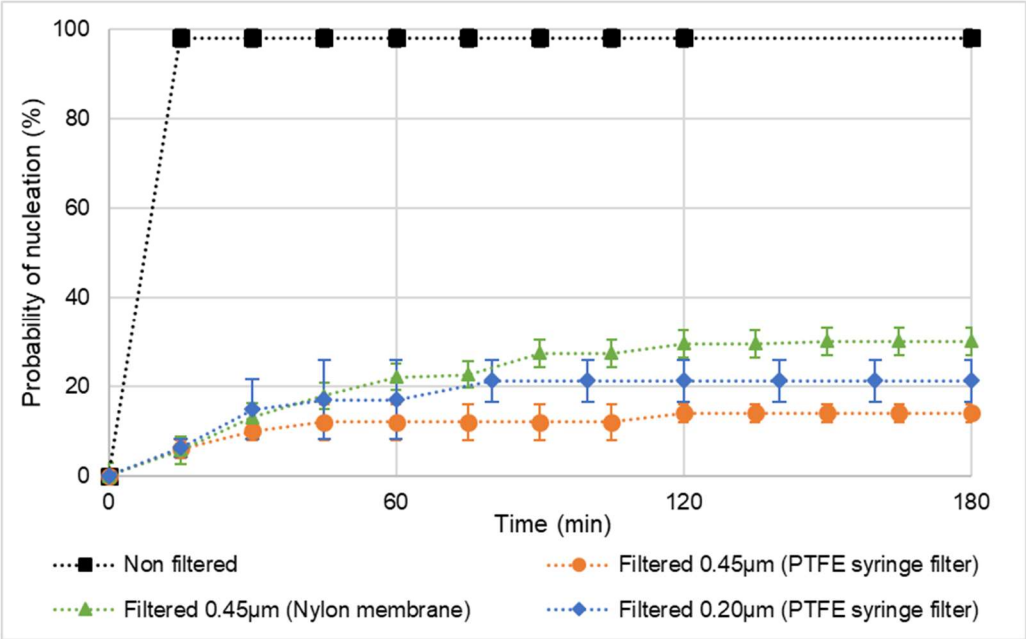

Figure 5-8-Evolution of the probability of nucleation versus time of irradiated aqueous EDS solutions (β=1.10) filtered by different methods (filtered with nylon membrane 0.45µm; PTFE syringe filter of 0.45µm and 0.2µm). (For non-filtered solution error bars are smaller than the size of the squares)

5.4.2 **Investigations on the chemical nature of the impurities removed by filtration**

The use of Nylon membrane filters offers the possibility to collect the filtered impurities in view to further physico-chemical analyses. After filtration of the hot solution of EDS (i.e., prior to its transfer in the vials), the white filter became orange, as shown in Figure 5-9. The filter was weighed before and after filtration: the mass of impurities divided by the mass of dissolved RT-EDS in the filtered solution gave, on average, a concentration of impurities of 0.14mg per gram of solid RT-EDS (i.e., 0.01%wt of impurities in the solid). It should be noted that impurities are not visually detectable in the unfiltered solutions, except for a slightly yellow appearance compared to the filtered solution that are completely transparent to the eyes. The impurities collected on the membrane filter were then analysed using XRD, ATR-FTIR and microscopy. Concerning XRD, no diffraction peaks were detected during the analysis (in a range from 2 to 100 2θ), which could mean that the impurities are amorphous or that the diffracting particles are too small to be detected. Moreover, the SEM picture hardly showed any distinct morphology of the particles (Figure 5-10), and SHG analyses did not revealed any SHG signal.

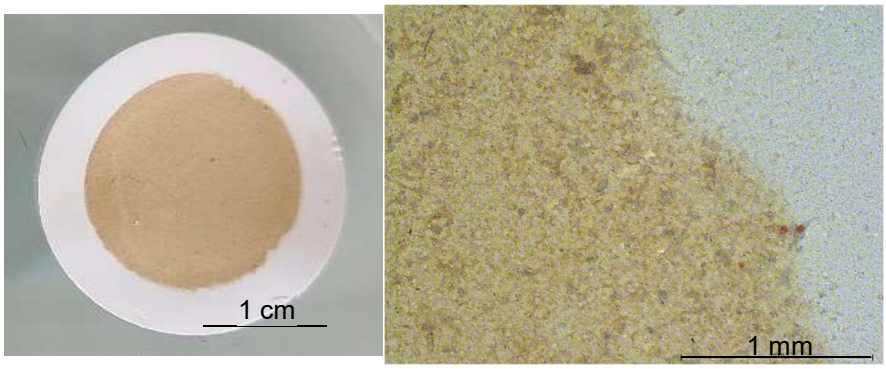

Figure 5-9-Visual aspect of the Nylon membrane filter after filtration of 30mL of EDS solution (β=1.10). On the right, the same membrane observed with optical microscope with magnification x30.

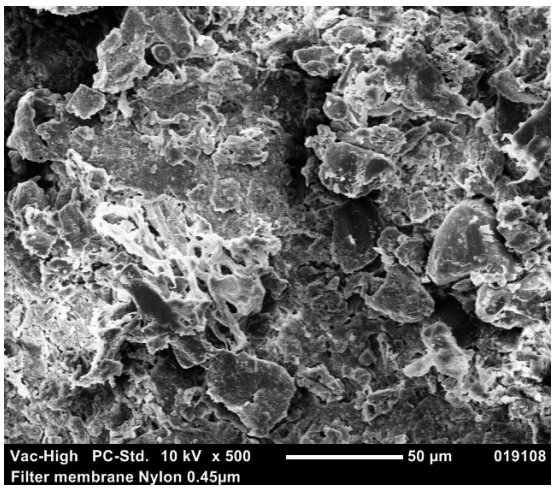

Figure 5-10-SEM analysis of the Nylon filter membrane

The ATR-FTIR spectra of the RT-EDS pure powder, the clean membrane filter and the membrane filter after filtration are shown in Figure 5-11. It can be seen that the filtered impurities show typical absorbance peaks at 1202, 1147, 1079, 504 and 461cm^{-1}. Those peaks are distinct from EDS powder and Nylon membrane. FTIR spectrum of the impurities were compared to possible reference spectra such as iron phosphate[11] as it was the impurity identified by Ward *et al.*[2]. Then other metallic references were compared, including stainless steel[12], iron oxide[13], chromium oxide[14] or nickel oxide[15]. No match with the experimental peaks of the collected impurities was found. The chemical nature of the impurity could not be determined using FTIR analyses.

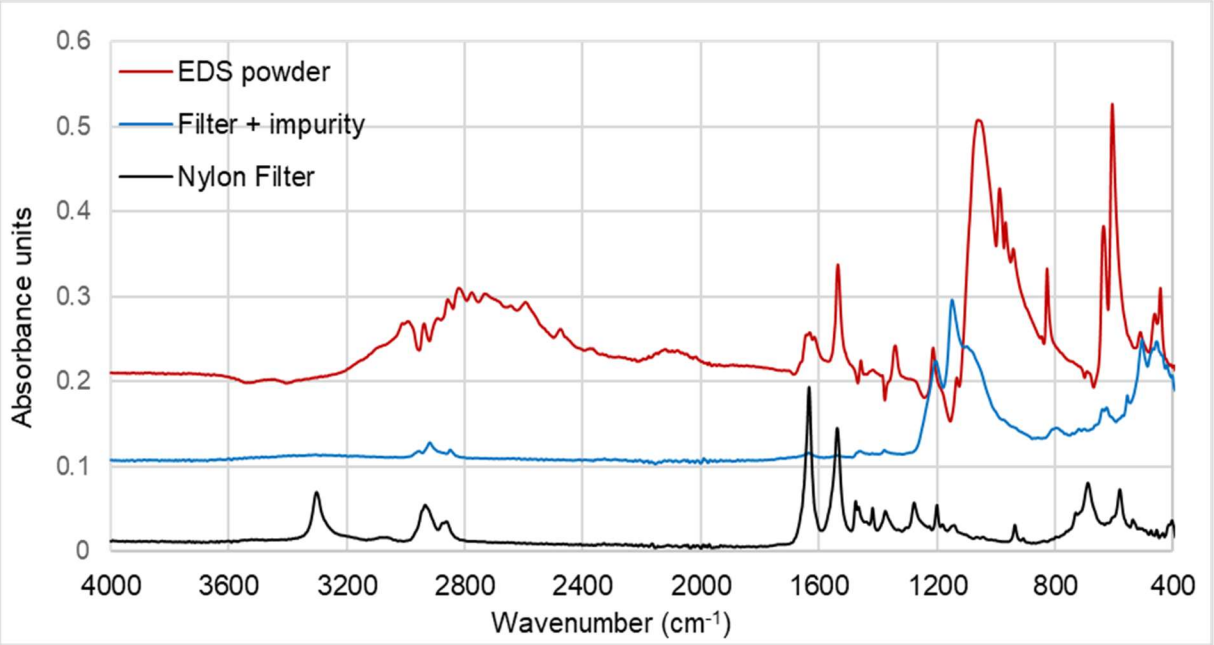

Figure 5-11- ATR-FTIR spectra of the Nylon filter membrane alone, the filter membrane with impurities and the solid RT-EDS. Absorbance of RT-EDS powder and filter + impurity has been Y-offset for clarity.

To conclude about the chemical nature of these filtered impurities, ICP-E (inductively coupled plasma – atomic emission) spectroscopy was used. For this analysis, filtration of the EDS aqueous solution was conducted using a PTFE filter membrane of 0.2µm pore size (Nylon filter membrane could not be used in this experiment because Nylon dissolved in the acidic conditions used hereafter). After filtration, the PTFE membrane containing the impurities was soaked in hydrochloric acid 35% for 24h in order to dissolve the impurities, prior to dilution with water (by a factor of ten). Dilution of the acidic solution was necessary to avoid damaging the plasma torch of the spectrometer. The same procedure was repeated using a clean PTFE filter membrane to create a control sample.

The results presented in Table 5-1 show that the impurities collected by the membrane filter mainly consist of metallic elements (Fe, Cr, Ni), with a composition similar to that of stainless steel. Indeed, stainless steel is an alloy of iron with at least 11%wt of chromium which gives the alloy some corrosion resistance properties[16]. Different types of stainless steel exist, involving the addition of nickel, molybdenum, sulphur or other elements in different concentration[17]. It should be mentioned that the concentration values given in Table 5-1 are only relative values: no separate calibration for each chemical element with standard solutions was performed. It should also be underlined that the ICP-E spectroscopy cannot detect all the element of the periodic table: some elements such as carbon, oxygen or nitrogen are indeed undetectable.

Table 5-1-List of the significantly detected elements by ICP-E analyses and their qualitative concentrations (in mg/L)

Element	Concentration (mg/L)		Difference
	Control sample	Impurity sample	
Iron (Fe)	3.30	8.10	4.80
Nickel (Ni)	0.28	0.76	0.48
Chromium (Cr)	0.06	0.71	0.65
Sulphur (S)	0.14	1.60	1.46

It is interesting to compare these analyses with those of Ward *et al*.[2] who studied the impurities collected by filtration of NH_4Cl supersaturated solutions and found, after ICP-OES and ICP-MS analysis, that the solid consisted mainly of iron, and a smaller part of phosphorus. They concluded that the impurity might be iron phosphate as it is insoluble in water and has a yellow-brown colour similar to the colour of the membrane after filtration. In the case of EDS solutions, our hypothesis is that the solid impurities of our EDS commercial lots come from the industrial production step: small steel particles may be scratched out from the tank walls or from the mechanical stirrer and pollute the batches of RT-EDS crystals. Moreover, it is known that corrosion of steel can occurs in industrial tank[18], the product of the corrosion is called rouge and contain iron oxide (rust) but also metallic oxide such as chromium or nickel according to the steel composition[19]. This would also match with the yellow-brownish colour observed on the filter after filtration.

5.4.3 Influence of controlled addition of impurities in EDS supersaturated solutions

In this section, the reported experiments aim at doping the filtered EDS aqueous solution by intentional addition of particles in order to check if the initial NPLIN kinetics (i.e., prior to filtration) can be retrieved. Furthermore, the use of different kind of particles can help to identify if all particles can enable the NPLIN phenomenon or if some are more suitable than others and thus to understand how these particles are involved in the NPLIN mechanism. The tested particles are (i) gold nanoparticles (ii) silver nanoparticles (iii) stainless steel particles and (iv) rust particles (See Chapter 3- §3.3.2 for more details on the particles). The concentrations of the particles in the doped solutions are given in Table 5-2. The concentration of rust particles has been established based on the measured impurity content of unfiltered solutions (i.e., 0.14 mg/g of RT-EDS). The concentration of stainless steel is much higher compared to the expected impurity content to compensate the fact that the powder settles in the bottom of the vial and that no surfactant has been used to help dispersion. We were limited by the fact that silver and gold nanoparticles were purchased as aqueous dispersions and only concentration of 0.006 mg/g could be achieved without changing the supersaturation of the solutions.

Table 5-2-Concentration of the particle added in supersaturated solution of EDS (mg per g of dissolved RT-EDS)

	Gold	Silver	Stainless Steel (316L)	Rust	Impurity removed
Concentration mg/g EDS	0.006	0.006	60	0.16	0.14

The NPLIN behaviour at 1064 nm of the different supersaturated doped solutions (β=1.10) exposed to 1 pulse at 34.8mJ is presented in Figure 5-12. For each condition, at least 2 sets of 25 samples were studied with 5 control samples. Even if none of the particles tested allowed to retrieve the nucleation behaviour of the non-filtered solutions, Figure 5-12 highlights that doped solutions exhibit higher probability of nucleation with reference to the filtered and undoped solutions. It is however interesting to consider that the different particles used for doping generate different NPLIN behaviours: For instance, at t=4h after irradiation, it appears that the solutions doped with silver nanoparticles have higher probability of nucleation (Pn=80%) compared to steel doped (Pn=70%), rust doped (Pn=55%) and gold doped (Pn=42%) solutions. This is all the more

remarkable if one considers that these nucleation trends are uncorrelated to the impurity concentrations: for instance, silver doped samples have higher nucleation probabilities compared to rust doped samples whereas the concentration of silver is 20 times lower than the concentration of rust. It is therefore possible to propose that the different behaviours could be due to different properties of the particles in solution, such as their absorption or diffusion properties of the laser light and heat transfer.

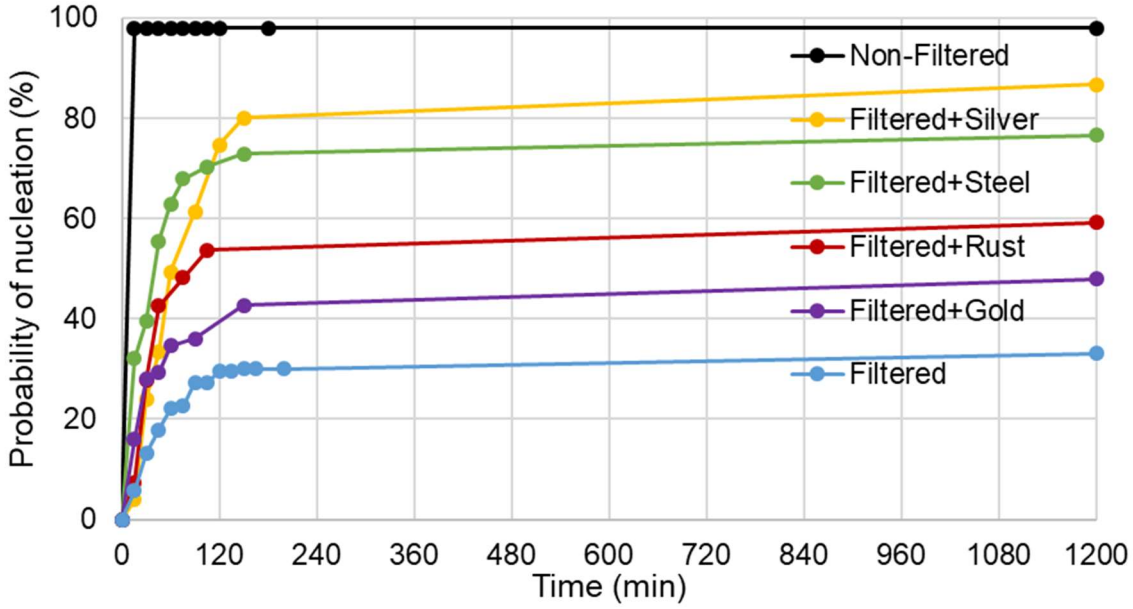

Figure 5-12-Evolution of the probability of nucleation versus time for supersaturated solution of EDS(β=1.10) doped with different impurity exposed to 1 pulse at 34.8mJ at 1064nm. Non-filtered and filtered solution are reference

If we compare the concentration of the particles in solution (Table 5-2), it is interesting to note that while solutions doped with gold or silver have the same impurity concentration (i.e., 0.006 mg/g of RT-EDS), the NPLIN kinetics are strongly different. Concerning silver doped solutions, it should be highlighted that while the nanoparticles concentration is considerably reduced with reference to the impurity concentration in unfiltered solutions (i.e., 0.14mg/g of RT-EDS), it is sufficient to re-increase the probability of nucleation to almost the same level than unfiltered solutions.

The fact that filtered doped solution does not follow the same kinetics as non-filtered solution could be due to a difference in composition, concentration or dispersion of the particles in the solution. Ward *et al.*[2] doped their aqueous NH_4Cl solution with iron-oxide (Fe_3O_4), they observed 100% of probability of nucleation for unfiltered and doped solution but only 60% for filtered solutions. Moreover, NH_4Cl filtered solutions gave on average one crystal per vial whereas unfiltered samples

gave 7.8±1.3 crystals per vial. Doping of filtered solution with Fe_3O_4 allows to retrieve similar number of nuclei (6.8±2.6), and addition of PEG to Fe_3O_4 increased the number of nuclei to 17.9±4.8. They concluded that the addition of surfactant should stabilize the dispersion of particle which produce more nucleation site.

5.4.4 Influence of the wavelength on the doped solution

The influence of the laser wavelength on NPLIN kinetics has been considered in several case studies[20–23] and it is generally admitted that this parameter has no influence on the NPLIN phenomenon (Chapter 2- §2.6.1) but the 532nm radiation is preferred because it is less likely to result in solution heating. In the context of our investigation, it is worth considering the characteristics of the nanoparticles in terms of absorbance (see Appendix A.2), which may behave differently at different irradiation wavelengths. In particular, the fact that gold nanoparticles are known to absorbs 520nm light prompted us to reinvestigate the NPLIN behaviour of doped EDS aqueous solutions at 532nm.

As discussed in Chapter 2- §2.4.4, the nanoparticle heating hypothesis poses that an insoluble colloidal impurity absorbs the laser light, resulting in a very localized temperature increase of the supersaturated solution surrounding the particle. Thus, we hypothesize that if the wavelength of the laser matches the absorption properties of the particles, then faster NPLIN kinetics would occur as more energy could be released.

In this context, the same experiments as those reported in section §5.4.3 were reproduced by changing only the laser wavelength from 1064nm to 532nm. The use of a frequency-doubling module (see Chapter 3- §3.4) to convert the 1064 nm pulses to 532nm pulses modifies the energy value at the output of the laser. Using an energy adjustment device, we settle the 532 nm pulse energy to 35.0mJ, a value which is close to the energy of 34.8 mJ delivered at 1064nm. Once again, the irradiated solutions were supersaturated at β=1.10 and irradiated with 1pulse. At least 2 sets of 25 samples were exposed to laser light, and 5 samples were not exposed for control. The concentrations of particles added in the solutions are the same than used in section 5.4.3 (Table 5-2).

Figure 5-13 presents the curves obtained for the different sets of solutions irradiated at 532nm. Overall, it can be seen that the use of the 532 nm radiation gives rise to much higher probabilities of nucleation compared to the experiments performed at 1064 nm (Figure 5-12). Alike the

experiments performed at 1064 nm, the results shown in Figure 5-13 highlight that different particle doping gives different NPLIN kinetics. For instance, at t=4h after irradiation, the solutions doped with rust or steel nanoparticles have the same highest probability of nucleation (Pn=95%) compared to silver doped (Pn=90%) and gold doped (Pn=85%) solutions.

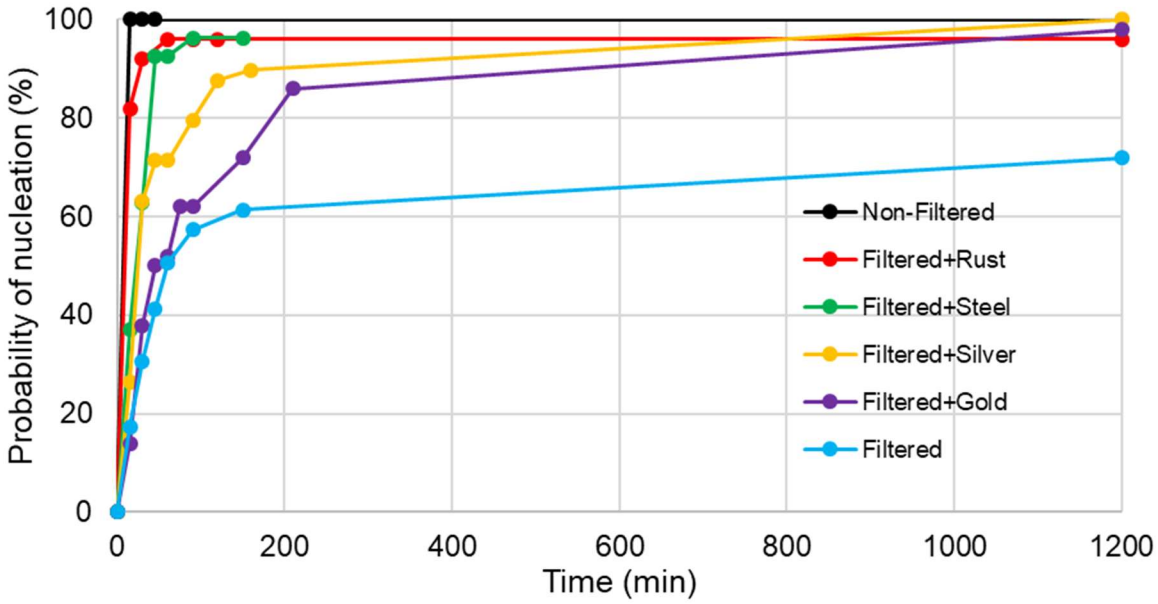

Figure 5-13-Evolution of the probability of nucleation versus time for supersaturated solution of EDS doped with a different impurity, exposed to 1pulse 35mJ at 532nm. Non-filtered and filtered solutions are references

Figure 5-14 compares the Pn(t)=f(t) curves obtained by conducting the NPLIN experiments at 532nm to those obtained at 1064nm for each type of treatment (i.e., non-filtered, filtered, doped with Ag, Au, Steel, Rust particles). It can be clearly seen that NPLIN experiments performed at 532nm are more efficient than those at 1064nm: for each type of particle tested, the green curve (532nm) is above the orange curve (1064nm) in every chart of Figure 5-14. In particular it should be highlighted that, even if the Pn(t)=f(t) curves for unfiltered samples are almost superimposable when working at 532 and 1064 nm, the filtered samples irradiated at 532 nm gives rise to a higher nucleation probability compared to that of filtered solutions irradiated at 1064 nm. It can also be observed that the Pn(t)=f(t) curves of samples doped with rust or steel and irradiated at 532 nm are almost superimposable to the curves obtained for un-filtered samples (i.e., very high kinetics of nucleation), whereas much slower NPLIN kinetics were observed at 1064 nm for these two types of particles. The Pn(t)=f(t) curves concerning silver doped solution seems to be less sensitive to the wavelength used for irradiation, but it should be underlined that the probability of nucleation under 1064 nm irradiation was already high.

Concerning gold nanoparticles, a similar behaviour to rust doped solution was observed with a probability of nucleation almost doubled at 532nm compared to 1064nm.

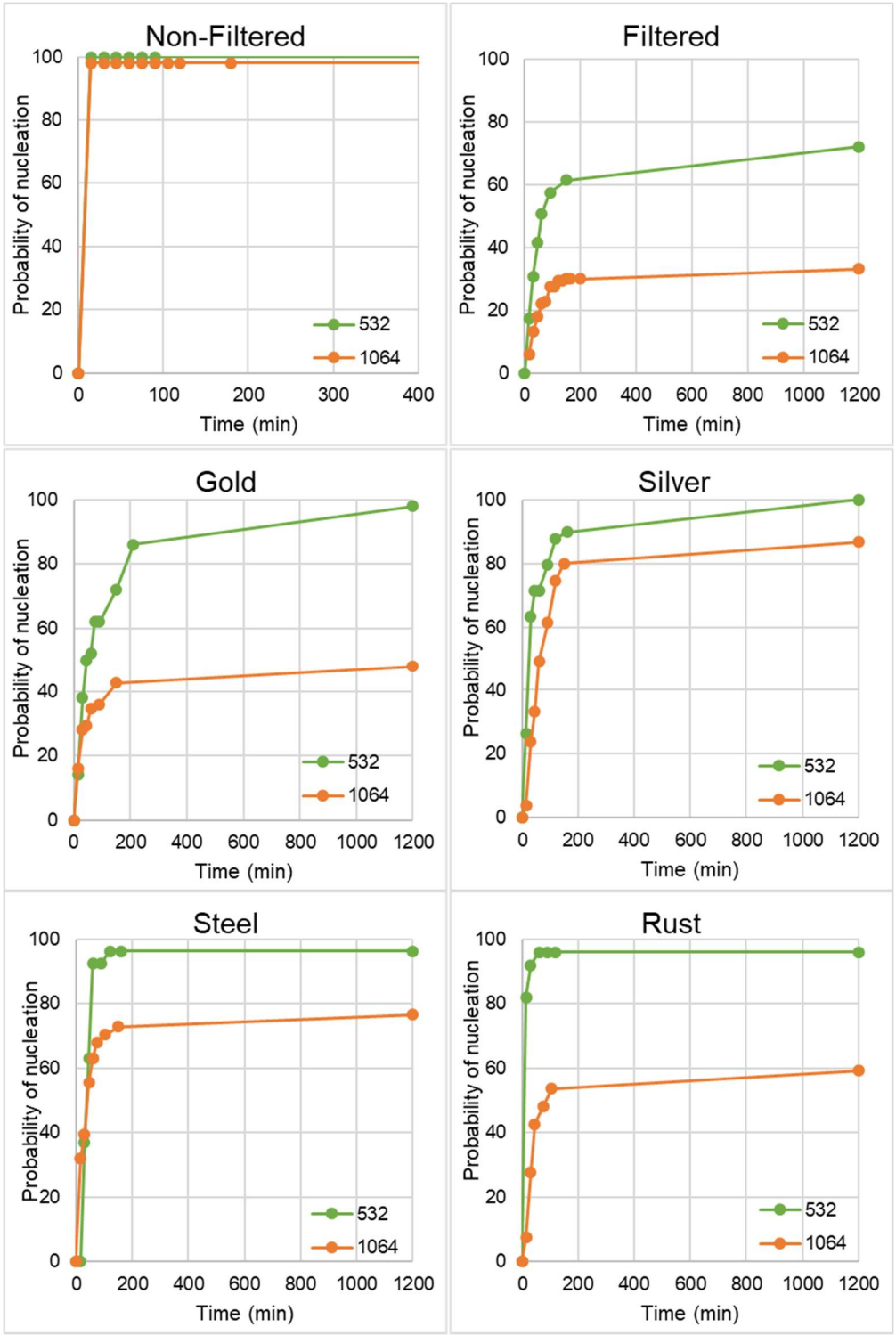

Figure 5-14-Influence of the wavelength on the NPLIN behaviour of filtered solution with different particles

It is therefore demonstrated that the addition of particles promotes the NPLIN phenomenon and enables to recover a high probability of nucleation after filtration. Besides, the wavelength of the laser is shown to have a stronger impact on the NPLIN kinetics than expected from literature data: the 532 nm radiation is more efficient than the 1064 nm to trigger nucleation. The effect is particularly striking when the solutions are doped with gold and rust nanoparticles. The UV-vis spectra of the different doped aqueous solutions have been measured (Appendix A.2) in order to evidence any correlation between the nucleation probability and the absorption impurities at (i) 1064nm and (ii) 532nm.

(i) At 1064nm, there is no absorbance of the impurity itself but, absorbance of water. No correlation between the NPLIN kinetics and the absorbance of particle could be established.

(ii) At 532 nm, absorption of water is lower than at 1064nm and so are solutions, particularly steel and silver. However, in the case of gold particles there is an absorption band at 532nm which is due to the particle and not to the water solvent. In the case of rust particle, it seems that there is also higher absorption due to the particle. The specific absorption of gold particle and rust could explain the important increase of probability of nucleation observed at 532nm.

Since RT-EDS is a molecular salt whose crystals exhibit supramolecular chirality, the following section focuses on the chirality of the crystals produced as a function of the polarization geometry used, of the wavelength of irradiation, and of the impurity profile.

5.5 Influence of polarized light on the crystallization of RT-EDS

Understanding chiral symmetry breaking is a major challenge in many scientific fields[24–26]: how can we control crystallization to selectively isolate one enantiomer? How can we explain that a racemic mixture evolves spontaneously towards homochirality[27]? Such are fundamental questions with deep implications that could partly explain the origin of life on earth[28,29]. Several studies evidenced stereospecific light-matter interactions during physico-chemical processes[30]. It was for instance evidenced that the use of circularly polarized light (CPL) can impact the stereoselectivity of several photochemical processes and de-symmetrize symmetric situations, including photochemical reactions (also called asymmetric photo-synthesis)[31–33], photoderacemizations[30,34], combined

with symmetry breaking to achieve deracemization[35,36]. Such type of stereoselective light-matter interactions have also been reported in the case of non-photochemical processes. For instance, it has been reported that the exposure of a solution of sodium chlorate during its evaporation to beta radiations with circularly polarized electron yields an asymmetric distribution of enantiomorphs[37]. Another example has been reported by Niinomi *et al*.[38] who demonstrated that the chirality of $NaClO_3$ crystal, produced from an aqueous solution doped with Ag nanoparticles, can be controlled by the direction of circularly polarized light of a continuous wave laser (532nm) irradiating the solution. Therefore, it seems that the use of the suitable light polarization can have a stereoselective impact on non-photochemical processes.

Can a similar effect be envisaged for NPLIN processes? Would it be possible to produce a single enantiomorph out of a racemic solution by triggering its stereoselective crystallization via the suitable light polarization? Several NPLIN studies tried to answer these questions focusing in particular on compounds exhibiting supramolecular chirality such as sodium chlorate[38–40] and 4,4'-dimethyl-chalcone.[41] In the case of 4,4'-dimethyl-chalcone (§2.4.1.2), Circularly polarized light does not influence the chirality of the compound, but linearly polarized light allows to increase the enantiomeric excess but without control of the enantiomorphs formed. In the case of sodium chlorate, it appears that the laser light (either RCP, LCP or LP) induces first the formation of an achiral metastable polymorph that converts into either one or the other enantiomorphs. Thus, within the framework of the OKE mechanism, stereoselective NPLIN deserves to be explored in the absence of more documented case studies.

Due to its supramolecular chirality, EDS is an ideal choice for conducting NPLIN stereoselective study. In addition, there is in average one crystal per vial that necessarily originates from NPLIN and with a chirality easily identified by polarised optical microscope. To this end, the crystals produced during NPLIN experiments were collected (after a growth time of 3hours) and examined with a polarizing microscope to determine the chirality the next day. Then, crystal enantiomeric excess (Cee) was calculated following Equation 5-1, where N_d and N_l represent respectively the number of d-crystals and the number of l-crystals.

$$Cee = \frac{N_d - N_l}{N_d + N_l} \qquad \textit{Equation 5-1}$$

The standard deviation (σ) weighted by the number of crystals in each vial is calculated with Equation 5-2 where N is the number of vials, w_i is the number of crystals in the vial i and x_i is the enantiomeric excess of vial i. The weighted mean is calculated by Equation 5-3.

$$\sigma = \sqrt{\frac{1}{N-1}\left[\frac{\sum(w_i(x_i-\bar{x})^2)}{\sum w_i}\right]} \qquad \textit{Equation 5-2}$$

$$\bar{x} = \frac{\sum w_i x_i}{\sum w_i} \qquad \textit{Equation 5-3}$$

5.5.1 **Non-filtered samples irradiated at 1064nm**

In the following experiments, different polarization geometries of the incident laser beam were used: linearly polarized light (LP), right circularly polarized light (RCP) and left circularly polarized light (LCP). For each polarization geometry, 100 vials (2 sets of 50 vials with 10 control samples) containing 1mL of non-filtered supersaturated solution of EDS (β=1.10) were exposed to 1 pulse at 34.8mJ (23 MW/cm²) at 1064nm. Assuming that the polarization geometry can control the Cee, it is expected to obtain an opposite chirality when using RCP or LCP (Cee=1 or Cee =-1) and a Cee of 0 when using LP or spontaneous nucleation. Table 5-3 shows no influence of laser polarization on the Cee, LCP and LP give the same Cee value of 0.02 and RCP gives a slightly higher value of -0.14.

Table 5-3-Results obtained for the NPLIN experiments of EDS solutions with Left (LCP), Right (RCP) circularly polarized, or Linear (LP) polarized laser light (1 pulse, 34.8 mJ). 100 vials were exposed to the laser for each polarization. N_{vial} is the number of vials that crystallized; $N_{crystal}$ is the total number of crystals; N_d is the total number of d-crystals; N_l is the total number of l-crystals; Cee is the crystal enantiomeric excess; σ is the standard deviation calculated with Equation5-2.

Polarization	N_{vial}	$N_{crystal}$	N_d	N_l	***Cee±σ***
LCP	89	194	99	95	0.02±0.07
RCP	86	190	81	109	-0.14±0.07
LP	91	249	127	122	0.02±0.06

It should be stressed that even for the same experimental conditions, the number of crystals produced varies from vial to vial, generally one or two crystals up to four in some cases. When several crystals are produced, it is not possible to distinguish which ones were generated by the laser pulse and which ones were secondary crystals. Even if these secondary crystals are more likely due to secondary nucleation triggered by the appearance of the laser induced single crystal, only vials exhibiting one single crystal

were considered in order to avoid counting crystals that were produced by second primary crystallization. Table 5-4 presents the Cee calculated from population of only one crystal per vial. The Cee values are quite high (0.1 for RCP, 0.2 for LCP and 0.3 for LP), but the standard deviation is also high (0.2), it indicates that more data would be necessary to obtain a suitable statistical confidence. The measured Cee are not high enough with reference to the standard deviation to establish a correlation between the polarization of the laser light and the preferential nucleation of one enantiomorph over the other.

Table 5-4-Summary of the Results Obtained for Nucleation of EDS Solutions with Left (LCP), Right (RCP) circularly polarized, or linear (LP) polarized laser light (1 pulse, 34.8 mJ). Only vials exhibiting one crystal have been counted. N_{vial} is the total number of vials that crystallized; $N_{crystal=1}$ is the number of vials that gave only a single crystal; N_d is the number of d-crystals; N_l is the number of l-crystals; Cee is the crystal enantiomeric excess; σ is the standard deviation calculated.

Polarization	N_{vial}	$N_{crystal=1}$	N_d	N_l	***Cee±σ***
LCP	89	21	8	13	-0.2±0.2
RCP	86	19	10	9	0.1±0.2
LP	91	20	13	7	0.3±0.2

Polarization geometry (RCP, LCP or LP) seems therefore not correlated to RT-EDS crystals chirality when irradiating unfiltered solutions at 1064nm. The knowledge obtained through our previous experiments (section 5.3) prompted us to investigate the impact of changing the wavelength to 532nm in conjunction with the use of nanoparticles on the Cee of produced crystals.

5.5.2 **Non-filtered samples irradiated at 532nm**

Table 5-5 presents the Cee obtained for the non-filtered solutions of EDS exposed to linear or left circular polarized light at 532nm (β=1.10, 1pulse at 35mJ, set of 25 vials for each polarization). In these conditions, as 12 crystals per vials were obtained on average, only 10 vials out of the set of 25 were observed under the microscope. Among the ca. 120 crystals observed, the chirality of only half of them could be determined due to the size and morphologies of some crystals. We however confirmed that the distribution of enantiomorphs among these ca. 60 individuals is representative of that of all the crystals found in the 25 vials and we conclude that there is a distribution close to 50/50 between each enantiomorphs, whatever the polarization used.

Table 5-5-Results obtained for nucleation of EDS solutions exposed to Left (LCP) circularly polarized laser light or linear (LP) polarized laser light at 532nm. N_{vial} is the number of vials analysed; $N_{crystal}$ is the total number of crystals; N_d is the total number of d-crystals; N_l is the total number of l-crystals; Cee is the crystal enantiomeric excess; σ is the standard deviation calculated

Polarization	N_{vial}	$N_{crystal}$	N_d	N_l	Cee±σ
LP	10	114	28	27	0.0±0.1
LCP	10	125	34	39	-0.07±0.08

When irradiating the unfiltered solution at 532nm with either LP or LCP, our data show that both conditions gives a Cee values close to 0. Thus, there is no correlation between the chirality of RT-EDS crystals and the polarization geometry used for NPLIN at 532 nm.

5.5.3 **Stainless steel doped sample**

Table 5-6 presents the Cee obtained for filtered and doped with steel solutions of EDS exposed to either linear or left circular polarized light at 1064 nm and at 532nm (β=1.10 1pulse at 34.8mJ (1064nm) or 35mJ (532nm)). The Cee calculated is closed to 0 indicating that there is no preference for an enantiomorph. No statistical study was done for the three other doping particles used but, a fraction of vial was checked and a similar number of d and l crystals were found in each vial.

Table 5-6-Results obtained for nucleation of EDS solution doped with steel particle exposed to left circularly polarized light (LCP) or linear polarized light (LP) at 1064nm and 532nm. N_{vial} is the number of vials analysed; $N_{crystal}$ is the total number of crystals; N_d is the total number of d-crystals; N_l is the total number of l-crystals; Cee is the crystal enantiomeric excess; σ is the standard deviation calculated

Wavelength	Polarization	N_{vial}	$N_{crystal}$	N_d	N_l	Cee±σ
1064nm	LP	12	15	7	8	-0.1±0.3
	LCP	12	20	9	11	-0.1±0.2
	Polarization	**N_{vial}**	**$N_{crystal}$**	**N_d**	**N_l**	**Cee±σ**
532nm	LP	26	83	35	32	0.0±0.1
	LCP	24	63	16	20	-0.1±0.2

To conclude about the impact of laser polarization geometry on the Cee of RT-EDS during NPLIN, the results showed no strong correlation between these two parameters. Further to this, the wavelength and the addition of particles seems to have no impact on the Cee of EDS.

5.6 MEAN NUMBER OF CRYSTALS AND MORPHOLOGIES

Through the different experimental conditions applied to nucleate RT-EDS via laser light, it was noticed differences in the number of crystals obtained per vials and sometimes also in morphologies (which led to difficulties for the identification of the chirality).

5.6.1 Morphologies of EDS crystals

Figure 5-15 shows different morphologies of crystals obtained from NPLIN. Typical crystals obtained from NPLIN are shown in Figure 5-15 A, they are flat with different thickness. The thickness of the crystals can sometimes hinder the determination of the chirality: For instance, the crystal shown in Figure 5-15 B is very bulky and it is difficult to orientate the 4_1 axis in the suitable direction. The Figure 5-15 C, shows an example of the case where several crystals are produced in the same vial. In this case it can be difficult to assign a handedness to each crystal, but the darkness and brightness have been used to account for the two chiralities.

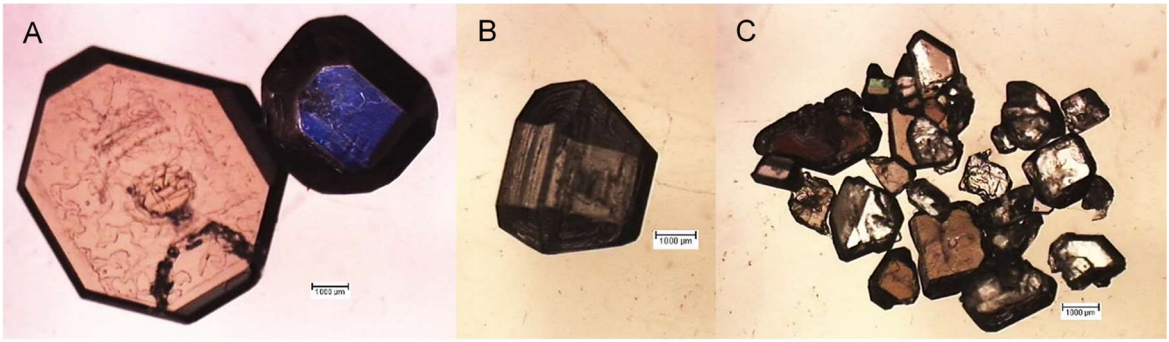

Figure 5-15-Example of RT-EDS crystals obtained via NPLIN. A- d and l-crystals obtained from 2 different vials. B- crystal with undetermined chirality C- numerous crystals obtained from one vial.

5.6.2 Mean number of crystals

Table 5-7 gives the mean number of crystals counted through the different experimental conditions.

First, one can note a slight difference between the mean number of crystals obtained via linear polarized light or circular polarized light, but it is not significant enough to consider an influence of the polarization on the number of nucleated crystals.

Then, a marked increase of the number of crystals is observed when changing the working wavelength from 1064nm to 532nm. The mean number of crystals is multiplied by a factor 5 in the case of non-filtered solutions and by a factor 2 for filtered+steel doped solutions. This is coherent with the increase in probability of nucleation observed in Figure 5-14.

Finally, it should be underlined that filtered solutions gave on average 1 single crystals per vial (data not shown in Table 5-7 due to the absence of statistical data). It is also worth noting that even after doping the filtered solution with nanoparticles, the mean number of crystals remains low and does not compare with the situation for unfiltered solutions, especially while working at 532 nm.

Table 5-7-Mean number of crystals per vial according to nucleation conditions (wavelength, filtration of solutions and polarization either LP: linear polarization or CP: circular polarization)

Nucleation conditions				
	1064nm		532nm	
	LP	CP	LP	CP
Non filtered	2.75	2.20	11.25	12.50
Filtered+Steel	1.25	1.67	3.25	2.74

5.7 DISCUSSION ON THE MECHANISM

5.7.1 OKE mechanism

In the context of the OKE mechanism, dissolved molecules align their most polarizable axis in the direction of the electromagnetic field during irradiation of the solution. It is expected that different polarization geometries could either trigger the nucleation of different polymorphs or impact differently the probability of nucleation (Chapter 2-§2.4.1.2). Based on this framework, we hypothesized that using either RCP or LCP laser light during NPLIN experiments could impact the handedness of the formed crystals. EDS was the ideal candidate for this study: (i) the NPLIN effect is very efficient (Figure 5-7), (ii) only few crystals are produced per irradiated vials (Table 5-7), (iii) the chirality of the crystals can be quickly determined by microscopy (Figure 5-2). The results shown in this chapter highlight that there is no correlation between the polarization geometry of the laser (either RCP, LCP or LP) and the chirality of the RT-EDS crystals produced by NPLIN (§5.5). This applies either at 532 or 1064 nm, and even if metallic nanoparticles are added to the solution (Table 5-6). It is also worth noting that the polarization of the light did not influence the probability of nucleation of EDS and had a very limited impact on the number of crystals produced by NPLIN (Table 5-7).

Although not shown in this chapter, we also conducted similar experiments using $NaClO_3$ (another compound exhibiting supramolecular chirality) and modafinic acid (a molecular compound exhibiting molecular chirality): the data are shown in Appendixes A.3.1 and A.3.2. The obtained statistics also revealed an absence of correlation between the chirality of the produced crystals and the polarization geometry of the laser.

5.7.2 **Nanoparticle heating**

The nanoparticle heating hypothesis states the presence of solid impurities inside the solutions and those particles interact with the laser to produce heat or pressure wave. Our results show that the EDS solutions contain insoluble impurity particles. These particles have been isolated on the filter membrane in order to try identifying them. The analysis of the impurities, particularly the ICPE analysis, led us to suspect stainless steel as the impurity and possibly the product of corrosion of steel : rouge.

The EDS solutions that were filtered showed an important decrease of the probability of nucleation compared to non-filtered solutions (Figure 5-8). This agrees with the study on K_2SO_4 (Chapter 4- §4.4) and the literature[1,2,42]. The impact of the impurities as part of the NPLIN mechanism is confirmed. However, the mechanism by which the phenomenon occurs remains not clear as the interaction between the light and the particle, and its consequence on the solution are unknown. More NPLIN case study are therefore required: although the impurity content might be different for each investigated compound, it could serve to identify a family of materials suitable to trigger NPLIN effects.

In our experiments, filtered solutions were doped with different particles in order to gain knowledge on the nature of the interaction between the laser and the particle and on the mechanism by which nucleation is induced. The NPLIN of doped solutions shows that the use of different kind of particle leads to different NPLIN behaviour. Indeed, for all tested particles, doping allows an increase of the probability of nucleation compared to filtered solutions but does not permit to reach the initial behaviour of non-filtered solutions. This is particularly true for the 1064nm wavelength. When using the 532 nm wavelength, the probability of nucleation of filtered+doped solutions is closer to the nucleation behaviour of unfiltered solutions.

Regarding the number of crystals produced by NPLIN: (i) filtration decreases the number of produced crystals, (ii) doping does not enable to produce the same number of crystals than non-filtered solution (especially at 532nm). All these results underline the importance of the laser wavelength and the presence (and nature) of insoluble impurities in solutions.

5.8 CONCLUSION

To conclude, it is first important to point out that the NPLIN effect of EDS was not previously reported in the literature. Therefore, this study demonstrates the possibility to nucleate easily RT-EDS via the NPLIN process, it is the most effective NPLIN effect we observed, decreasing EDS (β=1.10) nucleation from months to minutes with a single laser pulse.

The influence of the presence of impurities and the impact of filtration on the NPLIN kinetics have been clearly evidenced in EDS solutions. The analysis of the impurities by ICP-ES shows a metallic composition close to that of stainless steel or its degradation product, rouge. Finally, the addition of particle in filtered solution resulted in the increase of the probability of nucleation during NPLIN. The use of a 532nm wavelength enhanced the impact of the particle added on the NPLIN kinetics.

At the early stage of this PhD work, EDS was chosen due to its supramolecular chirality and it was the suitable candidate to investigate if the laser could control the enantiomorph produced by varying the polarization geometry. Our results showed that, with the conditions tested, no stereoselective nucleation could be observed.

5.9 REFERENCES

(1) Javid, N.; Kendall, T.; Burns, I. S.; Sefcik, J. Filtration Suppresses Laser-Induced Nucleation of Glycine in Aqueous Solutions. *Crystal Growth & Design* **2016**, *16* (8), 4196–4202. https://doi.org/10.1021/acs.cgd.6b00046.

(2) Ward, M. R.; Mackenzie, A. M.; Alexander, A. J. Role of Impurity Nanoparticles in Laser-Induced Nucleation of Ammonium Chloride. *Crystal Growth & Design* **2016**, *16* (12), 6790–6796. https://doi.org/10.1021/acs.cgd.6b00882.

(3) Santhakumari, N. C.; Vallabhan, C. P. G. Electrical Conductivity, Dielectric Properties and Phase Transition in Ethylenediammonium Sulphate Single Crystals. *Journal of Physics and Chemistry of Solids* **1992**, *53* (5), 697–701. https://doi.org/10.1016/0022-3697(92)90210-5.

(4) Sakurai, K. A Direct Determination of the Crystal Structure of Ethylenediammonium Sulphate. *J. Phys. Soc. Jpn.* **1961**, *16* (6), 1205–1213. https://doi.org/10.1143/JPSJ.16.1205.

(5) Ben-Ghozlen, M.-H.; Kamoun, S.; Pabst, I.; Paulus, H. Crystal structure of ethylenediammonium sulphate [H3N(CH2)2NH3]SO4. **1995**.

(6) Matsumoto, A.; Ide, T.; Kaimori, Y.; Fujiwara, S.; Soai, K. Asymmetric Autocatalysis Triggered by Chiral Crystal of Achiral Ethylenediamine Sulfate. *Chem. Lett.* **2015**, *44* (5), 688–690. https://doi.org/10.1246/cl.150052.

(7) Mnyukh, Y. *Fundamentals of Solid-State Phase Transitions, Ferromagnetism and Ferroelectricity. 1st Books, Fairfield, USA, p*; 2010.

(8) Jayaraman, K.; Choudhury, A.; Rao, C. N. R. Sulfates of Organic Diamines: Hydrogen-Bonded Structures and Properties. *Solid State Sciences* **2002**, *4* (3), 413–422. https://doi.org/10.1016/S1293-2558(02)01269-4.

(9) Kleinman, D. A. Theory of Second Harmonic Generation of Light. *Phys. Rev.* **1962**, *128* (4), 1761–1775. https://doi.org/10.1103/PhysRev.128.1761.

(10) DS BIOVIA. Material Studio.

(11) Yu, X.; Zhan, Q. Phosphate-Mineralization Microbe Repairs Heavy Metal Ions That Formed Nanomaterials in Soil and Water; 2019. https://doi.org/10.5772/intechopen.84296.

(12) Ma, C.; Yuan, C.; Cao, P. A Facile Method to Prepare a Hydrophilic/Hydrophobic Metal Surface by Peptide. *Materials* **2018**, *11*, 1289. https://doi.org/10.3390/ma11081289.

(13) Veneranda, M.; Aramendia, J.; Bellot-Gurlet, L.; Colomban, P.; Castro, K.; Madariaga, J. M. FTIR Spectroscopic Semi-Quantification of Iron Phases: A New Method to Evaluate the Protection Ability Index (PAI) of Archaeological Artefacts Corrosion Systems. *Corrosion Science* **2018**, *133*, 68–77. https://doi.org/10.1016/j.corsci.2018.01.016.

(14) Anandhi, J. T.; Rayer, S. L.; Chithambarathanu, T. Synthesis, FTIR Studies and Optical Properties of Aluminium Doped Chromium Oxide Nanoparticles by Microwave Irradiation at Different Concentrations. *cme* **2017**, *5* (2), 43–54. https://doi.org/10.13189/cme.2017.050204.

(15) Fardood, S. T.; Ramazani, A.; Moradi, S. A Novel Green Synthesis of Nickel Oxide Nanoparticles Using Arabic Gum. *ChemJMold* **2017**, *12* (1), 115–118. https://doi.org/10.19261/cjm.2017.383.

(16) *DOE Fundamentals Handbook*, U.S. Department of Energy.; Material science; 1993; Vol. volume 1 of 2.

(17) Davis, J. R. *Stainless Steels*; ASM International, 1994.

(18) Zaffora, A.; Di Franco, F.; Santamaria, M. Corrosion of Stainless Steel in Food and Pharmaceutical Industry. *Current Opinion in Electrochemistry* **2021**, *29*, 100760. https://doi.org/10.1016/j.coelec.2021.100760.

(19) Corbett, R. Rouging - a Discoloration of Stainless Steel Surfaces. *Materials performance(USA)* **2001**, *40* (2), 64–66.

(20) Kacker, R.; Dhingra, S.; Irimia, D.; Ghatkesar, M. K.; Stankiewicz, A.; Kramer, H. J. M.; Eral, H. B. Multiparameter Investigation of Laser-Induced Nucleation of Supersaturated Aqueous KCl Solutions. *Crystal Growth & Design* **2018**, *18* (1), 312–317. https://doi.org/10.1021/acs.cgd.7b01277.

(21) Barber, E. R.; Ward, M. R.; Ward, A. D.; Alexander, A. J. Laser-Induced Nucleation Promotes Crystal Growth of Anhydrous Sodium Bromide. *CrystEngComm* **2021**. https://doi.org/10.1039/D1CE01180D.

(22) Matic, J.; Sun, X.; Garetz, B. A.; Myerson, A. S. Intensity, Wavelength, and Polarization Dependence of Nonphotochemical Laser-Induced Nucleation in Supersaturated Aqueous Urea Solutions. *Crystal Growth & Design* **2005**, *5* (4), 1565–1567. https://doi.org/10.1021/cg050041c.

(23) Ward, M. R.; Alexander, A. J. Nonphotochemical Laser-Induced Nucleation of Potassium Halides: Effects of Wavelength and Temperature. *Crystal Growth & Design* **2012**, *12* (9), 4554–4561. https://doi.org/10.1021/cg300750c.

(24) Wagnière, G. H. *On Chirality and the Universal Asymmetry: Reflections on Image and Mirror Image*; John Wiley & Sons, 2007.

(25) Barron, L. D. *Molecular Light Scattering and Optical Activity*; Cambridge University Press, 2009.

(26) Bentley, R. Chirality in Biology. In *Reviews in Cell Biology and Molecular Medicine*; John Wiley & Sons, Ltd, 2006. https://doi.org/10.1002/3527600906.mcb.200200008.

(27) Kondepudi, D. K.; Asakura, K. Chiral Autocatalysis, Spontaneous Symmetry Breaking, and Stochastic Behavior. *Acc. Chem. Res.* **2001**, *34* (12), 946–954. https://doi.org/10.1021/ar010089t.

(28) Blackmond, D. G. The Origin of Biological Homochirality. *Cold Spring Harb Perspect Biol* **2010**, *2* (5), a002147. https://doi.org/10.1101/cshperspect.a002147.

(29) Goldanskii, V. I.; Kuz'min, V. V. Spontaneous Mirror Symmetry Breaking in Nature and the Origin of Life. *AIP Conference Proceedings* **1988**, *180* (1), 163–228. https://doi.org/10.1063/1.37867.

(30) Feringa, B. L.; van Delden, R. A. Absolute Asymmetric Synthesis: The Origin, Control, and Amplification of Chirality. *Angewandte Chemie International Edition* **1999**, *38* (23), 3418–3438. https://doi.org/10.1002/(SICI)1521-3773(19991203)38:23<3418::AID-ANIE3418>3.0.CO;2-V.

(31) Kagan, H.; Moradpour, A.; Nicoud, J. F.; Balavoine, G.; Tsoucaris, G. Photochemistry with Circularly Polarized Light. Synthesis of Optically Active

Hexahelicene. *J. Am. Chem. Soc.* **1971**, *93* (9), 2353–2354. https://doi.org/10.1021/ja00738a061.

(32) Sugahara, H.; Meinert, C.; Nahon, L.; Jones, N. C.; Hoffmann, S. V.; Hamase, K.; Takano, Y.; Meierhenrich, U. J. D-Amino Acids in Molecular Evolution in Space – Absolute Asymmetric Photolysis and Synthesis of Amino Acids by Circularly Polarized Light. *Biochimica et Biophysica Acta (BBA) - Proteins and Proteomics* **2018**, *1866* (7), 743–758. https://doi.org/10.1016/j.bbapap.2018.01.004.

(33) Kawasaki, T.; Sato, M.; Ishiguro, S.; Saito, T.; Morishita, Y.; Sato, I.; Nishino, H.; Inoue, Y.; Soai, K. Enantioselective Synthesis of Near Enantiopure Compound by Asymmetric Autocatalysis Triggered by Asymmetric Photolysis with Circularly Polarized Light. *J. Am. Chem. Soc.* **2005**, *127* (10), 3274–3275. https://doi.org/10.1021/ja0422108.

(34) Kucirka, J.; Shekhtman, A. G. On the Deracemization of a Chiral Molecular Beam by Interaction with Circularly Polarized Light. *Physics Letters A* **1996**, *221* (3–4), 273–276. https://doi.org/10.1016/0375-9601(96)00555-5.

(35) Noorduin, W. L.; Bode, A. A. C.; van der Meijden, M.; Meekes, H.; van Etteger, A. F.; van Enckevort, W. J. P.; Christianen, P. C. M.; Kaptein, B.; Kellogg, R. M.; Rasing, T.; Vlieg, E. Complete Chiral Symmetry Breaking of an Amino Acid Derivative Directed by Circularly Polarized Light. *Nature Chemistry* **2009**, *1* (9), 729–732. https://doi.org/10.1038/nchem.416.

(36) Meinert, C.; Hoffmann, S. V.; Cassam-Chenaï, P.; Evans, A. C.; Giri, C.; Nahon, L.; Meierhenrich, U. J. Photonenergy-Controlled Symmetry Breaking with Circularly Polarized Light. *Angewandte Chemie* **2014**, *126* (1), 214–218. https://doi.org/10.1002/ange.201307855.

(37) Mahurin, S.; McGinnis, M.; Bogard, J. S.; Hulett, L. D.; Pagni, R. M.; Compton, R. N. Effect of Beta Radiation on the Crystallization of Sodium Chlorate from Water: A New Type of Asymmetric Synthesis. *Chirality* **2001**, *13* (10), 636–640. https://doi.org/10.1002/chir.10007.

(38) Niinomi, H.; Sugiyama, T.; Tagawa, M.; Murayama, K.; Harada, S.; Ujihara, T. Enantioselective Amplification on Circularly Polarized Laser-Induced Chiral Nucleation from a $NaClO_3$ Solution Containing Ag Nanoparticles. *CrystEngComm* **2016**, *18* (39), 7441–7448. https://doi.org/10.1039/C6CE01464J.

(39) Barber, E. R.; Kinney, N. L. H.; Alexander, A. J. Pulsed Laser-Induced Nucleation of Sodium Chlorate at High Energy Densities. *Crystal Growth & Design* **2019**, acs.cgd.9b00951. https://doi.org/10.1021/acs.cgd.9b00951.

(40) Ward, M. R.; Copeland, G. W.; Alexander, A. J. Chiral Hide-and-Seek: Retention of Enantiomorphism in Laser-Induced Nucleation of Molten Sodium Chlorate. *The Journal of Chemical Physics* **2011**, *135* (11), 114508. https://doi.org/10.1063/1.3637946.

(41) Murphy, N. C.; Compton, R. N.; Pagni, R. M. Effect of Chiral and Achiral Perturbations on the Crystallization of 4,4‘-Dimethylchalcone from Ethyl Acetate. *Crystal Growth & Design* **2007**, *7* (2), 449–452. https://doi.org/10.1021/cg0680125.

(42) Ward, M. R.; Jamieson, W. J.; Leckey, C. A.; Alexander, A. J. Laser-Induced Nucleation of Carbon Dioxide Bubbles. *The Journal of Chemical Physics* **2015**, *142* (14), 144501. https://doi.org/10.1063/1.4917022.

Chapter 6. GENERAL DISCUSSION

Through our experiments, it was demonstrated that the polarization geometry of the laser has no influence on the NPLIN kinetics of potassium sulfate (K_2SO_4) and ethylenediamine sulfate (EDS), neither on the enantiomorphs produced in case of EDS. These results are in agreement with several studies that have been performed in the SMS laboratory, prior to this PhD work, concerning in particular sodium chlorate (see Appendix A.3.1).

Hence, we can ask: why does the polarization geometry have no influence on our compounds? Why is the Optical Kerr Effect not occurring during our experiments?

Is it related to laser intensity? Indeed, regarding articles reporting an influence of the polarization geometry during NPLIN[1–4], it can be noticed that the laser intensities at work are about 10 times higher compared to our set-up or to studies focusing on KCl NPLIN[5–7] (and most of the NPLIN studies). Nonetheless, the high intensities used in ref. 1-4 remains rather weak compared to the one estimated by simulation [8] to induced OKE. Moreover, we succeeded to induce NPLIN in urea supersaturated solution using lower intensity than used in literature. Thus , we believe that the laser intensity is not the limiting factor in our experiment.

*Is it related to the laser type (*i.e., *continuous wave (CW) vs pulsed laser)?* Indeed, symmetry breaking phenomena have been reported during crystallization of sodium chlorate under CPL irradiation by using continuous light exposure[9,10]. We believe that CW laser and pulsed laser may involve different phenomena and CW laser might be more suitable for stereoselective challenges. In particular, the publication by Niinomi *et al.*[11] reports an interesting chiral bias during the crystallization of $NaClO_3$: the use of RCP continuous light triggers the nucleation of one enantiomorph, whereas the use of LCP triggers the nucleation of the other enantiomorph. However, this phenomenon was shown to rely on a primary interaction between the CW laser light and insoluble nanoparticles of silver, which have been added on purpose to the $NaClO_3$ solutions. Actually, the study by Niinomi *et al*. is in good agreement with more recent concepts regarding the NPLIN mechanisms which poses that the laser light does not interact directly with the solute compound but requires some kind of handover material to “link” the laser light to nucleation. Recent publications highlight that such materials could be insoluble impurities present in solutions. [6,12,13]

At the early stage of this PhD work, we hypothesized that the insoluble particles could result from damaging the vial sides upon laser irradiation,

which could generate glass particles in the solution. To investigate this, AFM and SEM observations of the inner surfaces of an irradiated glass vial were compared to those of an unexposed glass vial. The results of these experiments are reported in Appendix A.4 and show no evidence of such light induced damages.

This hypothesis was further refuted by the fact that filtration of the supersaturated solutions prior to the exposure to the laser light strongly reduces the NPLIN phenomenon. The present work confirms that the probabilities of nucleation of irradiated EDS and K_2SO_4 solutions are strongly reduced upon filtration of the solution (once again prior to laser exposure), thus highlighting the presence of solid and insoluble impurities inside the mother solutions. The chemical nature of the impurities collected during filtration of EDS solutions was investigated in Chapter 5-§5.4.2 and consists in a complex mixture of metallic materials, resembling the composition of stainless steel. Thus, we suppose that these impurities are present in the EDS commercial lots and come from the industrial production stage.

As discussed in Chapter 5, the presence of such solid impurities plays a major role in the NPLIN mechanism since their partial removal results in a partial decrease of NPLIN probability. Further to this, we showed that doping on purpose the filtered solutions of EDS with several types of metallic materials enables to retrieve higher NPLIN kinetics with reference to non-filtered solutions. However, the efficiency of NPLIN depends on the nature of the added impurity and we found that some impurities are more efficient than others. This suggests that the efficiency of the handover mechanism depends on how strong the “light – impurity” interaction is.

It can be hypothesized that the NPLIN efficiency is related to the light absorption properties of the insoluble particles: higher absorbing materials may lead to more efficient NPLIN effects. This is supported by the fact that NPLIN of EDS solutions doped with several types of particles was strongly impacted by the use of different wavelengths. In particular, the NPLIN kinetics were favoured by irradiating the doped solutions with a 532 nm light. Although we measured the UV-Vis spectra of the doped EDS solutions, it was difficult to find a correlation between the absorption properties of the solutions and their nucleation efficiencies. This could be due to the very different impurity concentrations used during our study. More studies are required to better understand the nature of the interaction between the laser light and such impurities.

Then, if the addition of metallic particles in a filtered solution enables to retrieve a NPLIN effect, would it be possible to induce or improve a NPLIN effect in a system that does not, or hardly exhibits NPLIN, by doping the solutions?

We investigated this possibility using supersaturated aqueous solutions of racemic diprophylline (DPL). DPL is a chiral molecular compound which has been intensely studied by the SMS laboratory[14–16]. The compound is well known to have difficulties nucleating, especially from water (aqueous solutions with supersaturation ratio as high as β=3 can remain metastable for more than 24h). It was also highlighted by our experiments that crystallization of DPL aqueous solutions is hardly favoured by laser irradiation (See Appendix A.5).

We decided to dope the DPL aqueous solutions (β=3.25) with gold nanoparticles (at a concentration of 0.01mg/g of DPL). Solutions were then exposed to 1064 nm light, using either 241 mJ or 126 mJ per pulse. The solutions required a number of pulses as high as 600 to crystallize. Such a high number of pulses has also been used for the NPLIN of carbamazepine[3], sulfathiazole[4] or glycine[2,12,17] (at even higher energies) but obviously does not compare to the conditions used in Chapter 4 and 5. At least 30 samples were studied in each experimental condition, and for control samples. The same experiment was also performed in the absence of gold nanoparticles. Results are shown in Figure 6-1. At 240mJ (Figure 6-1a), it can be seen that the NPLIN kinetics of irradiated undoped solutions (NPLIN H_2O) is similar to that of spontaneous nucleation (i.e., Control samples - non-irradiated). In contrast, doping the solution with gold nanoparticles and irradiating has a clear impact: 24h after irradiation doped solutions have a nucleation probability of 33% whereas the probability is still 0% for irradiated but un-doped solutions. We therefore evidenced that it is possible to trigger the NPLIN effect in a system by suitable doping.

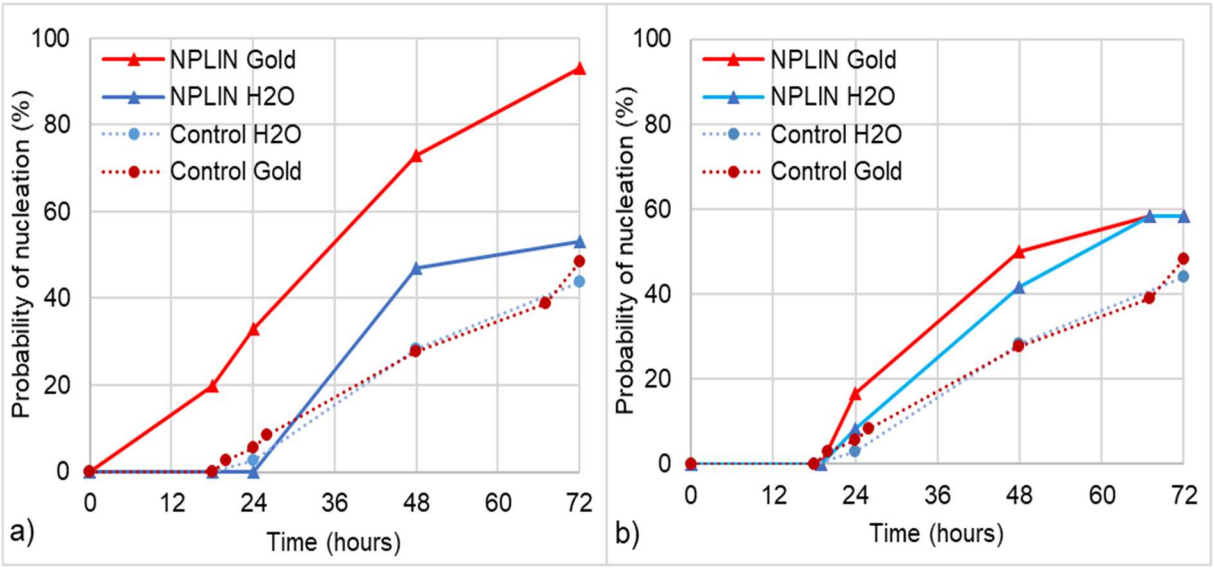

Figure 6-1-Probability of nucleation vs time for supersaturated solutions of DPL (β=3.25. Standard solution labelled H_2O (not doped) and doped solution with gold nanoparticles exposed to a) 600 pulses at 241mJ b) 600 pulses at 126mJ (1064nm). Point are experimental value and lines are guided to the eye and do not represent experimental behaviour.

However, using lower energy (126mJ per pulse, Figure 6-1b) the difference between doped solution and standard solution is narrower. It seems that the energy is not high enough to "activate" the gold nanoparticle. Solutions of gold nanoparticles are known to absorb at 520 nm : would this process "activation" be more efficient at 532 nm?

The same experiments were reproduced using 532nm light with 600 pulses at 122mJ. At least 30 samples were irradiated in each case. The results are presented in Figure 6-2 and show that: (i) the use of 532nm light leads to a higher probability of nucleation than 1064nm light, (ii) both doped gold solutions and standard solutions irradiated at 532 nm have a higher probability of nucleation and larger difference with reference to control (non-irradiated) samples. However, (iii) contrary to expectations, doping the solution with gold nanoparticle does not lead to a higher probability of nucleation at 532nm: after 36h the probability of nucleation of doped sample is lower than the one of standard samples.
Once again, it is possible that the energy used (122 mJ) is not high enough to "activate" the nanoparticles. Unfortunately, our laser set-up does not permit to reach an energy higher than 161mJ at 532nm. It could be expected that the NPLIN kinetics would be faster at higher energy at 532 nm.

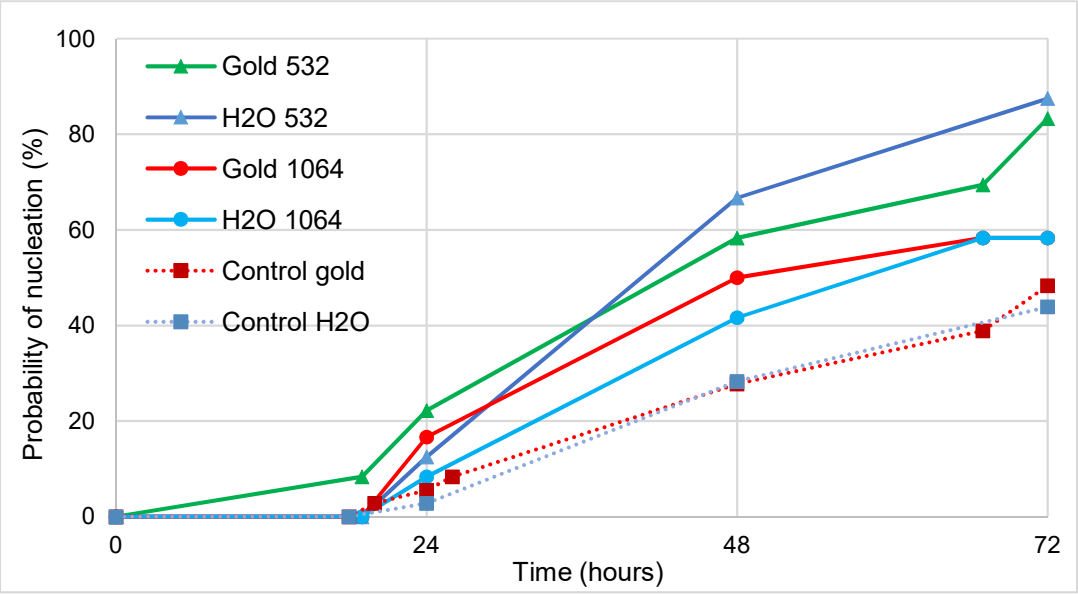

Figure 6-2-Probability of nucleation in function of time for supersaturated aqueous DPL solution and doped solution with gold (β=3.25), exposed to 600 pulses at 122mJ at 532nm compare to solutions exposed to 600 pulses at 126mJ at 1064nm.

These results underline that even if it is possible to trigger or improve the NPLIN effect by doping the solutions with insoluble metallic materials, other parameters should be considered, such as the laser wavelength, but also the energy transmitted to the solution.

The results reported in this PhD work also question how the nanoparticles, upon irradiation, interact with the solution and trigger the nucleation of the solute compound. It has been proposed that the energy absorbed by the particle is released upon its implosion, thus creating fresh nucleation sites. Another hypothesis is that the local heating of the solution provokes gas cavitation. Through the case of K_2SO_4 we showed that if cavitation occurs, the cavities formed do not consist of dissolved gas but rather of vaporized solvent. In this context, more investigations are required to understand this part of the mechanism, maybe by changing the wavelength since our investigations evidenced a clear impact of this parameter on the number of crystals produced.

To conclude, this PhD work shows that:

- The NPLIN mechanism relies, without doubt, on the presence of insoluble metallic particles in solution. Those particles most likely come from the industrial lot of solid compounds. It would be interesting to compare the NPLIN kinetics of a freshly synthesized sample with that of an industrial batch.

- NPLIN efficiency of a given system can be enhanced by voluntary doping of solutions with metallic nanoparticles and by tuning the working wavelength in relation to the absorption properties of the chosen particle. Understanding how exactly the particles interact with the laser light and induce the nucleation could permit to establish selection criteria regarding the chemical nature and concentration of the particles.
- The NPLIN kinetics is independent of the dissolved gas content which question the role, presence and nature of gas cavitation during NPLIN.

Of course, more studies are required to further understand the mechanism:

- Regarding the doping of solutions, it could be envisaged to use other kind of particles, particularly, non-metallic particles (e.g., carbon) to check if the NPLIN effect is limited to metallic impurities. Then, it would be of interest to investigate the influence of concentration of the particles added and their size (e.g., gold nanoparticles are available in size ranging from 5nm to 400nm). The use of a surfactant or even a gelling agent could be necessary to ensure sufficient dispersion of the particles.
- Besides, it would be helpful to determine the exact physicochemical nature of the solid impurities in the solutions. Dynamic light scattering could be used to measure the size of the impurities in the solution. Hence, we will be able to compare for each compound if the same impurities are involved. It would be very informative to interview the chemicals providers about these impurities.
- The NPLIN set-up could be coupled to a microscope and a camera to observe the first stage of NPLIN and conclude about the possible formation of bubbles using nanosecond unfocused laser. In addition, coupling the NPLIN set-up with a microfluidic set-up could also be useful to achieve a higher number of experiment and therefore more reliable statistics.

References:

(1) Matic, J.; Sun, X.; Garetz, B. A.; Myerson, A. S. Intensity, Wavelength, and Polarization Dependence of Nonphotochemical Laser-Induced Nucleation in Supersaturated Aqueous Urea Solutions. *Crystal Growth & Design* **2005**, *5* (4), 1565–1567. https://doi.org/10.1021/cg050041c.

(2) Sun, X.; Garetz, B. A.; Myerson, A. S. Supersaturation and Polarization Dependence of Polymorph Control in the Nonphotochemical Laser-Induced Nucleation (NPLIN) of Aqueous Glycine Solutions. *Crystal growth & design* **2006**, *6* (3), 684–689.

(3) Ikni, A.; Clair, B.; Scouflaire, P.; Veesler, S.; Gillet, J.-M.; El Hassan, N.; Dumas, F.; Spasojević-de Biré, A. Experimental Demonstration of the Carbamazepine Crystallization from Non-Photochemical Laser-Induced Nucleation in Acetonitrile and Methanol. *Crystal Growth & Design* **2014**, *14* (7), 3286–3299. https://doi.org/10.1021/cg500163c.

(4) Li, W.; Ikni, A.; Scouflaire, P.; Shi, X.; El Hassan, N.; Gémeiner, P.; Gillet, J.-M.; Spasojević-de Biré, A. Non-Photochemical Laser-Induced Nucleation of Sulfathiazole in a Water/Ethanol Mixture. *Crystal Growth & Design* **2016**, *16* (5), 2514–2526. https://doi.org/10.1021/acs.cgd.5b01526.

(5) Alexander, A. J.; Camp, P. J. Single Pulse, Single Crystal Laser-Induced Nucleation of Potassium Chloride. *Crystal Growth & Design* **2009**, *9* (2), 958–963. https://doi.org/10.1021/cg8007415.

(6) Kacker, R.; Dhingra, S.; Irimia, D.; Ghatkesar, M. K.; Stankiewicz, A.; Kramer, H. J. M.; Eral, H. B. Multiparameter Investigation of Laser-Induced Nucleation of Supersaturated Aqueous KCl Solutions. *Crystal Growth & Design* **2018**, *18* (1), 312–317. https://doi.org/10.1021/acs.cgd.7b01277.

(7) Ward, M. R.; Ballingall, I.; Costen, M. L.; McKendrick, K. G.; Alexander, A. J. Nanosecond Pulse Width Dependence of Nonphotochemical Laser-Induced Nucleation of Potassium Chloride. *Chemical Physics Letters* **2009**, *481* (1–3), 25–28. https://doi.org/10.1016/j.cplett.2009.09.049.

(8) Knott, B. C.; Doherty, M. F.; Peters, B. A Simulation Test of the Optical Kerr Mechanism for Laser-Induced Nucleation. *The Journal of Chemical Physics* **2011**, *134* (15), 154501. https://doi.org/10.1063/1.3574010.

(9) Cheng, A.-C.; Niinomi, H.; Omatsu, T.; Ishida, S.; Sasaki, K.; Sugiyama, T. Plasmonic Manipulation-Controlled Chiral Crystallization of Sodium Chlorate. *J. Phys. Chem. Lett.* **2020**, *11* (11), 4422–4426. https://doi.org/10.1021/acs.jpclett.0c01041.

(10) Mahurin, S.; McGinnis, M.; Bogard, J. S.; Hulett, L. D.; Pagni, R. M.; Compton, R. N. Effect of Beta Radiation on the Crystallization of Sodium Chlorate from Water: A New Type of Asymmetric Synthesis. *Chirality* **2001**, *13* (10), 636–640. https://doi.org/10.1002/chir.10007.

(11) Niinomi, H.; Sugiyama, T.; Tagawa, M.; Murayama, K.; Harada, S.; Ujihara, T. Enantioselective Amplification on Circularly Polarized Laser-Induced Chiral Nucleation from a $NaClO_3$ Solution Containing Ag Nanoparticles. *CrystEngComm* **2016**, *18* (39), 7441–7448. https://doi.org/10.1039/C6CE01464J.

(12) Javid, N.; Kendall, T.; Burns, I. S.; Sefcik, J. Filtration Suppresses Laser-Induced Nucleation of Glycine in Aqueous Solutions. *Crystal Growth & Design* **2016**, *16* (8), 4196–4202. https://doi.org/10.1021/acs.cgd.6b00046.

(13) Ward, M. R.; Mackenzie, A. M.; Alexander, A. J. Role of Impurity Nanoparticles in Laser-Induced Nucleation of Ammonium Chloride. *Crystal Growth & Design* **2016**, *16* (12), 6790–6796. https://doi.org/10.1021/acs.cgd.6b00882.

(14) Brandel, C.; Amharar, Y.; Rollinger, J. M.; Griesser, U. J.; Cartigny, Y.; Petit, S.; Coquerel, G. Impact of Molecular Flexibility on Double Polymorphism, Solid Solutions and Chiral Discrimination during Crystallization of Diprophylline Enantiomers. *Mol. Pharmaceutics* **2013**, *10* (10), 3850–3861. https://doi.org/10.1021/mp400308u.

(15) Viel, Q.; Brandel, C.; Cartigny, Y.; Eusébio, M. E. S.; Canotilho, J.; Dupray, V.; Dargent, E.; Coquerel, G.; Petit, S. Crystallization from the Amorphous State of a Pharmaceutical Compound: Impact of Chirality and Chemical Purity. *Crystal Growth & Design* **2017**, *17* (1), 337–346. https://doi.org/10.1021/acs.cgd.6b01566.

(16) Brandel, C.; Cartigny, Y.; Coquerel, G.; ter Horst, J. H.; Petit, S. Prenucleation Self-Assembly and Chiral Discrimination Mechanisms during Solution Crystallisation of Racemic Diprophylline. *Chemistry – A European Journal* **2016**, *22* (45), 16103–16112. https://doi.org/10.1002/chem.201602707.

(17) Liu, Y.; van den Berg, M. H.; Alexander, A. J. Supersaturation Dependence of Glycine Polymorphism Using Laser-Induced Nucleation, Sonocrystallization and Nucleation by Mechanical Shock. *Phys. Chem. Chem. Phys.* **2017**, *19* (29), 19386–19392. https://doi.org/10.1039/C7CP03146G.

APPENDICES

A.1 HOT-STAGE MICROSCOPY

The polymorphic transition of EDS was studied with a polarized light microscope equipped with a hot stage device (Linkam THMS 600). At around 225°C, a brighter zone appears and extends to the whole crystal with different colours at some points (Figure A-1), and this corresponds to the appearance of the HT-EDS phase. When looking at the cooling, the two events observed by DSC and XRD cannot be distinguished but an opacification of the crystal is observed. At the end of the cooling, the polymorphic transition results in the transformation of the single crystal into a polycrystalline solid, which is clearly confirmed by the coloured mosaic.

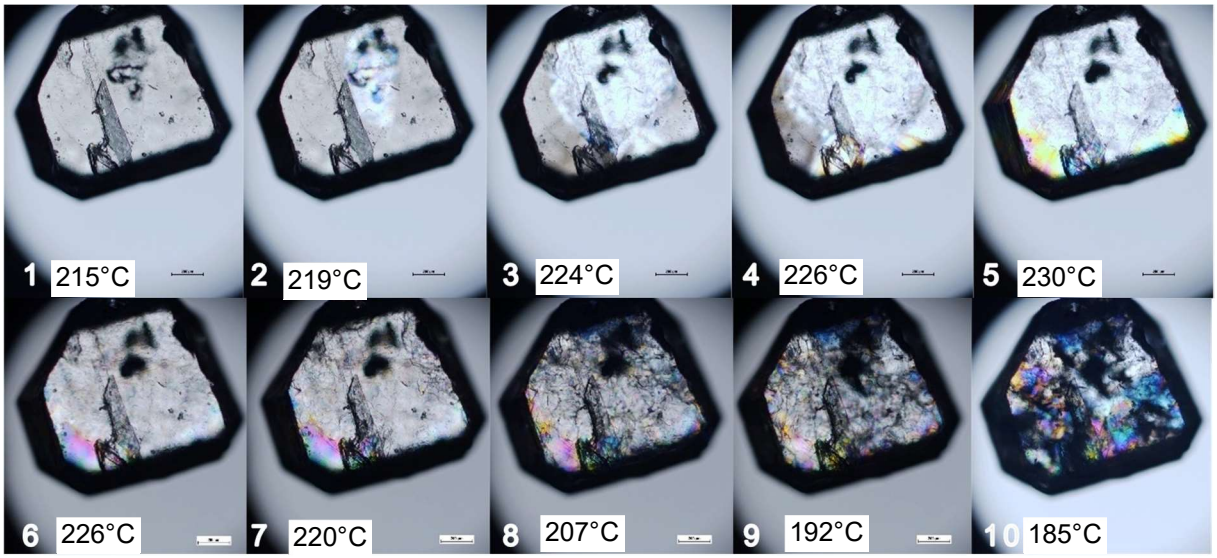

Figure A-1-EDS crystals seen under polarized light microscope (NIKON Eclipse LV100) upon heating (1-5) and upon cooling (6-10)

A.2 UV- VIS SPECTRA OF NANOPARTICLES USED

The UV-visible spectra of the particles in water were measured. Figure A-2 presents the different spectra obtained. The reference is the water spectrum. The spectrum obtained for water with addition of steel particles is quite similar. There is a peak of absorption for gold around 520nm and for silver at 400nm. Due to the absorption of water, all the solutions containing particles absorb more at 1064nm than at 532nm. In the case of rust particle, it seems that the spectrum is shifted to higher absorption values, the absorption is much higher than for the other solutions.

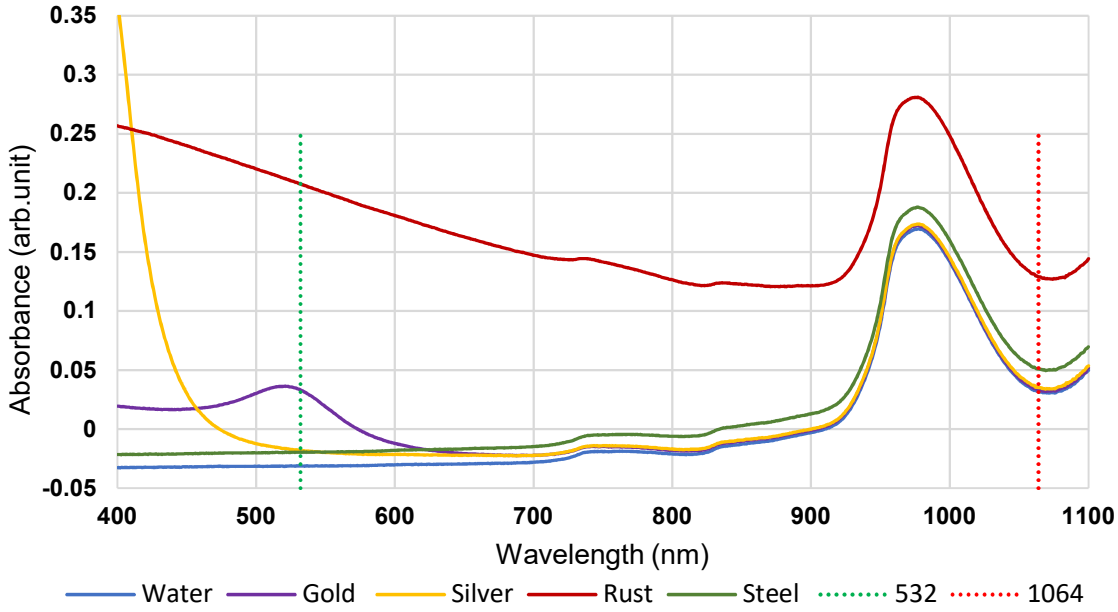

Figure A-2-UV-Vis spectra measured for different particles suspension in water

A.3 TRAINING REPORTS

A.3.1 Study of Sodium Chlorate (Laurianne FEUILLU)

During her training period, Laurianne has worked on the NPLIN of sodium Chlorate ($NaClO_3$) in water, with the same set-up used in this PhD work. She was asked to study the influence of the laser polarization geometry on the chirality of the crystals produced by NPLIN ($NaClO_3$ exhibits supramolecular chirality). The results are presented in Table A-1 and Table A-2, respectively for linear polarization and circular polarization. No correlation is observed between the polarization geometry and the chirality of the crystals produced.

Table A-1-Chirality of $NaClO_3$ crystals obtained by NPLIN with linearly polarized light for different supersaturation (β). % blue and %brown each corresponding to one enantiomorph either d or l . % racemic corresponds to sample in which both enantiomorph were present.

	Experiment number	Number of Crystallized Samples	%Blue	%Brown	%Racemic
β=1.07	1	21	52,4	28,6	19,1
	2	19	21,1	31,6	47,4
	3	12	25,0	41,7	33,3
	4	31	16,1	22,6	29,0
	5	9	11,1	77,8	11,1
	6	3	33,3	66,7	00,0
	7	10	40,0	40,0	20,0
	Spontaneous nucleation	43	44,2	46,5	9,3
	Total	148	32,4	38,5	22,3

β=1.04	1	6	83,3	16,7	00,0
	2	5	40,0	60,0	00,0
	3	24	33,3	45,8	20,8
	4	10	30,0	60,0	10,0
	5	20	30,0	60,0	10,0
	Total	65	36,9	50,8	12,3
β=1.06	1	15	46,7	46,7	6,7
	2	10	30,0	50,0	20,0
	Spontaneous nucleation	8	12,5	25,0	62,5
	Total	33	33,3	42,4	24,3

Table A-2-Chirality of $NaClO_3$ crystals obtained by NPLIN with Circularly polarized light.

	Experiment number	Number of Crystallized Samples	% Blue	%Brown	%Racemic
β=1.07	1	18	44,4	33,3	22,2
	2	26	34,6	53,9	11,5
	3	40	35,0	32,5	32,5
	4	8	50,0	50,0	0,0
	5	25	36,0	40,0	24,0
	6	7	28,6	71,4	0,0
	7	7	28,6	57,1	14,3
	8	7	28,6	42,9	28,6
	Total	138	36,2	42,8	21,0

A.3.2 Study of Modafinil Acid (Aurélien LEMERCIER)

Through his training period, Aurélien has worked on different compounds including modafinil acid which is a chiral molecule as shown in Figure A-3. Solutions of β=1.2 of modafinil acid in methanol were exposed to either linear or circular polarization. The enantiomeric excess was determined by polarimetry, the results are presented in Table A-3 and show no correlation between optical rotation and polarization geometry.

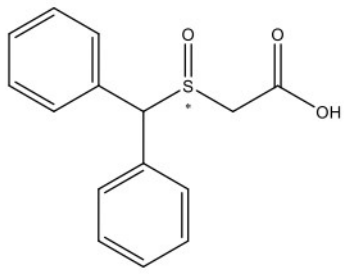

*Figure A-3-Chemical structure of Modafinil acid, * indicate the stereogenic center*

Table A-3-Mean optical rotation for modafinil acid exposed to linear or circular polarization compared to control sample (non-irradiated) for at least 42 samples.

	Control sample	Linear polarization	Circular polarization
Optical rotation (°)	0.175	0.288	0.311

A.4 AFM AND SEM ANALYSIS

After the exposition of vial filled with water to 100 pulses at 85.6mJ, the irradiated section of vial was cut to perform AFM and SEM analysis

Pictures obtained from AFM analysis are presented in (Figure A-4). The measured roughness values are presented in Table A-4, the average roughness (Ra) and maximum roughness (Rz) for the three samples are of the same order of magnitude.

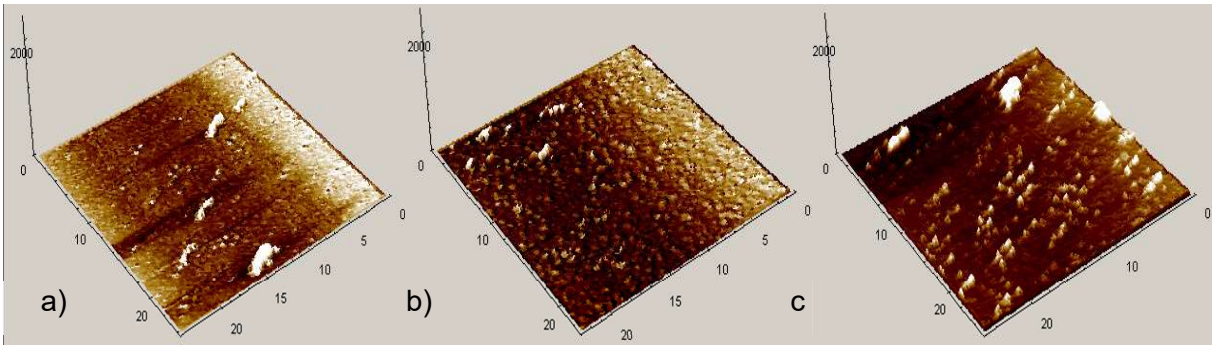

Figure A-4-3D representation of the inner surface roughness of the vial measured by atomic force microscopy (AFM). a) a piece of control vial without any laser exposure, b) and c) a piece of vial exposed to 100pulses at 85.6mJ respectively the entry face and the exit face of the laser beam. The size of the surface analysed is 25µmx25µm

Table A-4-Roughness average (Ra) and maximum roughness (Rz) measured for control vial and irradiated vial (entry face and exit face of the laser beam)

	Roughness average (Ra)	Roughness max (Rz)
Control Vial	7nm	340nm
Irradiated Vial (Entry)	18nm	453nm
Irradiated Vial (Exit)	20nm	380nm

The images obtained from SEM are presented in Figure A-5, no impact of laser can be seen compared to the control vial.

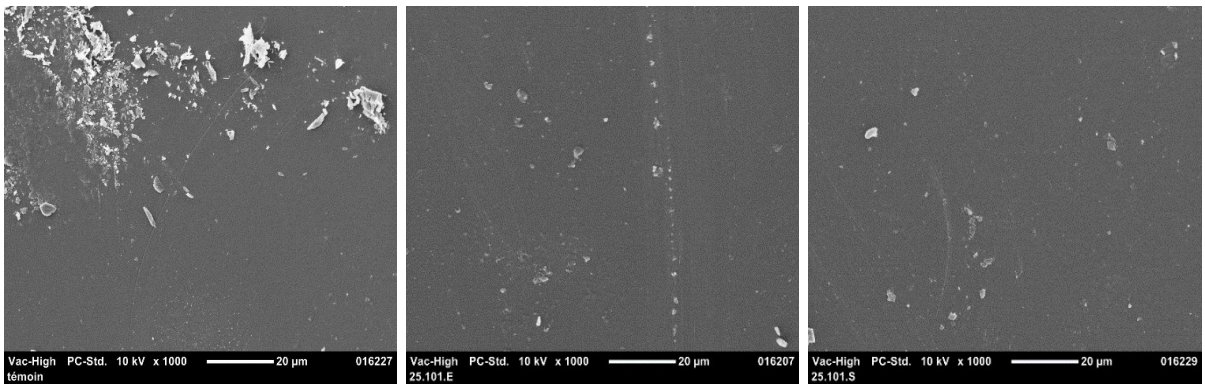

Figure A-5-Scanning electron microscopy (SEM) images. From left to right: control vial, vial entry face and vial exit face of the laser beam.

A.5 THE DIPROPHYLLINE AQUEOUS SYSTEM NPLIN BEHAVIOUR

A.5.1 Introduction

Diprophylline (DPL) is a chiral drug used in the treatment of respiratory disorders, also named 7-(2,3-Dihydroxy-propyl)theophylline, it is a derivative of theophylline. The molecules are presented in Figure A-6. The intrinsic chirality and polymorphism of DPL were first interesting for our NPLIN study, but the interest then shifted to the long induction times observed and the low reactivity of DPL with laser light (i.e., Limited (or non-observable) NPLIN effect)

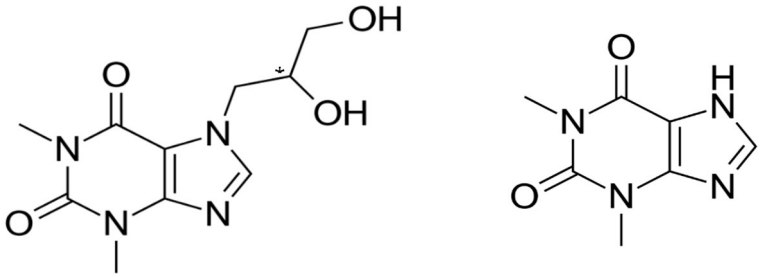

*Figure A-6-Chemical structure of diprophylline (*chiral carbon) on the left and theophylline on the right*

A.5.2 Solubility of Diprophylline

Racemic DPL (RI) is soluble in polar solvent such as water, dimethylformamide or dimethyl sulfoxide and poorly soluble in methanol and isopropyl alcohol[1]. In this study, as only aqueous solutions are concerned, the solubility curve of DPL in water was established by gravimetry. Wu *et al.*[2] examined the solubility of DPL in different solvents including water and correlated experimental data to thermodynamics model. They used the isothermal saturation method and determined the solubility in molar fraction via HPLC analysis. Their data were converted from molar fraction to mass fraction in order to compare with our experimental solubility data. The results are shown in Figure A-7. There is a difference between our experimental data and the solubility data of Wu *et al* which can be due to the different techniques used to measure solubility. For this study, we choose to consider the solubility value we measured at the working temperature of 20°C, so 9.5%wt.

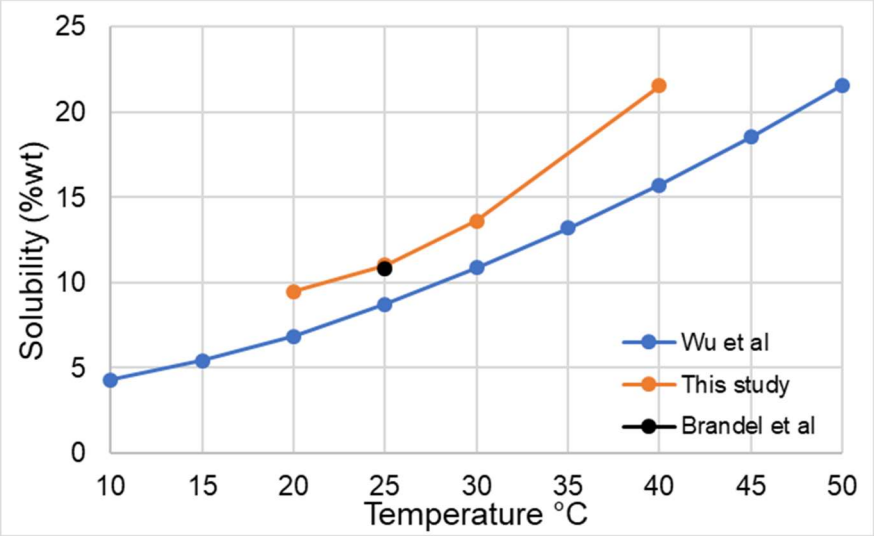

Figure A-7-Solubility determine in this study in weight percentage of (RS)-DPL in water in function of temperature compare to others studies[1,2]

A.5.3 Spectroscopy UV-vis

The UV-vis spectrum of saturated aqueous DPL solution was measured to evaluate the possible absorption of the molecule and eliminate the probability of photochemical reactions. Figure A-8 shows the absorbance spectra of DPL and water. The absorption of DPL aqueous solutions mainly originates from water with a slight increase of the absorbance at the two wavelengths studied (1064nm and 532nm) which is not significative and will not lead to photochemical reaction.

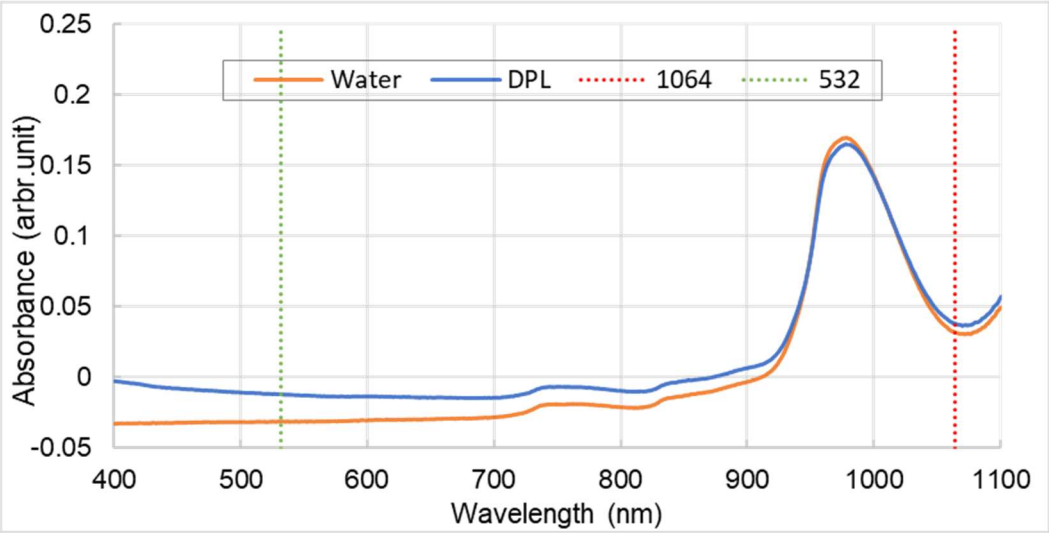

Figure A-8-UV-vis spectra of saturated DPL aqueous solution and water.

A.5.4 NPLIN experiments

Figure A-9a) shows the behaviour of DPL supersaturated solution of β=3.5, exposed to 600pulses at 241mJ (at least 20 samples for both NPLIN and control). In the end the control samples have a higher probability of nucleation than the samples exposed to laser. In Figure A-9b), when β=3.25, the NPLIN effect is not clear as spontaneous nucleation occurs simultaneously. Therefore, there is no strong effect of the laser on the DPL solutions contrary to the compound observed in Chapter 4 and 5.

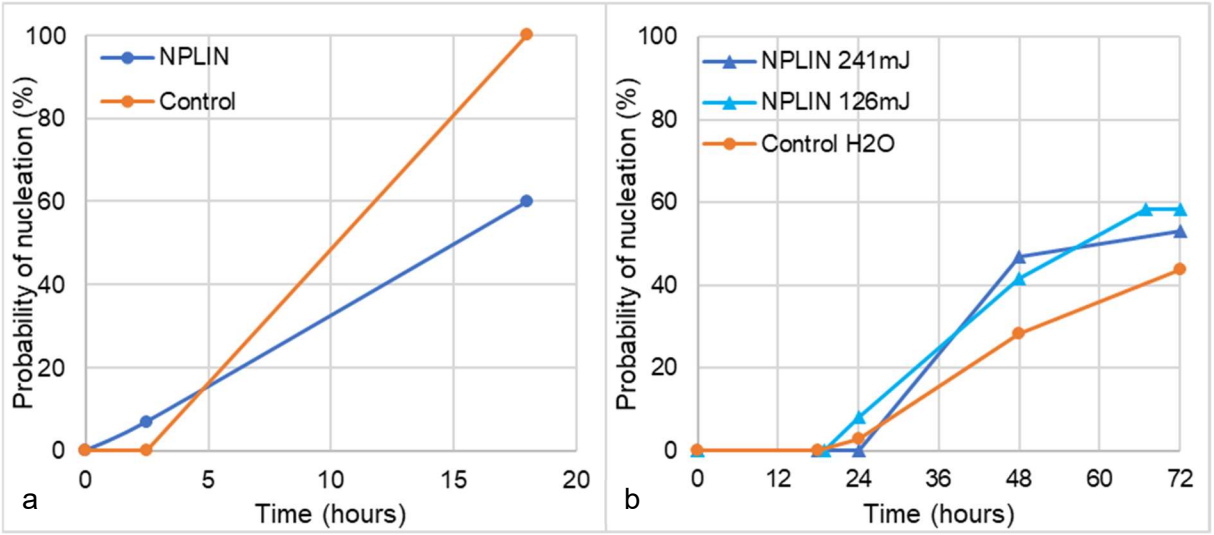

Figure A-9-Probability of nucleation over time for aqueous DPL solution exposed to 1064nm laser a) β=3.5 exposed to 600pulses at 241mJ with and b) β=3.25 exposed to 600pulses at 241mJ or 126mJ.

A.5.5 Description of the crystals obtained

The crystals obtained are needle like crystals but “agglomerated” in urshin like structure, as shown in Figure A-10 and Figure A-11. Both spontaneous nucleation and NPLIN gave the same kind of crystals. The solid structure obtained via NPLIN and spontaneous nucleation was checked by X-ray diffraction and confirmed that it is form RI.

Figure A-10-Pictures of the DPL crystals obtained in 1mL vial, on the left aqueous solution and on the right gold doped aqueous solution.

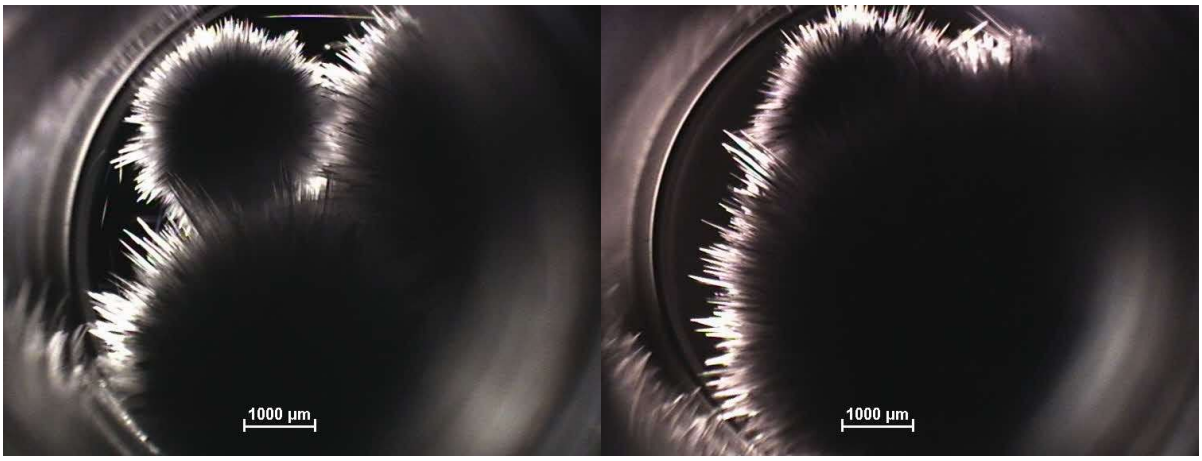

Figure A-11-Pictures of DPL crystals observed with microscope on the left aqueous solution and on the right gold doped aqueous solution.

(1) Brandel, C. Structural Purity and Solid-Solid Transitions in Molecular Crystals, university of Rouen Normandie, **2014**.

(2) Wu, Y.; Gao, J.; Yan, S.; Wu, C.; Hu, B. The Dissolution Behaviour and Apparent Thermodynamic Analysis of Diprophylline in Pure and Mixed Solvents. *The Journal of Chemical Thermodynamics* **2019**, *138*, 297–303. https://doi.org/10.1016/j.jct.2019.06.007.

Abstract

The non-photochemical laser induced nucleation (NPLIN) phenomenon occurs by irradiation of a supersaturated solution with a high energy pulsed nanosecond laser. NPLIN allows temporal control (decrease of induction time) and spatial control (nucleation inside the irradiated area) of nucleation. However, the interaction between the laser light and the supersaturated solution is not well understood. Several mechanisms have been proposed to explain NPLIN, such as the Optical Kerr Effect or the nanoparticle heating mechanism. The aim of this PhD work is to contribute to the general understanding of the NPLIN mechanism.

Beside a comprehensive review of literature concerning NPLIN, this manuscript reports our investigation regarding two compounds: Potassium Sulfate and Ethylenediamine Sulfate. In both cases, the laser enables a marked reduction of induction times compared to spontaneous nucleation. For Potassium Sulfate, the influence of dissolved gas content in solution was examined in order to evaluate the cavitation mechanism. For Ethylenediamine Sulfate, the influence of filtration and doping of solutions through voluntary addition of particles were studied. Moreover, the supramolecular chirality of Ethylenediamine Sulfate permits to study the possible stereoselectivity of the process. Finally, the different mechanisms are reviewed according to our findings, allowing to open new ways of research concerning NPLIN.

Key-Words: *Nucleation, Non-Photochemical, Laser, NPLIN, Mechanism, Potassium Sulfate, Ethylenediamine Sulfate, Nanoparticle, Filtration*

Résumé

La nucléation non-photochimique induite par laser (NPLIN) est un phénomène faisant appel à un laser pulsé à haute énergie, souvent nanoseconde, pour initier la nucleation au sein d'une solution sursaturée. La NPLIN permet un contrôle temporel de la nucléation (diminution du temps d'induction) ainsi qu'un contrôle spatial (nucleation dans la zone irradiée). Cependant, l'interaction entre le laser et la solution sursaturée, permettant la nucléation, n'est pas clairement définie. Plusieurs mécanismes ont été proposés pour expliquer le phénomène NPLIN, tel que l'Effet Kerr Optique (OKE), ou le chauffage de nanoparticules. L'objectif de cette thèse est d'aider à la compréhension du mécanisme NPLIN.

En plus d'une analyse complète de la littérature concernant la NPLIN, ce manuscrit présente nos recherches sur deux composés : le sulfate de potassium et le sulfate d'éthylenediamine. Il a été démontré pour chacun l'influence du laser sur la réduction du temps d'induction par rapport à une nucleation spontanée. Dans le cas du sulfate de potassium, l'influence de la composition en gaz dissout dans la solution a été examiné dans le but d'évaluer le mécanisme de cavitation. Dans le cas du sulfate d'éthylenediamine, l'influence de la filtration et du dopage des solutions par ajout volontaire de particules a été examiné. De plus, la chiralité supramoléculaire du sulfate d'éthylenediamine a permis d'étudier la possibilité d'un contrôle stéréosélectif du NPLIN. Enfin, les différents mécanismes sont discutés en lien avec les résultats obtenus , permettant d'ouvrir de nouvelles voies de recherches concernant la NPLIN.

Mots-clés : *Nucléation, Non-Photochimique, Laser, NPLIN, Mécanisme, Sulfate de Potassium, Sulfate d'éthylenediamine, Nanoparticule, Filtration*